INFORMATION TO USERS

8107350

KIM, TAE JUNG

A HYBRID METHOD WHICH COMBINES A MOMENT METHOD CURRENT WITH AN ASYMPTOTIC CURRENT

The Ohio State University   PH.D.   1980

University Microfilms International

300 N. Zeeb Road, Ann Arbor, MI 48106

A HYBRID METHOD WHICH COMBINES A MOMENT METHOD CURRENT
WITH AN ASYMPTOTIC CURRENT

DISSERTATION

Presented in Partial Fulfillment of the Requirements for
the Degree Doctor of Philosophy in the Graduate
School of The Ohio State University

By
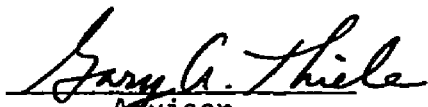
Tae Jung Kim, B.S.E.E., M.S.E.E.

******

The Ohio State University
1980

Reading Committee:

Professor Jack H. Richmond
Professor Robert G. Kouyoumjian
Professor Gary A. Thiele

Approved by

Adviser
Department of Electrical
Engineering

ACKNOWLEDGMENTS

VITA

March 27, 1945.....	Born, Seoul, Korea
1968...............	B.S.E.E., Seoul National University, Seoul, Korea
1970-1973..........	Teaching Assistant, Seoul National University, Seoul, Korea
1972...............	M.S.E.E., Seoul National University, Seoul, Korea
1976..............	M.S.E.E., University of Cincinnati, Cincinnati, Ohio
1976-1978.........	Graduate Student, the Ohio State University, Columbus, Ohio
1978-1980.........	Graduate Research Associate Electro-Science Laboratory, The Ohio State University, Columbus, Ohio

Fields of Study

Major Field: Electrical Engineering
Studies in Antenna Theory: Professor Gary A. Thiele
Studies in Electromagnetic Theory: Professor Robert G. Kouyoumjian
Studies in Communication Theory: Professor Claud E. Warren
Studies in Applied Mathematics: Professor John T. Scheick
Studies in Physics: Professor Richard N. Boyd

TABLE OF CONTENTS

LIST OF FIGURES

CHAPTER I

INTRODUCTION

In electromagnetic problems the main task is usually to determine the current distribution on the surface of a scatterer. It is a relatively simple problem to obtain other parameters we desire from a knowledge of the surface current distribution. Obtaining the current distribution usually means we must solve integral equations derived from Maxwell's equations and the boundary conditions.

One of the well known methods for solving integral equations is the moment method [6],[12],[16], which converts the integral equation to linear algebraic equations having as many unknowns as the number of basis functions used to approximate the surface current on the scattering body. Even though the moment method gives us relatively accurate results for arbitrarily shaped bodies, its practical use is usually limited to bodies which are not large in terms of a wavelength.

Another powerful method, which is known as the geometrical theory of diffraction (GTD), was introduced by Keller (1953). GTD is a ray optical method which uses the leading terms of the asymptotic approximation to the integral of interest. Recently, Kouyoumjian and Pathak [5] have developed new formulations for diffraction coefficients which produce the better results in the transition regions.

1

Usually GTD is known as a high frequency method since it has an advantage when applied to scatterers which are electrically large. However, GTD solutions are available only for relatively simple canonical geometries.

Although both methods considered above provide us with relatively accurate results in their own applications, there are many electromagnetic problems which cannot be solved by either method alone. To solve such problems by using to advantage the two methods mentioned above, recently, hybrid techniques which combine them have been developed. One approach, which has been introduced by Thiele and Newhouse [2] in 1975, combines moment methods with the GTD (i.e., MM-GTD techniques). This technique extends the moment method through the use of the GTD to obtain a new modified impedance matrix for the moment method solution. The application of this method was demonstrated by solving the problems such as a monopole near a conducting wedge, a monopole at the center of a flat plane or a circular disc, and a monopole near a conducting step. A little later in the same year, Burnside and his colleagues [3] showed another hybrid approach by combining the GTD with the moment method (i.e., GTD-MM technique). In this technique, the diffraction coefficient is treated as an unknown coefficient in the moment method and was determined by numerical techniques. The application of the method was demonstrated by obtaining the surface currents on a perfectly conducting wedge, and square and circular cylinders. Later Mittra [7],[8], also

introduced a new approach for combining the integral equation and the GTD by using the fact that the Fourier transform of the unknown surface current is proportional to the scattered far field and demonstrated its applications to a perfectly conducting infinite strip of zero thickness, a thin conducting rectangular plate, and later to a circular cylinder in two dimensions.

The GTD-MM method which combines the GTD with the moment method, requires a priori knowledge of the asymptotic form of the current away from the diffraction or moment method region. Therefore, the GTD-MM technique considered above is difficult to apply to arbitrarily shaped bodies where the GTD current forms are not known a priori.

In this paper a new hybrid method which overcomes the disadvantage mentioned above is presented. This method which combines the moment method with an asymptotic technique as orginally introduced by Molinet [1], does not need any priori knowledge of current forms away from the moment method regions. Thus, the hybrid method of this paper offers an advantage in solving for currents in GTD transition regions where the form of the current is often difficult to determine. Further, this hybrid method, which uses the geometrical optics current as the dominant contributor to the initial current, works surprisingly well even for extremely small bodies in the Rayleigh region. One would expect this technique to work well for large bodies since it uses the geometrical optics current which is asymptotic with respect to frequency. The fact that it also works well for low frequency is indeed an unexpected bonus.

3

The integral equations originally introduced for this new hybrid method, were derived for the wedge problem and are not suitable for other shaped bodies. Therefore, in Chapter II, we consider the general theory for the method and also derive the general integral equations which are suitable for arbitrarily shaped bodies. In the derivation of the equations the asymptotic currents are assumed to approximately represent the dominant currents on the surfaces of a conducting body. Then the difference current between the approximate and exact currents is obtained by using the moment method in the moment method regions which are formed around the shadow boundary regions or around sharp geometrical discontinuities. In the next step, we determine the currents in the non-moment method regions by obtaining the contribution to the surface currents induced by the currents in the moment method regions. The process may be repeated to obtain higher order solutions.

Applications of the method to a perfectly conducting wedge, square and circular cylinders in two dimensions are considered in Chapters III, IV, and V, respectively. In Chapter VI, extension of our hybrid method to the three dimensional geometry is also considered by using a perfectly conducting sphere as an example. The results of the surface currents on a wedge and a square cylinder were compared with the solutions from the GTD whose diffraction coefficients are based on the results derived by Kouyoumjian and Pathak [5]. On the other hand, for a circular cylinder and a sphere, the comparisons were made with the exact eigenfunction solutions.

4

Usually for bodies having only plane surfaces, the general integral equations for the method reduce to relatively simple forms, but not for bodies composed of curved surfaces. Also observing those equations for the plane surfaces, we can realize that singularity problems are not involved in them. However, this problem will arise for curved surfaces and must be considered for more accurate results. Theoretically when we evaluate the principle value of integration, we must exclude the singular point for numerical integration, but practically we exclude the patch of a finite area containing the singular point instead of just the singular point. We see that this practical calculation will increase errors as long as the surface is not divided into very many subpatches so that the patch areas become very small. However, considering the computer running time and memory storage, it may not be efficient to divide the surface into so many divisions. Therefore, in Chapters V and VI we derive some constants which will roughly provide the contribution lost by excluding the finite patch area instead of a single point for the evaluation of the principle value of integration, and the effect of those constants is shown by comparing the results with and without them. By using those constants in the integral equations for the method, we can decrease the number of divisions for numerical integrations and thus computing time to obtain the same results that can be obtained by increased number of divisions.

In the examples which are considered in Chapters III, IV, V, and VI, the impedance matrix for the moment method is derived exactly for the wedge, but approximately for the square and circular cylinders, and the sphere. Even though we can derive the more accurate expression for it, it may not be useful for numerical calculations because of its complexity.

In Chapter VII, summary and conclusions are presented along with some of the advantages and disadvantages of this method.

CHAPTER II

GENERAL THEORY

2.1 First Order Approximation

Let's consider an arbitrary shaped 3-dimensional perfectly conducting body illuminated by a plane wave as shown in Figure 2.1. We divide the total surface S of the body into S^ℓ and S^S which represent the lit and shadowed regions, respectively. The separation boundary of S is the shadow boundary which is shown by the line AB in Figure 2.1. In addition, we split each of these regions into two regions, a moment method region (MM-region) and an asymptotic region (AS-region) which are represented, respectively by S^ℓ_{MM} and S^ℓ_{AS} in the lit region or by S^S_{MM} and S^S_{AS} in the shadow region. Therefore, we can write the following expressions regarding the surfaces.

$$S^\ell = S^\ell_{MM} + S^\ell_{AS} \tag{2.1}$$

$$S^S = S^S_{MM} + S^S_{AS} \; . \tag{2.2}$$

Usually the moment method region is smaller than the asymptotic region.

Next let the total current be denoted by $\overline{J}^\ell(\overline{R})$ in the lit region and by $\overline{J}^S(\overline{R})$ in the shadowed region. The current can then be expressed in terms of $\overline{J}^\ell_{MM}(\overline{R})$ and $\overline{J}^\ell_{AS}(\overline{R})$ or $\overline{J}^S_{MM}(\overline{R})$ and $\overline{J}^S_{AS}(\overline{R})$ as

7
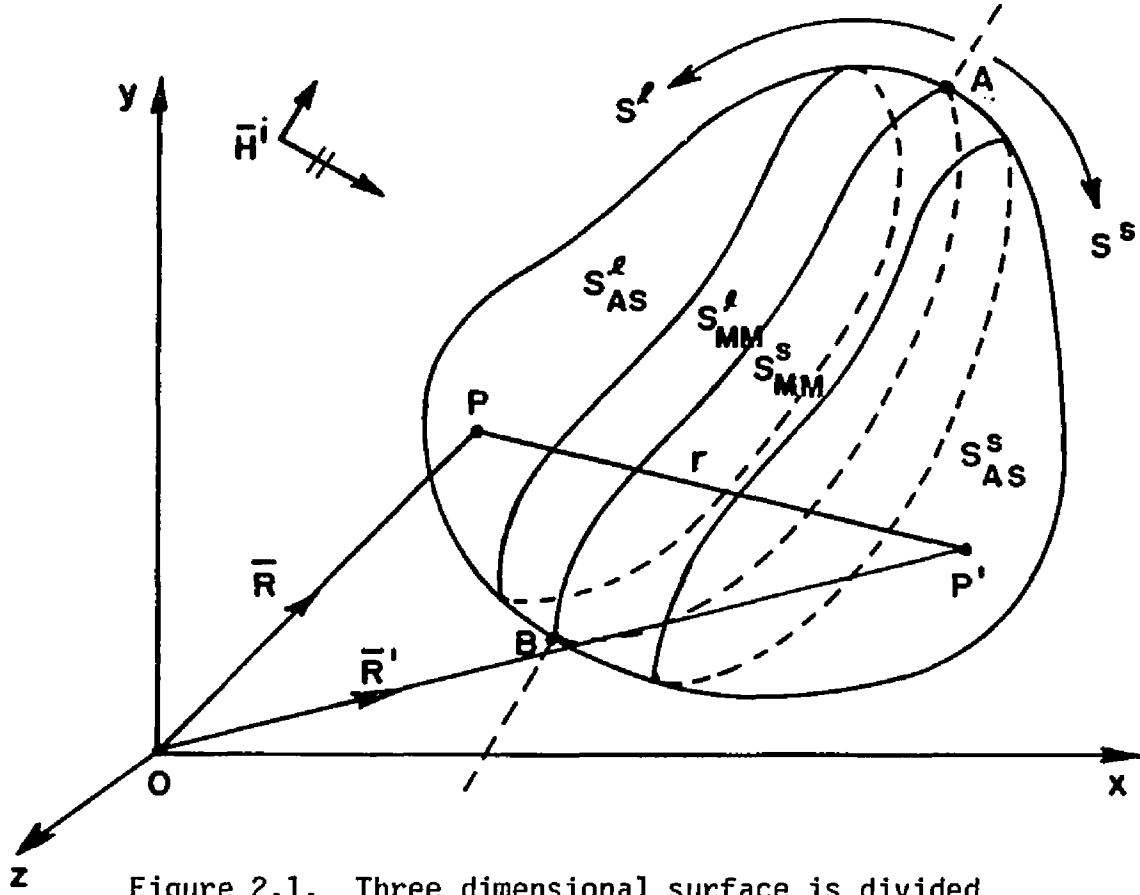
Figure 2.1. Three dimensional surface is divided into four regions.

$$J^{\ell}(\overline{R}) = J_{MM}^{\ell}(\overline{R}) + J_{AS}^{\ell}(\overline{R}) \tag{2.3}$$

$$J^{s}(\overline{R}) = J_{MM}^{s}(\overline{R}) + J_{AS}^{s}(\overline{R}) \tag{2.4}$$

where $J_{MM}^{\ell}(\overline{R})$ and $J_{MM}^{s}(\overline{R})$ are the total currents on S_{MM}^{ℓ} and S_{MM}^{s}, respectively, and $J_{AS}^{\ell}(\overline{R})$ and $J_{AS}^{s}(\overline{R})$ represent the total currents on S_{AS}^{ℓ} and S_{AS}^{s}, respectively.

We will use the usual form of Maue's magnetic field integral equation to derive the general equations for our hybrid method. The

8

current at an observation point P (see Figure 2.1) will satisfy the magnetic field integral equation given by

$$\bar{J}(\bar{R}) = 2\hat{n}\times\bar{H}^i(\bar{R}) + 2\hat{n}\times\int_S \bar{J}(\bar{R}') \times \nabla'G(r)ds' \qquad (2.5)$$

where $\bar{R}$ and $\bar{R}'$ are the position vectors of the observation point P and the source point P', respectively, and $r = |\bar{R}-\bar{R}'|$ is the distance between the points P and P'. The unit vector $\hat{n}$ is outward and normal to the surface at P. $\bar{H}^i(\bar{R})$ is the incident magnetic field at P on the surface. The symbol f represents the principle value of integration.

The free space Green's function G(r) for the two dimensional problem is given by

$$G(r) = \frac{1}{4j} H_0^{(2)}(\beta r) \qquad (2.6)$$

and for the three-demensional problem is given by

$$G(r) = \frac{e^{-j\beta r}}{4\pi r} \qquad (2.7)$$

where $H_0^{(2)}(\beta r)$ is the zero order second kind Hankel function, and β is the free space propagation constant. Now $\nabla'G(r)$, where the prime refers to the coordinate system of the source points, can be obtained as

$$\nabla'G(r) = -\frac{\beta}{4j} H_1^{(2)}(\beta r) r' \qquad (2.8)$$

9

for the two-dimensional problem and

$$\nabla'G(r) = - (j\beta + \frac{1}{r}) \frac{e^{-j\beta r}}{4\pi r} \hat{r}' \qquad (2.9)$$

for the three-dimensional problem, where $\hat{r}'$ is the unit vector in the direction of $\bar{R}'-\bar{R}$, and $H_1^{(2)}(\beta r)$ is the first order second kind Hankel function. The time dependent factor $e^{j\omega t}$ is suppressed throughout.

The integration surface S in Equation (2.5) can be divided into S^ℓ and S^S, and according to those integration regions, the integral can be separated into two parts. For observation points in the lit region, the current $\bar{J}^\ell(\bar{R})$ will satisfy Equation (2.5) or the following equation.

$$\bar{J}^\ell(\bar{R}) = 2\hat{n}x\bar{H}^i(\bar{R}) + 2\hat{n} \times \int_{S^\ell} \bar{J}^\ell(\bar{R}') \times \nabla'G(r)ds'$$

$$+ 2\hat{n} \times \int_{S^S} \bar{J}^S(\bar{R}') \times \nabla'G(r)ds' \qquad (2.10)$$

The second and third terms are the currents induced by the currents at source points in the lit and shadowed regions, respectively.

Since the current $\bar{J}^S(\bar{R}')$ is usually small compared to $\bar{J}^\ell(\bar{R}')$, the third term of Equation (2.10) may be small compared to the second term, and also both of them are small compared to the optics term $2\hat{n}x\bar{H}^i(\bar{R})$, we can ignore the third term in Equation (2.10) and make the approximation of

10

$$\bar{J}^{\ell}(\bar{R}) \simeq \bar{J}^{\ell}_{op}(\bar{R}) \qquad (2.11)$$

where the optics region current $\bar{J}^{\ell}_{op}(\bar{R})$ is given by

$$\bar{J}^{\ell}_{op}(\bar{R}) = 2\hat{n}x\bar{H}^i(\bar{R}) + 2\hat{n}x \int_{S^{\ell}} \bar{J}^{\ell}_{op}(\bar{R}') \times \nabla'G(r)ds' \qquad (2.12)$$

Also we can write the following integral equation for observation points on the shadowed region.

$$\bar{J}^S(\bar{R}) = 2\hat{n}x\bar{H}^i(\bar{R}) + 2\hat{n}x \int_{S^{\ell}} \bar{J}^{\ell}(\bar{R}') \times \nabla'G(r)ds'$$

$$+ 2\hat{n}x \int_{S^S} \bar{J}^S(\bar{R}') \times \nabla'G(r)ds' \quad . \qquad (2.13)$$

If we replace $\bar{J}(\bar{R}')$ in Equation (2.13) by the approximate current $\bar{J}^{\ell}_{op}(\bar{R}')$, which is given in Equation (2.12), then the current $\bar{J}^S(\bar{R})$ is no longer exact, but instead is approximate. If we represent this approximation by $\bar{J}^S_{op}(\bar{R})$, then Equation (2.13) becomes

$$\bar{J}^S_{op}(\bar{R}) \simeq 2\hat{n}x\bar{H}^i(\bar{R}) + 2\hat{n}x \int_{S^{\ell}} \bar{J}^{\ell}_{op}(\bar{R}') \times \nabla'G(r)ds'$$

$$+ 2\hat{n}x \int_{S^S} \bar{J}^S_{op}(\bar{R}') \times \nabla'G(r)ds' \quad . \qquad (2.14)$$

Since $\bar{J}^{\ell}_{op}(\bar{R})$ in Equation (2.12) and $\bar{J}^S_{op}(\bar{R})$ in Equation (2.14) are approximations for $\bar{J}^{\ell}(\bar{R})$ and $\bar{J}^S(\bar{R})$, respectively, additional currents are required to determine the correct currents on both surfaces.

Let these additional currents be $\overline{I}^{\ell}(\overline{R})$ and $\overline{I}^S(\overline{R})$ on the surfaces S^{ℓ} and S^S, respectively. Then the exact currents in both the regions are

$$\overline{J}^{\ell}(\overline{R}) = \overline{J}^{\ell}_{op}(\overline{R}) + \overline{I}^{\ell}(\overline{R}) \tag{2.15}$$

$$\overline{J}^S(\overline{R}) = \overline{J}^S_{op}(\overline{R}) + \overline{I}^S(\overline{R}) \quad . \tag{2.16}$$

According to Equations (2.3) and (2.4), the currents $\overline{I}^{\ell}(\overline{R})$ and $\overline{I}^S(\overline{R})$ can be expressed as

$$\overline{I}^{\ell}(\overline{R}) = \overline{I}^{\ell}_{MM}(\overline{R}) + \overline{I}^{\ell}_{AS}(\overline{R}) \tag{2.17}$$

$$\overline{I}^S(\overline{R}) = \overline{I}^S_{MM}(\overline{R}) + \overline{I}^S_{AS}(\overline{R}) \quad . \tag{2.18}$$

Then from Equations (2.3), (2.4), (2.15), (2.16), (2.17), and (2.18) we can express the total currents on the regions S^{ℓ}_{MM}, S^S_{MM}, S^{ℓ}_{AS}, and S^S_{AS} as

$$\overline{J}^{\ell}_{MM}(\overline{R}) = \overline{J}^{\ell}_{op}(\overline{R}) + \overline{I}^{\ell}_{MM}(\overline{R}) \tag{2.19}$$

$$\overline{J}^S_{MM}(\overline{R}) = \overline{J}^S_{op}(\overline{R}) + \overline{I}^S_{MM}(\overline{R}) \tag{2.20}$$

and

$$\overline{J}^{\ell}_{AS}(\overline{R}) = \overline{J}^{\ell}_{op}(\overline{R}) + \overline{I}^{\ell}_{AS}(\overline{R}) \tag{2.21}$$

$$\overline{J}_{AS}^{S}(\overline{R}) = \overline{J}_{op}^{S}(\overline{R}) + \overline{T}_{AS}^{S}(\overline{R}) \quad .\tag{2.22}$$

The currents at observation points on the moment method region also will satisfy Equation (2.5). Hence,

$$\overline{J}_{MM}^{\ell}(\overline{R}) = 2\hat{n}x\overline{H}^{i}(\overline{R}) + 2\hat{n}x \int_{S^{\ell}} \overline{J}^{\ell}(\overline{R}') \times \nabla'G(r)ds'$$

$$+ 2\hat{n}x \int_{S^{S}} \overline{J}^{S}(\overline{R}') \times \nabla'G(r)ds' \tag{2.23}$$

and

$$\overline{J}_{MM}^{S}(\overline{R}) = 2\hat{n}x\overline{H}^{i}(\overline{R}) + 2\hat{n}x \int_{S^{\ell}} \overline{J}^{\ell}(\overline{R}') \times \nabla'G(r)ds'$$

$$+ 2\hat{n}x \int_{S^{S}} \overline{J}^{S}(\overline{R}') \times \nabla'G(r)ds' \quad .\tag{2.24}$$

Substituting Equations (2.15), (2.16), (2.19), and (2.20) into Equations (2.23) and (2.24), and then using Equations (2.17) and (2.18), we obtain the following two equations.

$$\overline{J}_{op}^{\ell}(\overline{R}) + \overline{T}_{MM}^{\ell}(\overline{R}) = 2\hat{n}x\overline{H}^{i}(\overline{R}) + 2\hat{n}x \int_{S^{\ell}} \overline{J}_{op}^{\ell}(\overline{R}') \times \nabla'G(r)ds'$$

$$+ 2\hat{n}x \int_{S_{MM}^{\ell}} \overline{T}_{MM}^{\ell}(\overline{R}') \times \nabla'G(r)ds' + 2\hat{n}x \int_{S_{AS}^{\ell}} \overline{T}_{AS}^{\ell}(\overline{R}') \times \nabla'G(r)ds'$$

$$+ 2\hat{n}x \oint_{S^S} \overline{J}^S_{op}(\overline{R}') \times \nabla'G(r)ds' + 2\hat{n}x \oint_{S^S_{MM}} \overline{I}^S_{MM}(\overline{R}') \times \nabla'G(r)ds'$$

$$+ 2\hat{n}x \oint_{S^S} \overline{J}^S_{op}(\overline{R}') \times \nabla'G(r)ds' + 2\hat{n}x \oint_{S^S_{MM}} \overline{I}^S_{MM}(\overline{R}') \times \nabla'G(r)ds'$$

$$+ 2\hat{n}x \oint_{S^S_{AS}} \overline{I}^S_{AS}(\overline{R}') \times \nabla'G(r)ds' \qquad\qquad (2.25)$$

and

$$\overline{J}^S_{op}(\overline{R}) + \overline{I}^S_{MM}(\overline{R}) = 2\hat{n}x\overline{H}^i(\overline{R}) + 2\hat{n}x \oint_{S^\ell} \overline{J}^\ell_{op}(\overline{R}') \times \nabla'G(r)ds'$$

$$+ 2\hat{n}x \oint_{S^\ell_{MM}} \overline{I}_{MM}(\overline{R}') \times \nabla'G(r)ds' + 2\hat{n}x \oint_{S^\ell_{AS}} \overline{I}^\ell_{AS}(\overline{R}') \times \nabla'G(r)ds'$$

$$+ 2\hat{n}x \oint_{S^S} \overline{J}^S_{op}(\overline{R}') \times \nabla'G(r)ds' + 2\hat{n}x \oint_{S^S_{MM}} \overline{I}^S_{MM}(\overline{R}') \times \nabla'G(r)ds'$$

$$+ 2\hat{n}x \oint_{S^S_{AS}} \overline{I}^S_{AS}(\overline{R}') \times \nabla'G(r)ds' \quad . \qquad\qquad (2.26)$$

Subtracting Equation (2.12) from Equation (2.25) and Equation (2.14) from Equation (2.26), we obtain the currents in the lit and shadowed moment method regions which are given by

14

$$\bar{I}_{MM}^{\ell}(\bar{R}) = 2\hat{n}x \int_{S_{MM}^{\ell}} \bar{I}_{MM}^{\ell}(\bar{R}')x\nabla'G(r)ds' + 2\hat{n}x \int_{S_{MM}^{s}} \bar{I}_{MM}^{s}(\bar{R}')x\nabla'G(r)ds'$$

$$+ 2\hat{n}x \int_{S^{s}} \bar{J}_{op}^{s}(\bar{R}')x\nabla'G(r)ds' + 2\hat{n}x \int_{S_{AS}^{\ell}} \bar{I}_{AS}^{\ell}(\bar{R}')x\nabla'G(r)ds'$$

$$+ 2\hat{n}x \int_{S_{AS}^{s}} \bar{I}_{AS}^{s}(\bar{R}')x\nabla'G(r)ds' \qquad (2.27)$$

and

$$\bar{I}_{MM}^{s}(\bar{R}) = 2\hat{n}x \int_{S_{MM}^{\ell}} \bar{I}_{MM}^{\ell}(\bar{R}')x\nabla'G(r)ds' + 2\hat{n}x \int_{S_{MM}^{s}} \bar{I}_{MM}^{s}(\bar{R}')x\nabla'G(r)ds'$$

$$+ 2\hat{n}x \int_{S_{AS}^{\ell}} \bar{I}_{AS}^{\ell}(\bar{R}')x\nabla'G(r)ds' + 2\hat{n}x \int_{S_{AS}^{s}} \bar{I}_{AS}^{s}(\bar{R}')x\nabla'G(r)ds'$$

$$(2.28)$$

Since there are four unknown currents $\bar{I}_{MM}^{\ell}(\bar{R})$, $\bar{I}_{MM}^{s}(\bar{R})$, $\bar{I}_{AS}^{\ell}(\bar{R})$, and $\bar{I}_{AS}^{s}(\bar{R})$ in two equations, we cannot solve for them without making proper approximations. In Equation (2.27) it is clearly seen that the current term containing $\bar{J}_{op}^{s}(\bar{R}')$ is dominant. However, it is hard to compare the other current terms with each other analytically. As we know, the currents on the right side of Equation (2.27) represent the currents induced by $\bar{J}_{op}^{s}(\bar{R})$ and the currents in the moment and asymptotic method regions.

Now considering that observation points are limited to the moment method region and that the current in the nearest region to the observation points will most contribute to the current at the observation points, we can ignore those current terms containing $\bar{T}_{AS}^{\ell}(\bar{R}')$ or $\bar{T}_{AS}^{S}(\bar{R}')$ in both Equations (2.27) and (2.28) to derive the first order approximations for $\bar{T}_{MM}^{\ell}(\bar{R})$ and $\bar{T}_{MM}^{S}(\bar{R})$. Therefore, the first order approximations for $\bar{T}_{MM}^{\ell}(\bar{R})$ and $\bar{T}_{MM}^{S}(\bar{R})$ can be written as

$$\bar{T}_{MM}^{\ell}(\bar{R}) \simeq 2\hat{n}x \int_{S_{MM}^{\ell}} \bar{T}_{MM}^{\ell}(\bar{R}')x\nabla'G(r)ds' + 2\hat{n}x \int_{S_{MM}^{S}} \bar{T}_{MM}^{S}(\bar{R}')x\nabla'G(r)ds'$$

$$+ 2\hat{n}x \int_{S^{S}} \bar{J}_{op}^{S}(\bar{R}')x\nabla'G(r)ds' \qquad (2.29)$$

and

$$\bar{T}_{MM}^{S}(\bar{R}) \simeq 2\hat{n}x \int_{S_{MM}^{\ell}} \bar{T}_{MM}^{\ell}(\bar{R}')x\nabla'G(r)ds' + 2\hat{n}x \int_{S_{MM}^{S}} \bar{T}_{MM}^{S}(\bar{R}')x\nabla'G(r)ds'$$

$$(2.30)$$

We should realize that without ignoring those current terms containing $\bar{T}_{AS}^{\ell}(\bar{R}')$ or $\bar{T}_{AS}^{S}(\bar{R}')$ in Equations (2.27) and (2.28), we cannot derive equation sets which can be solved by the moment method. On the other hand, since the current $\bar{J}_{op}^{S}(\bar{R}')$ is known, we can solve Equations (2.29) and (2.30) simultaneously using the moment method. By the same procedure, we can derive integral equations for $\bar{T}_{AS}^{\ell}(\bar{R})$ and $\bar{T}_{AS}^{S}(\bar{R})$.

16

However, we can write down directly those equations by noting that the currents on the asymptotic regions also satisfy Equations (2.29) and (2.30) for their first order approximations. Thus, we can write the following equations for $\overline{T}_{AS}^{\ell}(\overline{R})$ and $I_{AS}^{S}(\overline{R})$.

$$\overline{T}_{AS}^{\ell}(\overline{R}) \simeq 2\hat{n}x \int_{S_{MM}^{\ell}} \overline{T}_{MM}^{\ell}(\overline{R}')x\nabla'G(r)ds' + 2\hat{n}x \int_{S_{MM}^{S}} \overline{T}_{MM}^{S}(\overline{R}')x\nabla'G(r)ds'$$

$$+ 2\hat{n}x \int_{S^{S}} \overline{J}_{op}^{S}(\overline{R}')x\nabla'G(r)ds' \qquad (2.31)$$

and

$$\overline{T}_{AS}^{S}(\overline{R}) \simeq 2\hat{n}x \int_{S_{MM}^{\ell}} \overline{T}_{MM}^{\ell}(\overline{R}')x\nabla'G(r)ds' + 2\hat{n}x \int_{S_{MM}^{S}} \overline{T}_{MM}^{S}(\overline{R}')x\nabla'G(r)ds'$$

$$(2.32)$$

$\overline{T}_{AS}^{\ell}(\overline{R})$ and $\overline{T}_{AS}^{S}(\overline{R})$ can be obtained simply by substituting the pre-determined currents $\overline{T}_{MM}^{\ell}(\overline{R})$ and $\overline{T}_{MM}^{S}(\overline{R})$ into Equations (2.31) and (2.32).

The above first order approximations may not be enough to give the correct surface currents on some complex bodies. Therefore, we will derive equations for the second order approximations for $\overline{T}_{MM}^{\ell}(\overline{R})$ and $\overline{T}_{MM}^{S}(\overline{R})$ in the next section.

17

$$\overline{I}_{MM}^{S}(\overline{R}) \simeq \overline{I}_{1}^{S}(\overline{R}) + 2\hat{n}_{s}\times \oint_{S_{AS}^{\ell}} \; [2\hat{n}_{\ell}\times \oint_{S_{MM}^{\ell}} \; \overline{I}_{MM}^{\ell}(\overline{R}'')\times\nabla''G(r_1)ds'']\times\nabla'G(r_2)ds'$$

$$+ \; 2\hat{n}_{s}\times \oint_{S_{AS}^{\ell}} \; [2\hat{n}_{\ell}\times \oint_{S_{MM}^{S}} \; \overline{I}_{MM}^{S}(\overline{R}'')\times\nabla''G(r_1)ds'']\times\nabla'G(r_2)ds'$$

$$+ \; 2\hat{n}_{s}\times \oint_{S_{AS}^{S}} \; [2\hat{n}_{s}\times \oint_{S_{MM}^{\ell}} \; \overline{I}_{MM}^{\ell}(\overline{R}'')\times\nabla''G(r_1)ds'']\times\nabla'G(r_2)ds'$$

$$+ \; 2\hat{n}_{s}\times \oint_{S_{AS}^{S}} \; [2\hat{n}_{s}\times \oint_{S_{MM}^{S}} \; \overline{I}_{MM}^{S}(\overline{R}'')\times\nabla''G(r_1)ds'']\times\nabla'G(r_2)ds'$$

$$+ \; 2\hat{n}_{s}\times \oint_{S_{AS}^{\ell}} \; [2\hat{n}_{\ell}\times \oint_{S^{S}} \; \overline{J}_{op}^{S}(\overline{R}'')\times\nabla'G(r_1)ds'']\times\nabla'G(r_2)ds' \qquad (2.34)$$

where $\overline{I}_{1}^{\ell}(\overline{R})$ and $\overline{I}_{1}^{S}(\overline{R})$ are the first order approximations for $\overline{I}_{MM}^{\ell}(\overline{R})$ and $\overline{I}_{MM}^{S}(\overline{R})$, respectively, and $\hat{n}_{\ell}$ and $\hat{n}_{s}$ are the unit normal vectors in the lit and shadowed surfaces, respectively. Also r_1 and r_2 are given by

$$r_1 = |\overline{R}'-\overline{R}''| \qquad (2.35)$$

$$r_2 = |\overline{R}-\overline{R}'| \qquad (2.36)$$

The second order approximations for $T_{AS}^{\ell}(\bar{R})$ and $T_{AS}^{S}(\bar{R})$ have the same expressions as those for $T_{MM}^{\ell}(\bar{R})$ and $T_{MM}^{S}(\bar{R})$, respectively, except that observation points are moved from the moment method regions to the asymptotic regions.

If we repeat the same procedure, we can obtain equations which will give us higher order approximations for $T_{MM}^{\ell}(\bar{R})$ and $T_{MM}^{S}(\bar{R})$. Numerically this procedure can be achieved easily by iterative methods.

2.3 Summary and Discussion

We have derived all equations for the first and second order approximations that are necessary for the method. For summary and later convenience, we will write those equations for the first order approximations here again

$$\bar{J}_{op}^{\ell}(\bar{R}) = 2\hat{n}x\bar{H}^{i}(\bar{R}) + 2\hat{n}x \int_{S^{\ell}} \bar{J}_{op}^{\ell}(\bar{R}')x\nabla'G(r)ds' \qquad (2.37)$$

$$\bar{J}_{op}^{S}(\bar{R}) = 2\hat{n}x\bar{H}^{i}(\bar{R}) + 2\hat{n}x \int_{S^{\ell}} \bar{J}_{op}^{\ell}(\bar{R}')x\nabla'G(r)ds'$$

$$+ 2\hat{n}x \int_{S^{S}} \bar{J}_{op}^{S}(\bar{R}')x\nabla'G(r)ds' \qquad (2.38)$$

20

$$\bar{I}_{MM}^{\ell}(\bar{R}) = 2\hat{n}x \int_{S_{MM}^{\ell}} \bar{I}_{MM}^{\ell}(\bar{R}')x\nabla'G(r)ds' + 2\hat{n}x \int_{S_{MM}^{S}} \bar{I}_{MM}^{S}(\bar{R}')x\nabla'G(r)ds'$$

$$+ 2\hat{n}x \int_{S^S} \bar{J}_{op}^{S}(\bar{R}')x\nabla'G(r)ds' \qquad (2.39)$$

$$\bar{I}_{MM}^{S}(\bar{R}) = 2\hat{n}x \int_{S_{MM}^{\ell}} \bar{I}_{MM}^{\ell}(\bar{R}')x\nabla'G(r)ds' + 2\hat{n}x \int_{S_{MM}^{S}} \bar{I}_{MM}^{S}(\bar{R}')x\nabla'G(r)ds'$$

$$(2.40)$$

The Green's function has an r^{-1} singularity as the observation point P approaches the source point P' on the surface of the body. Since the second term of Equation (2.37) and the third term of Equation (2.38) become zero if P and P' are on the same straight surface, the singularity problem is not involved in the planar surface. However, there will be as many singular points as observation points for a curved surface such as in a circular cylinder or a sphere.

Theoretically the principle value of integration is evaluated by excluding the singular point, but practically it is done by excluding the finite patch area containing the singular point. Therefore, this exclusion of the patch may cause some errors in the surface current calculations. This problem will be considered in more detail in Chapters V and VI.

21

When we use the iterative method to solve for $J_{op}^{\ell}(\bar{R})$ and $J_{op}^{S}(\bar{R})$ in Equations (2.37) and (2.38), we have to consider convergence of the result. We cannot prove mathematically that the iterative method produces a convergent result, but instead we must insure it by numerical calculation.

Also it appears that there are no distinct ways to determine the extent of the moment method region in practical numerical calculations. However, by numerical results it will be seen that the extent of the moment method region does not affect the surface current significantly. Therefore we can use an arbitrary size for the MM-region according to the size of the body. This is very desirable for practical applications of this method, because if the currents are much dependent on the extent of the MM-region, the method will not be reliable. Usually for a finite dimensioned body, from one third to half of the size of the body will be reasonable for the moment method region. If we increase the MM-region, we may get better results, but we have to sacrifice the computer running time. Also there will be a limit to increasing the MM-region by the limit of computer memory storages.

CHAPTER III

PERFECTLY CONDUCTING WEDGE

3.1 Integral Equations

Consider the wedge geometry in Figure 3.1, where the one side of the wedge is illuminated by a TE plane wave and the other side is shadowed. We set up the moment method regions around the edge, which are represented by C^ℓ_{MM} and C^S_{MM} in the lit and shadowed regions, respectively. For the wedge problem, the currents $\bar{J}^\ell_{op}(\bar{R})$ and $\bar{J}^S_{op}(\bar{R})$ in Equations (2.12) and (2.14) can be reduced to

$$\bar{J}^\ell_{op}(\bar{R}) = 2\hat{n}x\bar{H}^i(\bar{R}) \tag{3.1}$$

and

$$\bar{J}^S_{op}(\bar{R}) = 2\hat{n}x\bar{H}^i(\bar{R}) + 2nx \int_{C^\ell} \bar{J}^\ell_{op}(\bar{R}')x\nabla'G(r)d\ell' \quad . \tag{3.2}$$

Also the first order approximate currents in the MM-region can be simplified as

$$\bar{I}^\ell_{MM}(\bar{R}) = 2\hat{n}x \int_{C^S_{MM}} \bar{I}^S_{MM}(\bar{R}')x\nabla'G(r)d\ell' + 2\hat{n}x \int_{C^S} \bar{J}^S_{op}(\bar{R}')x\nabla'G(r)d\ell'$$

$$\tag{3.3}$$

and

$$\overline{T}_{MM}^{S}(\overline{R}) = 2\hat{n}x \oint_{C_{MM}^{\ell}} \overline{T}_{MM}^{\ell}(\overline{R}')x\nabla'G(r)d\ell' \quad . \tag{3.4}$$

The expressions for $\overline{T}_{AS}^{\ell}(\overline{R})$ and $\overline{T}_{AS}^{S}(\overline{R})$ are exactly same as Equations (3.3) and (3.4), respectively, except that the observation points are moved to the asymptotic region. Therefore, it is not necessary to write those equations here.

Now let us consider the case where both sides of the wedge are illuminated by a plane wave as in Figure 3.2. For this geometry, the currents $\overline{J}_{op}^{A}(\overline{R})$ and $\overline{J}_{op}^{B}(\overline{R})$, where A and B stand for the two surfaces of the wedge, can be expressed as

$$\overline{J}_{op}^{A}(\overline{R}) = 2\hat{n}x\overline{H}^{i}(\overline{R}) + 2\hat{n}x \oint_{C^{B}} \overline{J}_{op}^{B}(\overline{R}')x\nabla'G(r)d\ell' \tag{3.5}$$

$$\overline{J}_{op}^{B}(\overline{R}) = 2\hat{n}x\overline{H}^{i}(\overline{R}) + 2\hat{n}x \oint_{C^{A}} \overline{J}_{op}^{A}(\overline{R}')x\nabla'G(r)d\ell' \quad . \tag{3.6}$$

The exact current on the surface A, $\overline{J}_{EX}^{A}(\overline{R})$, can be obtained from

$$\overline{J}_{EX}^{A}(\overline{R}) = 2\hat{n}x\overline{H}^{i} + 2\hat{n}x \oint_{C^{B}} \overline{J}_{EX}^{B}(\overline{R}')x\nabla'G(r)d\ell'$$

$$+ 2\hat{n}x \oint_{C^{A}} \overline{J}_{EX}^{A}(\overline{R}')x\nabla'G(r)d\ell' \quad . \tag{3.7}$$

24
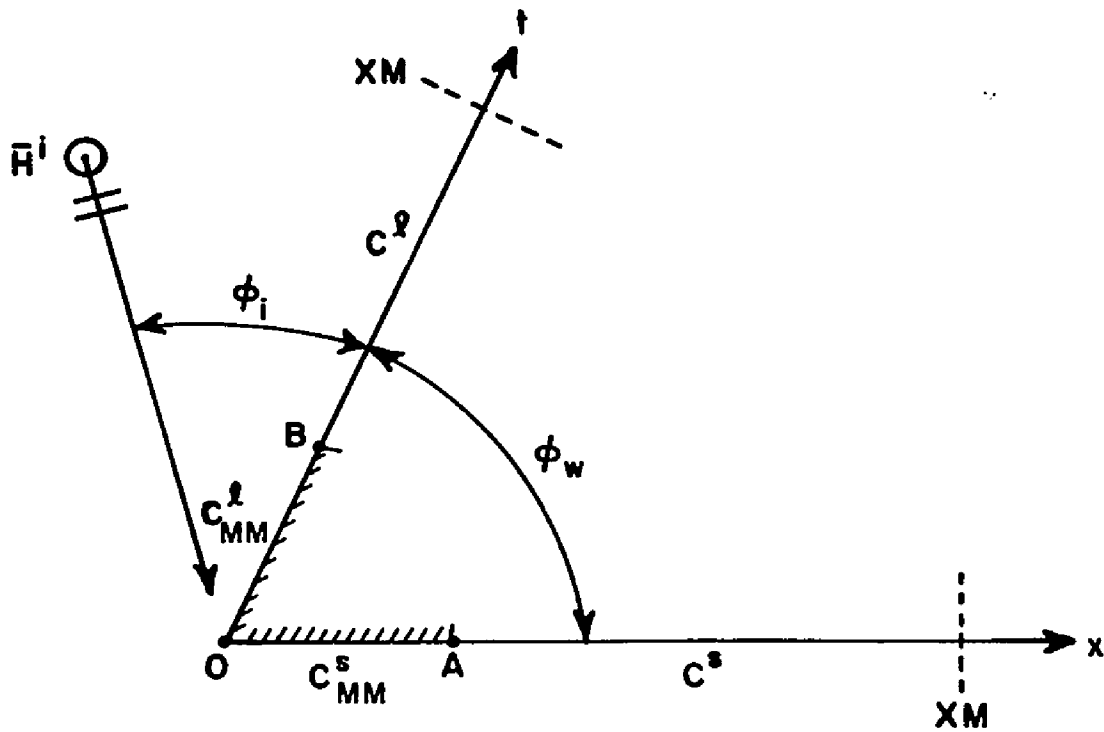
Figure 3.1.   Wedge illuminated by a TE plane wave, where one side
is lit and the other is shadowed.
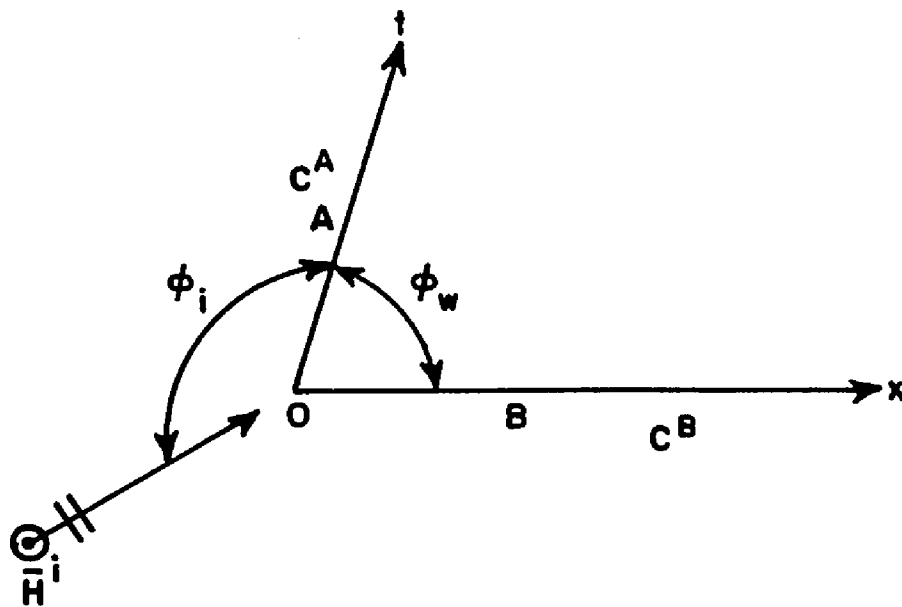
Figure 3.2.   Wedge illuminated by a TE plane wave, where
both sides are lit.

25

and

$$r = \sqrt{\ell^2 + \ell'^2 - 2\ell\ell'\cos\phi_w} \qquad (3.11)$$

The above result can be readily obtained from the geometry in Figure 3.3. Substitution of Equation (3.9) in Equation (3.8) leads to

$$I_{MM}^{\ell}(\ell) = 4 \int_{C_{MM}^{S}} \int_{C_{MM}^{\ell}} I_{MM}^{\ell}(\ell')G_w(\ell'',\ell')G_w(\ell,\ell'')d\ell'd\ell''$$

$$+ 2 \int_{C^S} J_{op}^S(\ell')G_w(\ell,\ell')d\ell' \qquad . \qquad (3.12)$$
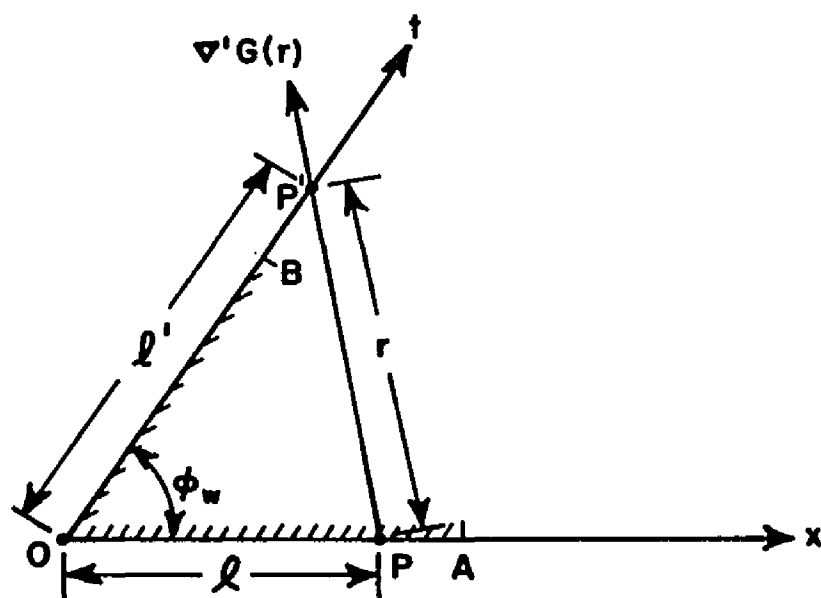
Figure 3.3. Geometry showing relationship between ℓ, ℓ', and ϕ_w in a wedge.

27

Now we will use the pulse basis functions and the point matching technique to solve for I_{MM} in Equation (3.12). Let $I_{MM}^{\ell}(\ell)$ be expressed by the series

$$I_{MM}^{\ell}(\ell) = \sum_{n=1}^{N} I_{n}^{\ell} P(\ell - \ell_{n}) \qquad (3.13)$$

where

$$P(\ell) = \begin{cases} 1 & \text{for} \quad |\ell - \ell_{n}| < \frac{\Delta \ell}{2} \\ \\ 0 & \text{elsewhere.} \end{cases} \qquad (3.14)$$

and $\Delta \ell = \frac{XM}{N}$ where XM represents the integration limit for numerical integration, and N is a number of subintervals.

Substituting Equation (3.13) into Equation (3.12) and rearranging terms, we have

$$\sum_{n=1}^{N} I_{n}^{\ell} [P(\ell - \ell_{n}) - 4 \int_{C_{MM}^{S}} G_{w}(\ell', \ell_{n}) G_{w}(\ell, \ell') \Delta \ell \, d\ell']$$

$$= 2 \int_{C^{S}} J_{op}^{S}(\ell') G_{w}(\ell, \ell') d\ell' \qquad . \qquad (3.15)$$

Multiplying both sides of Equation (3.15) by $\delta(\ell - \ell_{m})$, integrating over C_{MM}^{ℓ}, and dividing them by $\Delta \ell$, we have

$$\sum_{n=1}^{N} I_n^{\ell} [P(\ell_m - \ell_n) - 4 \int_{C_{MM}^S} G_w(\ell', \ell_n) G_w(\ell_m, \ell') \Delta\ell \, d\ell']$$

$$= 2 \int_{C^S} J_{op}^S(\ell') G_w(\ell_m, \ell') d\ell' \quad . \tag{3.16}$$

Expressing Equation (3.16) in matrix form

$$[Z_{mn}^{\ell}] [I_n^{\ell}] = [V_m^{\ell}], \quad m, n = 1, 2, \ldots, N. \tag{3.17}$$

allow us to identify the elements of the impedance matrix $[Z_{mn}^{\ell}]$ as

$$Z_{mn}^{\ell} = P(\ell_m - \ell_n) - 4 \int_{C_{MM}^S} G_w(\ell', \ell_n) G_w(\ell_m, \ell') \Delta\ell \, d\ell' \tag{3.18}$$

where $\quad m, n = 1, 2, 3, \ldots, N$

Usually the second term of Equation (3.18) will be small compared to the first term. The elements of the voltage matrix $[V_m^{\ell}]$ are determined by

$$V_m^{\ell} = 2 \int_{C^S} J_{op}^S(\ell') G_w(\ell_m, \ell') d\ell' \quad , \quad m = 1, 2, \ldots, N. \tag{3.19}$$

29

3.3 Numerical Results

We found some limitations in application of this method to a wedge after having tried several wedges with the various wedge angles and wave incident directions. It will be seen in the examples which follow that if the wedge angle (ϕ_w) or the wave incident angle (ϕ_i) is small, a large integration limit (XM) is required to obtain acceptable results. For example, if ϕ_w is 90° and ϕ_i is 30°, then XM $\simeq 60\lambda$ is needed for a desirable result. However, if we decrease ϕ_i to 10°, we cannot expect a desirable result even with a value of XM larger than 100λ. This means that for the grazing incident wave, it is not possible to obtain an acceptable result. Also we see that the wedge with very small wedge angle meets the same difficulty.

These limitations do not limit the method theoretically, but do impose a practical limitation for the wedge geometry. Since we deal with finite structures in actual problems, these limitations may not appear in other practical problems.

We obtained the surface currents on the lit and shadowed regions up to 5.0λ from the edge. The 5.0λ distance was divided into 100 sub-intervals for numerical integration, and 10 pulse basis functions were used in the 0.5λ wide moment method region. All the results were compared with independent GTD solutions. Figure 3.4 shows the results for $\phi_w=\phi_i=90^o$. It is seen that the magnitude and phase of the surface currents on both regions are in very good agreement with the GTD solutions. In Figure 3.5, which is for $\phi_w=90^o$ and $\phi_i=30^o$, we can recognize a little difference in the magnitude of the shadow region current

in the region from 4.0λ to 5.0λ. Note that this result was obtained with XM=60λ and about thirty minutes of computing time. The results for the surface currents for the geometry in which both surfaces are illuminated by the incident wave are shown in Figure 3.6. In this case, as we mentioned before, the moment method region current was not used to obtain the total surface current. The agreement with the GTD solutions are shown to be very good except in the region less than 0.2λ. We show the results for $\phi_w=120^O$ and $\phi_i=30^O$ in Figure 3.7 and quite good agreements with the GTD results are indicated except near 5.0λ. However, for the reverse geometry (i.e., for $\phi_w=30^O$ and $\phi_i=120^O$) the results become worse as shown in Figures 3.8 and 3.9. The results in Figures 3.8 and 3.9 were obtained with the extent of the moment method region (C_{MM}) of 0.5λ and 1.0λ, respectively. As was expected, better results were obtained with the larger C_{MM}. Even though many discrepancy points are observed on the magnitude curve for C_{MM}=0.5λ the results are still acceptable except in the region very near the edge. Of course, better results can be obtained with increased XM in both the geometries considered above.

By observing Figures 3.10 and 3.11 which are for C_{MM}=0.25λ and 1.0λ, respectively, we can realize the effect of the size of C_{MM}. Those results show that the extent of the moment method does not affect the surface currents significantly. As we increased or decreased the size of C_{MM} for these curves, the width of the pulse used in the moment method region was kept constant as 0.05λ.

31

It is seen from the results in Figures 3.8 to 3.10 that as the wedge angle or the wave incident angle is decreased, the dependencey of the surface current on the extent of the moment method is increased.

Usually the GTD solutions for the surface currents on the wedge are in very good agreement with exact solutions except for the region very near to the edge. In Figure 3.12, the GTD and our hybrid method solutions for the currents in that region (i.e., up to 0.05λ from the edge) are compared with exact solution for the 90° wedge and incident angles. It is seen that the error of the GTD currents becomes large as the observation point approaches the edge and also that overall agreement of our hybrid method solution with exact solution is a little better than that of the GTD.

All the results in this chapter were obtained with the second order approximation. Also, by experience, the second order approximations were seen to be enough for acceptable results. We see that fast convergence of the iterative method is possible with the application of this method to a planar surface. This will be reinforced later by considering a square cylinder in Chapter IV.
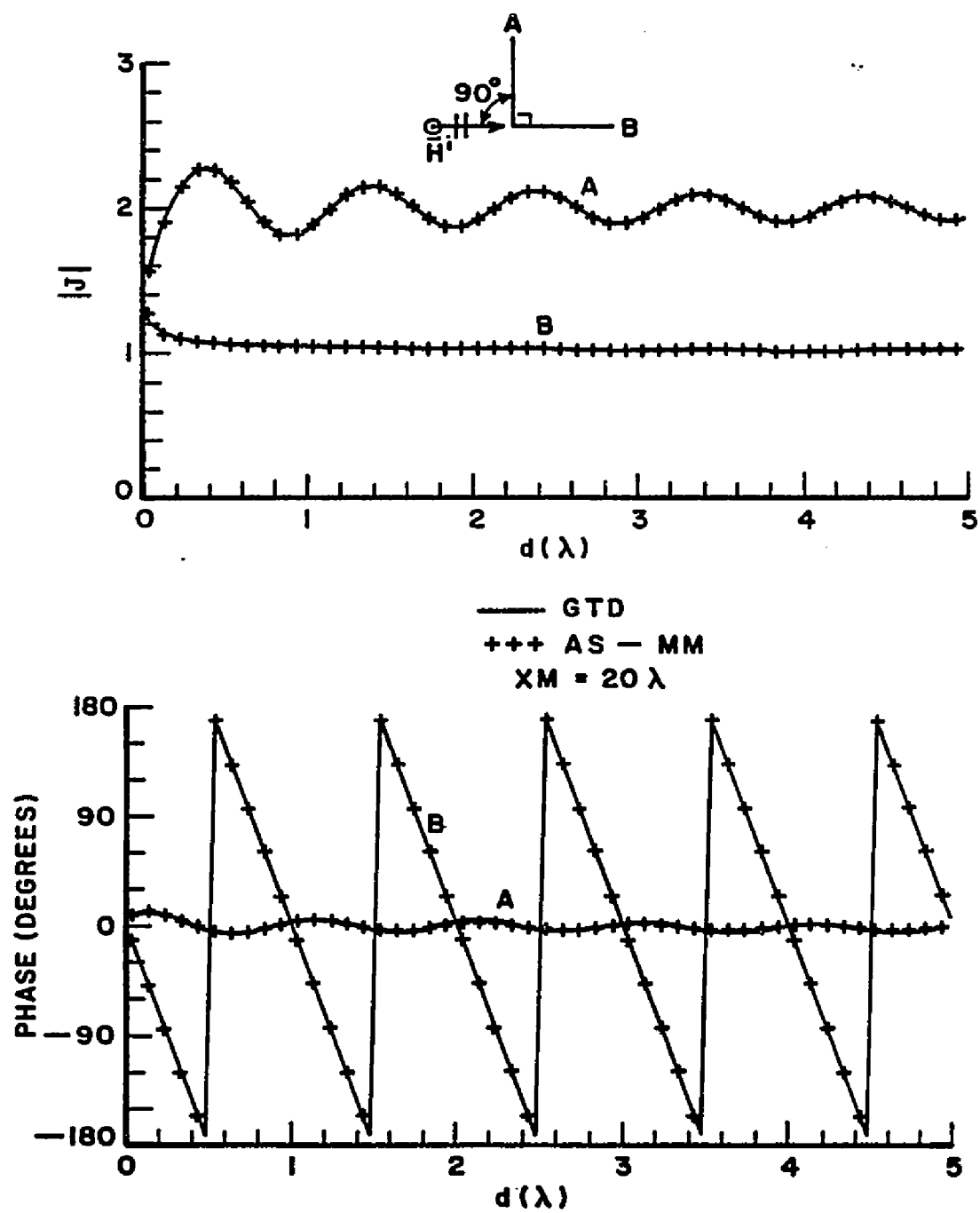
Figure 3.4.   Currents on a wedge for $\phi_w = 90^o$, $\phi_i = 90^o$, $C_{MM} = 0.5\lambda$, and $XM = 20\lambda$.
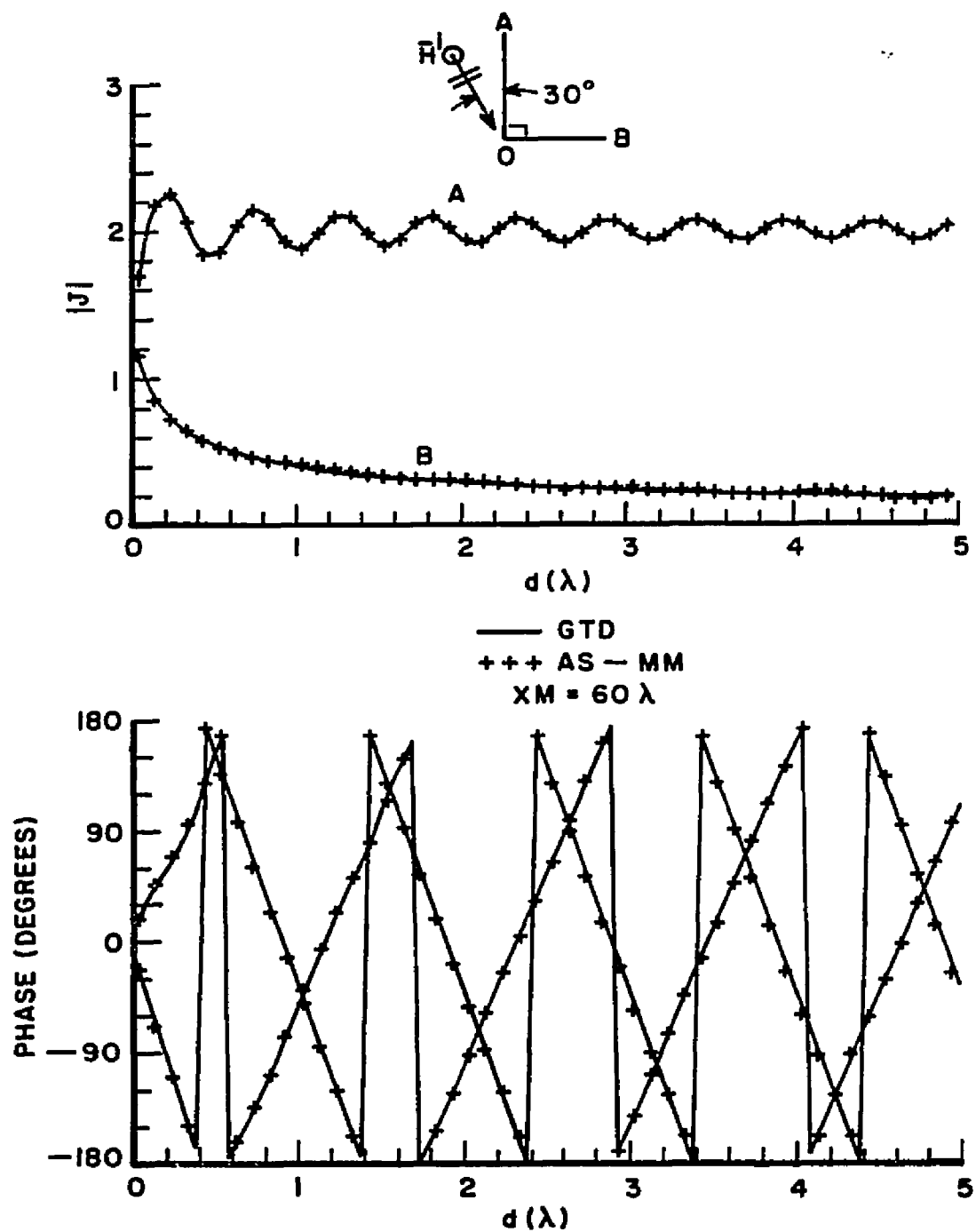
Figure 3.5. Currents on a wedge for $\phi_w=90^\circ$, $\phi_i=30^\circ$, $C_{MM}=0.5\lambda$, and $XM=60\lambda$.
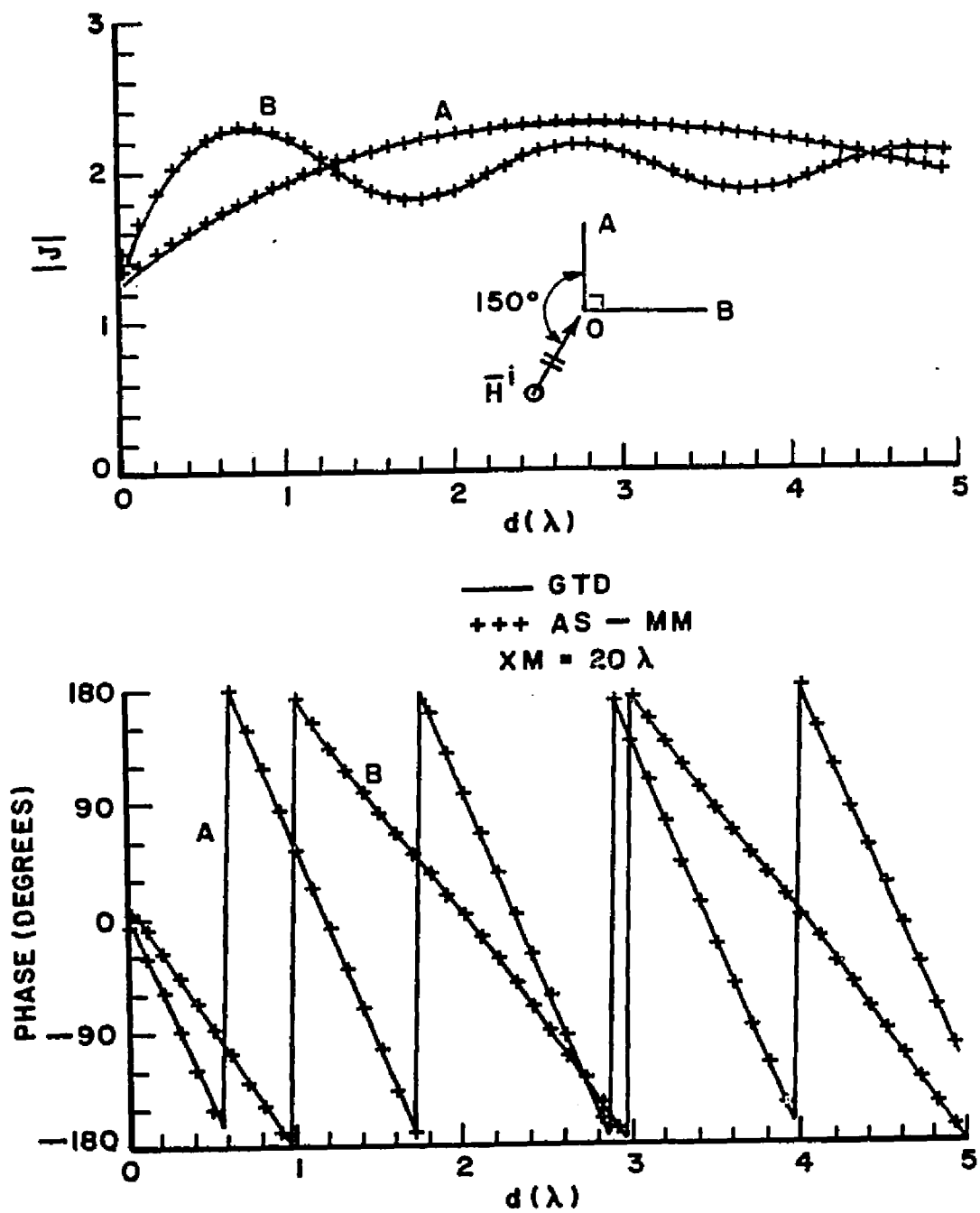
Figure 3.6. Currents on a wedge for $\phi_w=90^o$, $\phi_i=150^o$, and XM=20λ.
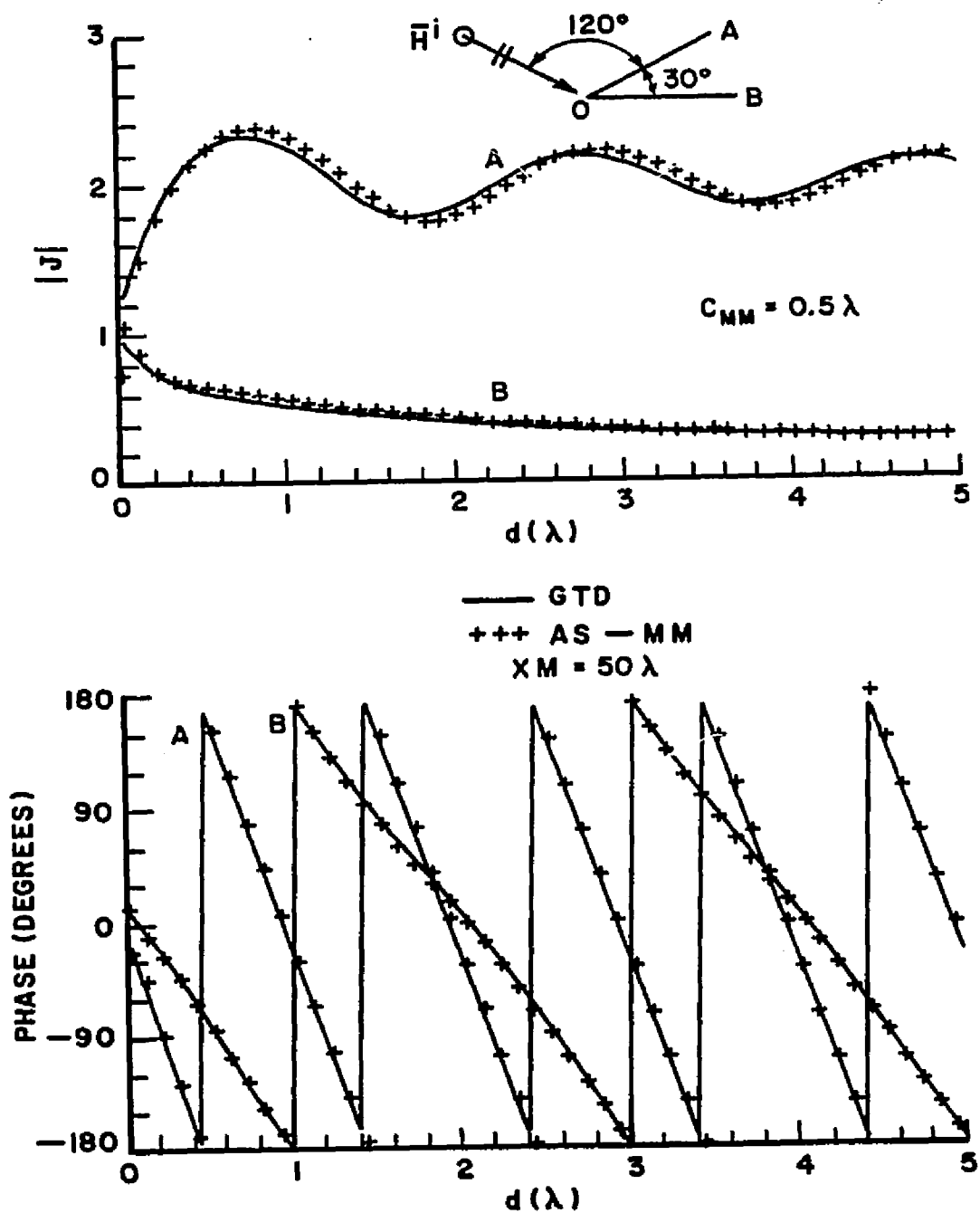
Figure 3.8.   Currents on a wedge for $\phi_w = 30°$, $\phi_i = 120°$, $C_{MM} = 0.5\lambda$, and $XM = 50\lambda$.
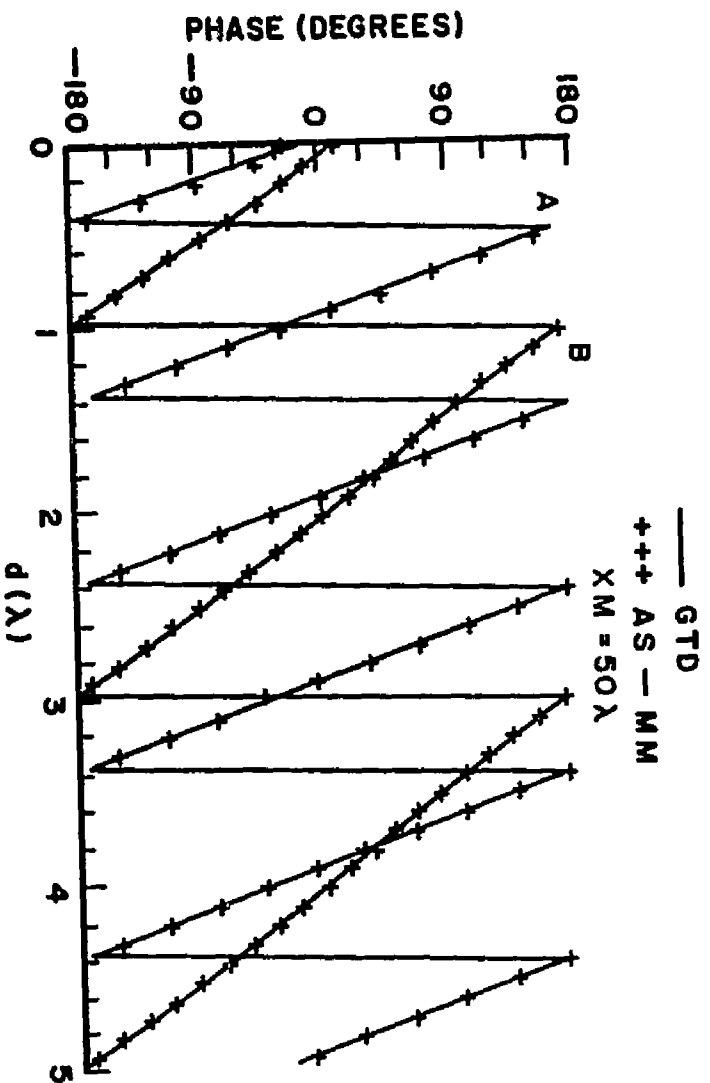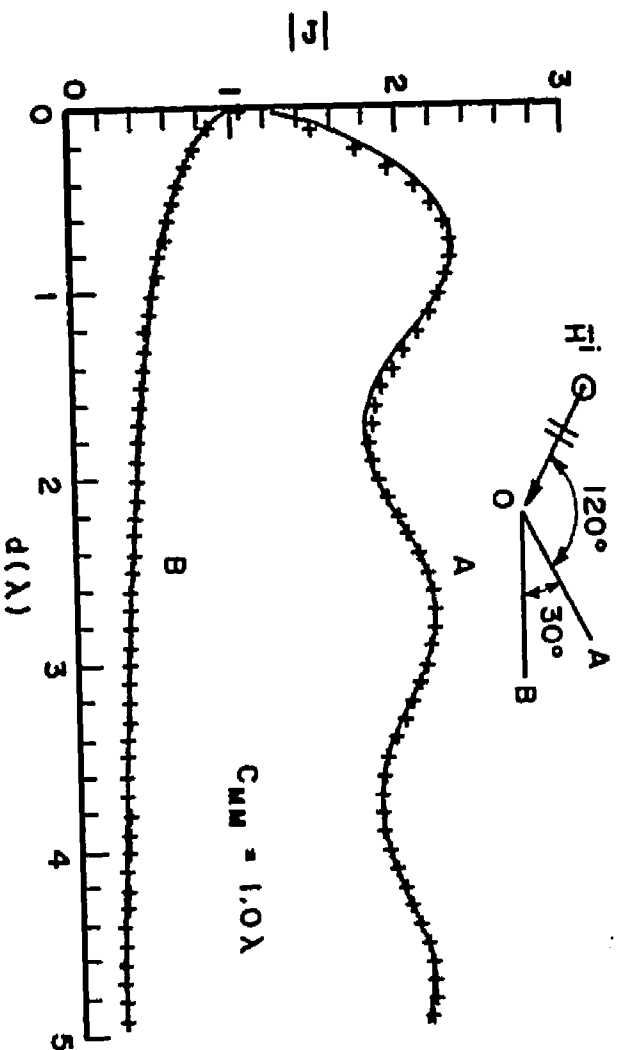
Figure 3.9. Currents on a wedge for $\phi_w = 30°$, $\phi_i = 120°$, $C_{MM} = 1.0\lambda$, and $XM = 50\lambda$.

38
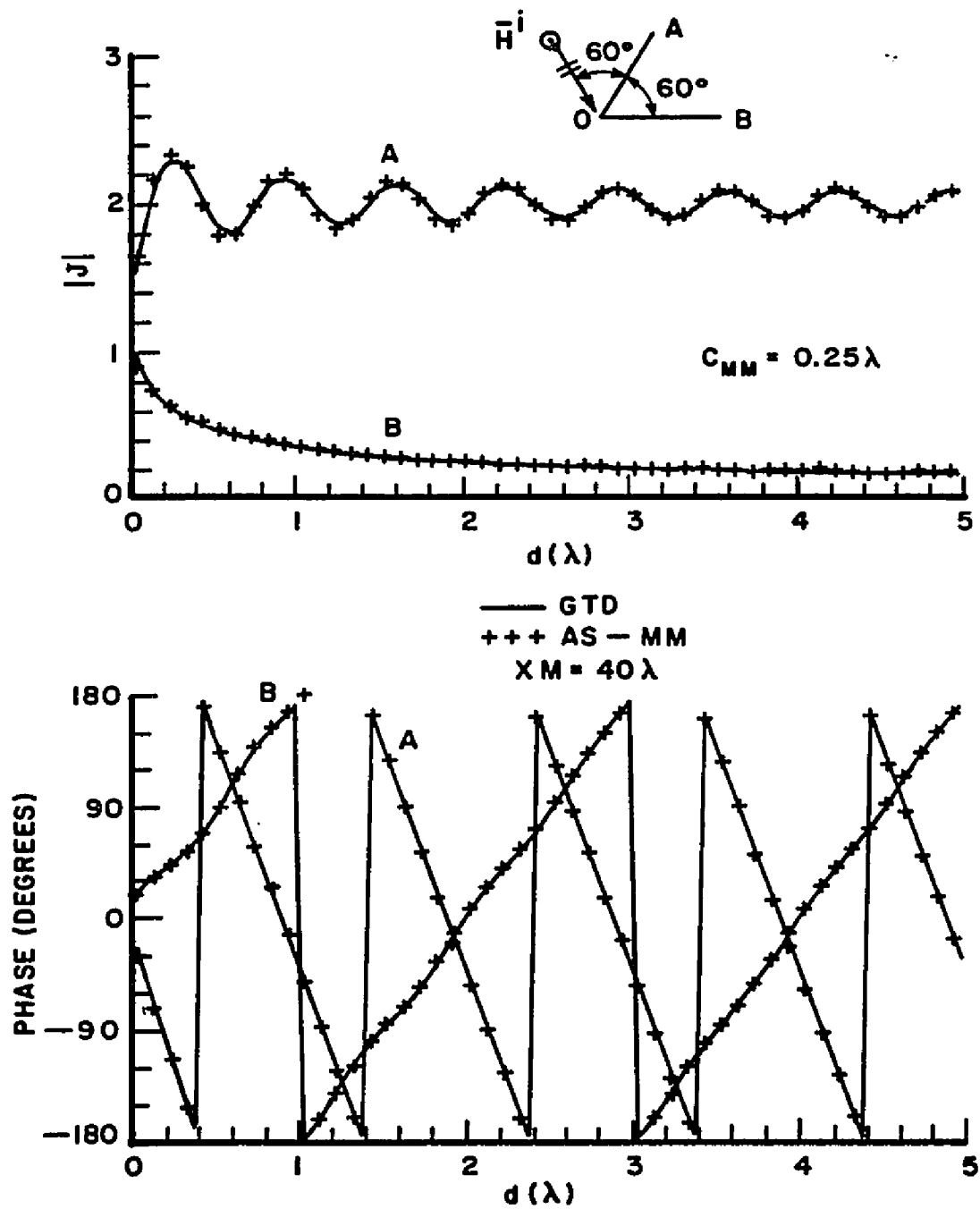
Figure 3.10.   Currents on a wedge for ϕ_w=60°, ϕ_i=60°, C_{MM}=0.25λ, and XM=40λ.

39
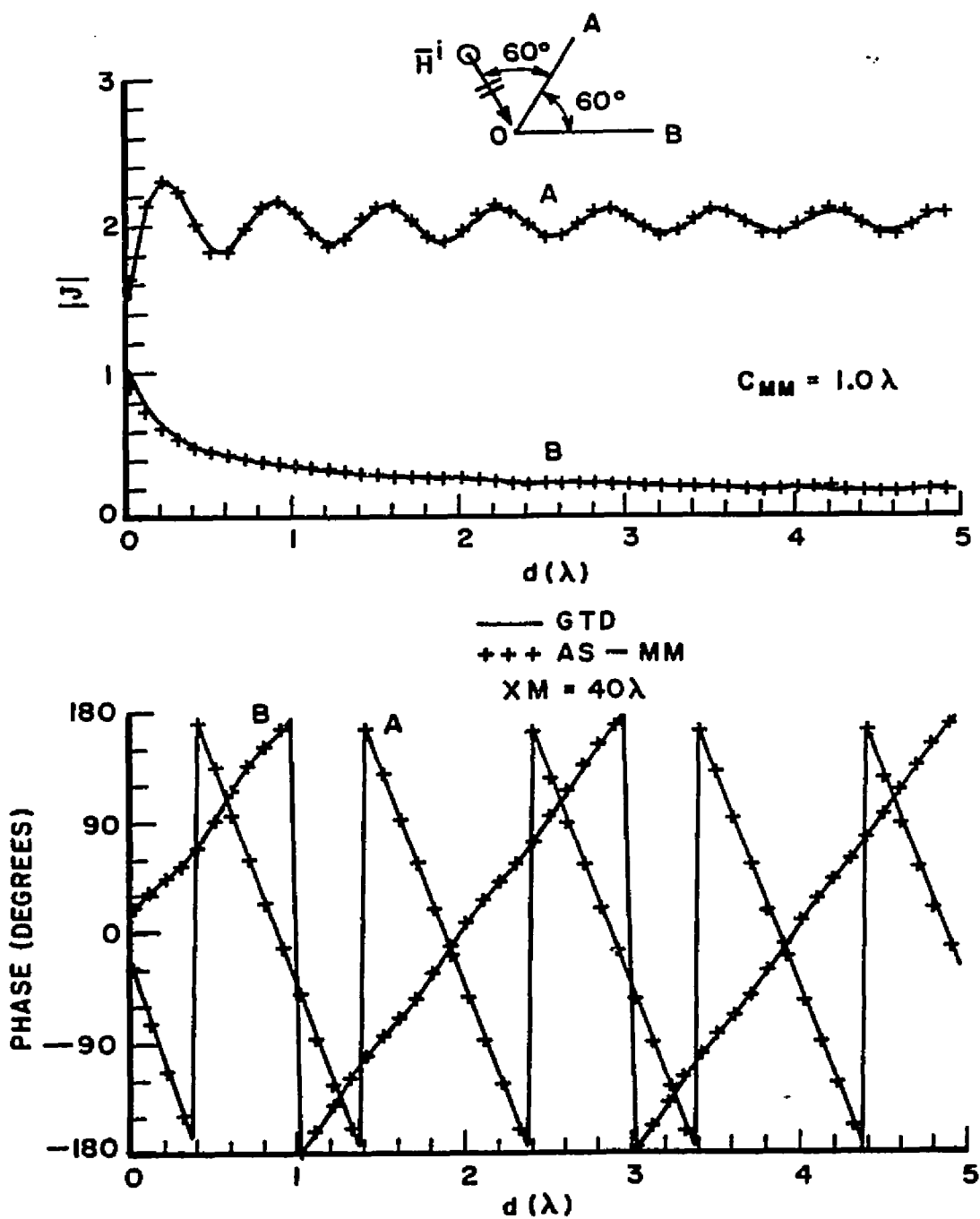
Figure 3.11. Currents on a wedge for $\phi_W=60^o$, $\phi_i=60^o$, $C_{MM}=1.0\lambda$, and $XM=40\lambda$.
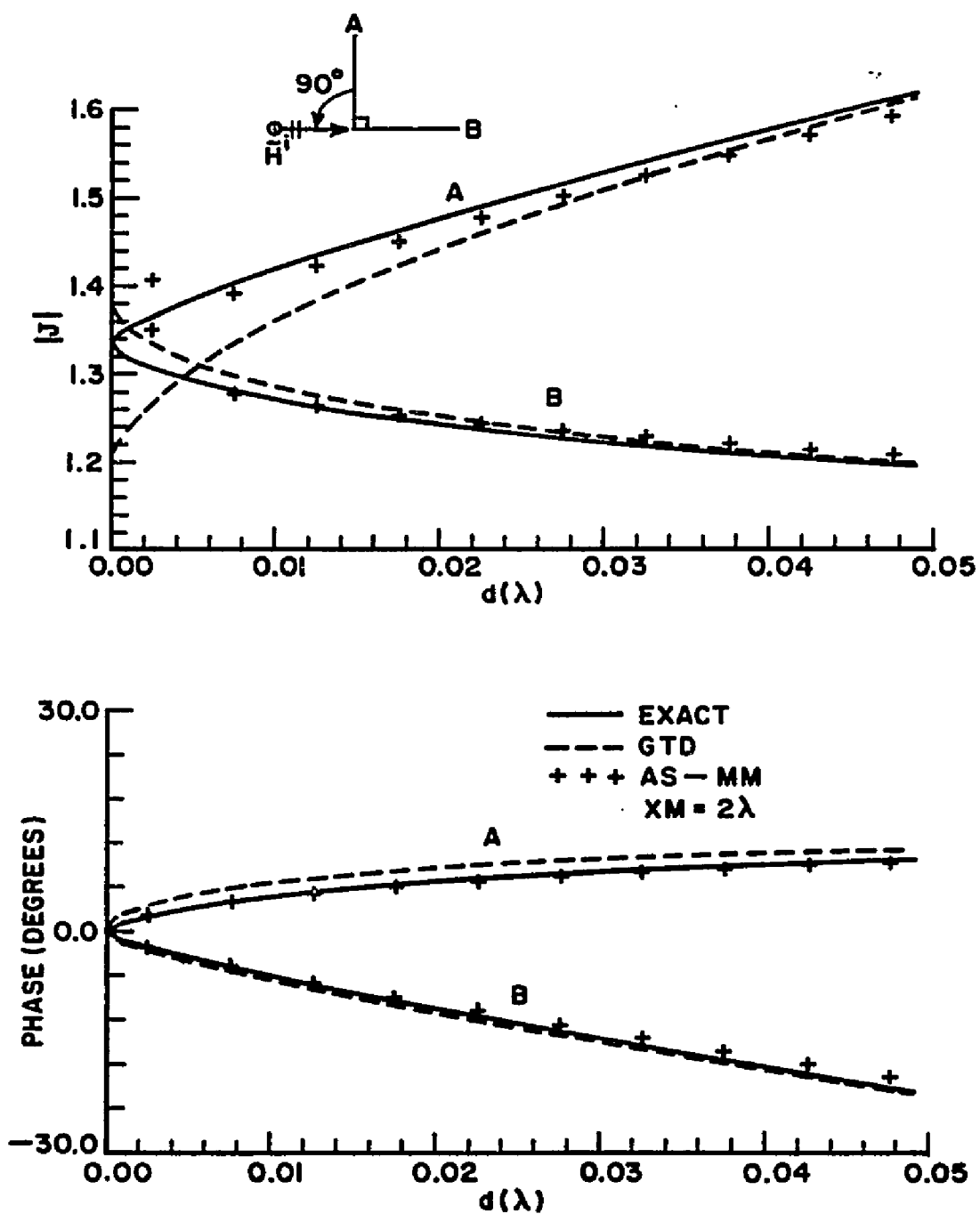
Figure 3.12. Currents on a wedge in the region very near to the edge for $\phi_W=90^0$, $\phi_i=90^0$, $C_{MM}=0.5\lambda$, and $XM=2\lambda$.

41

CHAPTER IV

SQUARE CYLINDER

4.1 Integral Equations

The geometry of a perfectly conducting square cylinder in two-dimensions is shown in Figure 4.1. A TE plane wave is incident on the square cylinder with an incident angle θ_i. For convenience, we represent the surfaces AB, BC, CD, and DA by C^1, C^2, C^3, and C^4, respectively. The moment method regions are set up around the four edges of the square cylinder and are denoted by C_{MM}^1, C_{MM}^2, C_{MM}^3, and C_{MM}^4, respectively on the surfaces C^1, C^2, C^3, and C^4.

It is assumed in this geometry that the surfaces C^1 and C^4 are lit and that the surfaces C^2 and C^3 are shadowed. Therefore the incident angle θ_i must be between 90° and 180° for the following equations which are derived below.

The currents $\overline{J}_{op}^1(\overline{R})$ and $\overline{J}_{op}^4(\overline{R})$ in the lit regions can be expressed as

$$\overline{J}_{op}^1(\overline{R}) = 2\hat{n}_1 \times \overline{H}_i(\overline{R}) + 2\hat{n}_1 \times \int_{C^4} \overline{J}_{op}^4(\overline{R}') \times \nabla' G(r) d\ell' \qquad (4.1)$$

and

$$\overline{J}_{op}^4(\overline{R}) = 2\hat{n}_4 \times \overline{H}^i(\overline{R}) + 2\hat{n}_4 \times \oint_{c^1} \overline{J}_{op}^1(\overline{R}') \times \nabla' G(r) d\ell' \quad . \tag{4.2}$$

Also the shadow region currents $\overline{J}_{op}^2(\overline{R})$ and $\overline{J}_{op}^3(\overline{R})$ can be written as

$$\overline{J}_{op}^2(\overline{R}) = 2\hat{n}_2 \times \overline{H}^i(\overline{R}) + 2\hat{n}_2 \times \sum_{\substack{k=1 \\ k \neq 2}}^{4} \oint_{c^k} \overline{J}_{op}^k(\overline{R}') \times \nabla' G(r) d\ell'$$

and

$$\overline{J}_{op}^3(\overline{R}) = 2\hat{n}_3 \times \overline{H}^i(\overline{R}) + 2\hat{n}_3 \times \sum_{\substack{k=1 \\ k \neq 3}}^{4} \oint_{c^k} \overline{J}_{op}^k(\overline{R}') \times \nabla' G(r) d\ell' \tag{4.4}$$

where $\hat{n}_1$, $\hat{n}_2$, $\hat{n}_3$, and $\hat{n}_4$ are the outward unit normal vectors to the surfaces c^1, c^2, c^3, and c^4, respectively.

The first order approximate currents in the four moment method regions can be obtained from:

$$\overline{I}_{MM}^1(\overline{R}) = 2\hat{n}_1 \times \sum_{k=2}^{4} \oint_{c_{MM}^k} \overline{I}_{MM}^k(\overline{R}') \times \nabla' G(r) d\ell' + 2\hat{n}_1 \times \sum_{k=2}^{3} \oint_{c^k} \overline{J}_{op}^k(\overline{R}') \times \nabla' G(r) d\ell' ;$$

$$\tag{4.5}$$

$$\overline{I}_{MM}^4(\overline{R}) = 2\hat{n}_4 \times \sum_{k=1}^{3} \oint_{c_{MM}^k} \overline{I}_{MM}^k(\overline{R}') \times \nabla' G(r) d\ell' + 2\hat{n}_4 \times \sum_{k=2}^{3} \oint_{c^k} \overline{J}_{op}^k(\overline{R}') \times \nabla' G(r) d\ell' ;$$

$$\tag{4.6}$$

$$T_{MM}^2(\overline{R}) = 2\hat{n}_2 x \sum_{\substack{k=1 \\ k\neq 2}}^{4} \int_{C_{MM}^k} \overline{T}_{MM}^k(\overline{R}') x \nabla' G(r) d\ell' \quad ; \tag{4.7}$$

$$T_{MM}^3(\overline{R}) = 2\hat{n}_3 x \sum_{\substack{k=1 \\ k\neq 3}}^{4} \int_{C_{MM}^k} \overline{T}_{MM}^k(\overline{R}') x \nabla' G(r) d\ell' \quad . \tag{4.8}$$
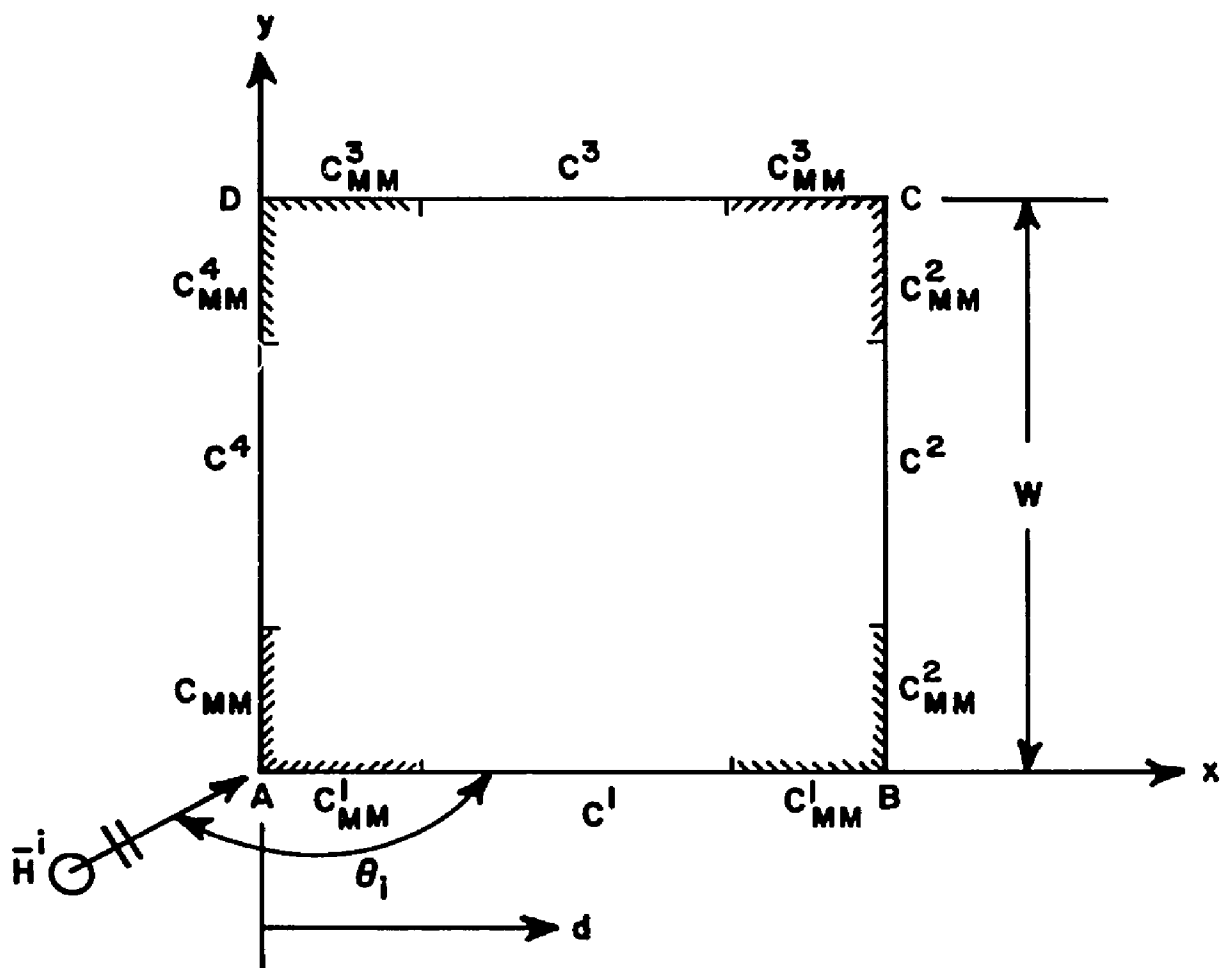
Figure 4.1. Surface divisions in a square cylinder in two dimensions.

The expressions for the currents in the asymptotic regions are the same as Equations (4.5) to (4.8) except that the observation points are moved from the MM-regions to the AS-regions.

Observing all these equations we can see that the observation and source points are not on the same surface in any one equation. Therefore as in the wedge case in Chapter III, the singularity problem (i.e., exclusion of an entire patch containing the singular point) does not appear in the square cylinder case.

The currents $\bar{J}_{op}^{1}(\bar{R})$ and $\bar{J}_{op}^{4}(\bar{R})$ can be solved simultaneously by the iterative method. After substituting these currents into the equations for $\bar{J}_{op}^{2}(\bar{R})$ and $\bar{J}_{op}^{3}(\bar{R})$, they also can be solved by the same technique.

4.2   Impedance Matrix

The moment method is used to solve Equations (4.5) to (4.8). For this purpose, we use simple pulse basis functions in the point-matching technique.

As we expect from the equations we derived, the resulting impedance matrix will be very complicated because there are four unknown currents involved in the calculations. Therefore, we will obtain an approximate expression for the matrix by ignoring certain terms in the equations. For the sake of clarity, expressing Equations (4.5) to (4.8) in scalar forms, we have

$$I_{MM}^1(\ell) = 2 \sum_{k=2}^{4} \oint_{C_{MM}^k} I_{MM}^k(\ell')G_q(\ell,\ell')d\ell' + 2 \sum_{k=2}^{3} \oint_{C^k} J_{op}^k(\ell')G_q(\ell,\ell')d\ell'$$

$$(4.9)$$

$$I_{MM}^4(\ell) = 2 \sum_{k=1}^{3} \oint_{C_{MM}^k} I_{MM}^k(\ell')G_q(\ell,\ell')d\ell' + 2 \sum_{k=2}^{3} \oint_{C^k} J_{op}^k(\ell')G_q(\ell,\ell')d\ell'$$

$$(4.10)$$

$$I_{MM}^2(\ell) = 2 \sum_{\substack{k=1 \\ k\neq 2}}^{4} \oint_{C_{MM}^k} I_{MM}^k(\ell')G_q(\ell,\ell')d\ell', \qquad (4.11)$$

and

$$I_{MM}^3(\ell) = 2 \sum_{\substack{k=1 \\ k\neq 3}}^{4} \oint_{C_{MM}^k} I_{MM}^k(\ell')G_q(\ell,\ell')d\ell'. \qquad (4.12)$$

The result of the differentiation of the Green's function with the associated vector calculation is expressed as $G_q(\ell,\ell')$, which is given by

$$G_q(\ell,\ell') = - \frac{\beta}{4j} H_1^{(2)}(\beta r) \frac{\ell}{\sqrt{\ell^2 + \ell'^2}} . \qquad (4.13)$$

46

If we substitute Equations (4.10) to (4.12) into Equation (4.9) repeatedly, we obtain an equation which has one unknown current $I_{MM}^1(\ell)$ and is composed of multiple integrals containing $I_{MM}^1(\ell')$ in their integrands. After ignoring the triple and higher multiple integral terms, we have

$$I_{MM}^1(\ell) = 4 \sum_{k=2}^{4} \oint_{C_{MM}^k} \oint_{C_{MM}^1} I_{MM}^1(\ell')G_q(\ell'',\ell')G_q(\ell,\ell'')d\ell'd\ell''$$

$$+ Q(\ell)+2 \oint_{C_{MM}^4} Q(\ell')G_q(\ell,\ell')d\ell' \qquad (4.14)$$

where

$$Q(\ell) = 2 \sum_{k=2}^{3} \oint_{C^k} J_{op}^k(\ell')G_q(\ell,\ell')d\ell' \qquad . \qquad (4.15)$$

Assume that the solution of Equation (4.14) can be expressed in the series form of

$$I_{MM}^1(\ell) = \sum_{n=1}^{N} I_n^1 P(\ell - \ell_n) \qquad (4.16)$$

where

$$P(\ell) = \begin{cases} 1 & \text{for } |\ell - \ell_n| < \dfrac{\Delta\ell}{2} \\ \\ 0 & \text{elsewhere.} \end{cases} \qquad (4.17)$$

47

and $\Delta\ell = \frac{W}{N}$, N is a number of subintervals in W.

Inserting Equation (4.16) in Equation (4.14) and rearranging terms, we have

$$\sum_{n=1}^{N} I_n^1 \left[P(\ell-\ell_n) - 4 \sum_{k=2}^{4} \oint_{C_{MM}^k} G_q(\ell',\ell_n)G_q(\ell,\ell')\Delta\ell d\ell' \right]$$

$$= Q(\ell) + 2 \oint_{C_{MM}^4} Q(\ell')G_q(\ell,\ell')d\ell' \quad .$$

(4.18)

Multiplying both sides of Equation (4.18) by $\delta(\ell-\ell_m)$, m=1,2,...N, integrating them over the surface C_{MM}^1, and dividing both sides by $\Delta\ell$, we have

$$\sum_{n=1}^{N} I_n^1 \left[P(\ell_m-\ell_n) - 4 \sum_{k=2}^{4} \oint_{C_{MM}^k} G_q(\ell',\ell_n)G_q(\ell_m,\ell')\Delta\ell d\ell' \right]$$

$$= Q(\ell_m) + 2 \oint_{C_{MM}^4} Q(\ell')G_q(\ell_m,\ell')d\ell' \quad , \quad m=1,2,...,N$$

(4.19)

from which I_n^1 can be determined by solving a matrix equation of the type

48

$[Z_{mn}^1]\ [I_n^1] = [V_m^1],\quad m,n=1,2,\ldots,N.$ The elements of the imped-

ance matrix $[Z_{mn}^1]$ are obtained from

$$Z_{mn}^1 = P(\ell_m - \ell_n) - 4 \sum_{k=2}^{4} \int_{C_{MM}^k} G_q(\ell', \ell_n) G_q(\ell_m, \ell') \Delta\ell \, d\ell' \qquad (4.20)$$

where $m,n=1,2,3,\ldots,N$.

Also the elements of the voltage matrix $[V_m^1]$ are determined by

$$V_m^1 = Q(\ell_m) + 2 \int_{C_{MM}^4} Q(\ell') G_q(\ell_m, \ell') \, d\ell' \qquad m=1,2,\ldots,N. \qquad (4.21)$$

In Equation (4.20) the most dominant term is

$$\int_{C_{MM}^4} G_q(\ell', \ell_n) G_q(\ell_m, \ell') \Delta\ell \, d\ell'$$

which is due to the surface current on the lit surface C_{MM}^4. Therefore

for the simpler form of Z_{mn}^1, we can ignore all other terms except the

dominant term.

49

4.3   Numerical Results

For numerical integration, the length of one side W of a square cylinder was divided into 60 subintervals. The moment method region C_{MM}^k(k=1,2,3,4) was set up with one half of W in it's length. Therefore the extent of the moment method region (C_{MM}) will be changed according to the size of the cylinder. However, as we have seen in the wedge problem, the current on the surface of a square cylinder also will not be affected by C_{MM}, as we will see later in the numerical results.

Numerical calculations were performed for various cylinder sizes and angles of the incident field, and comparisons were made with independent GTD solutions. For the GTD solutions, up to triply diffracted fields were considered, and the diffraction coefficient formulas obtained by Kouyoumjian and Pathak were used. The magnitude and phase of the surface current on a 0.7λ square cylinder with the wave incident angle $\theta_i = 95^o$ are shown in Figure 4.2. It is seen that overall agreement with the GTD solutions is very good except that the phase of the current on the deep shadowed region (C^3) deviates slightly from the GTD result. Also the result for a square cylinder with W=1.2λ and $\theta_i = 120^o$, which is shown in Figure 4.3, is seen to be in very good agreement with the GTD solution.

Results for larger W, that is W=3.0λ and 4.2λ are, respectively shown in Figures 4.4 and 4.5. We see that overall agreements are quite good with slight deviations in the deep shadow region. Although we obtained results for square cylinders up to 4.2λ on a side, the method does not show any limits on the size of a cylinder or on the wave

incident angle. Next let us examine the results of the surface cur-
on a 3.0 square cylinder with $C_{MM}=0.5\lambda$ and 2.0λ, respectively in
Figures 4.6 and 4.7. The number of pulse basis functions in C_{MM} is
proportional to C_{MM}, and the width of the pulse is kept constant at
0.05 for those data. By comparing Figure 4.6 with Figure 4.7, we
can realize that the larger C_{MM} makes the result slightly better,
especially in the deep shadow region. However, it is clearly seen
that the extent of the moment method region does not affect the surface
current significantly.

It is well known that a square cylinder can have an interior
resonance problem since the integral equation has a nonunique solution
at the resonant frequencies. The moment method produces an erroneous
solution for the surface current on a square cylinder at those resonant
frequencies. The geometries of the square cylinders which correspond
to the resonant frequencies are determined by

$$W = \frac{1}{2}\sqrt{m^2+n^2}\;\lambda \qquad\qquad m,n=0,1,2,3,\ldots \qquad\qquad (4.22)$$

from which we can find an infinite number of square cylinders which
are in the resonance mode. Some of these geometries are obtained
from Equation (4.22) are given by $W=0.5\lambda$, 0.707λ, 1.0λ, 1.118λ, 1.5λ,
1.58λ, 2.0λ, 2.121λ, 3.0λ, 3.041λ,... . For a square cylinder, the
resonant frequencies are so sharply defined that we may not detect
the resonance phenomena even at frequencies deviated very slightly
from them.

Figure 4.8 shows the results of the surface currents on the 0.707λ square cylinder with $\theta_i = 95^o$ which is one of the geometries having an interior resonance. Three methods, the GTD, moment, and hybrid methods are used to obtain those results. It is seen that the moment method produces erroneous results in both the magnitude and phase of the current. Also when the same square cylinder with $\theta_i = 120^o$ is tried, the moment method solutions become worse as shown in Figure 4.9.

On the other hand, our hybrid method solutions do not show any resonance phenomena and instead show very good agreement with the GTD solutions in both cases of $\theta_i = 95^o$ and 120°. Results for $W = 1.118\lambda$, which also correspond to one of the resonant geometries, are given in Figure 4.10. Our solution does not show any resonance effect.

It is worthwhile to mention that the GTD and our hybrid method solutions for $W = 0.705\lambda$ (which is slightly different from 0.707λ) have remarkably good agreement with the moment method solutions as shown in Figure 4.11.
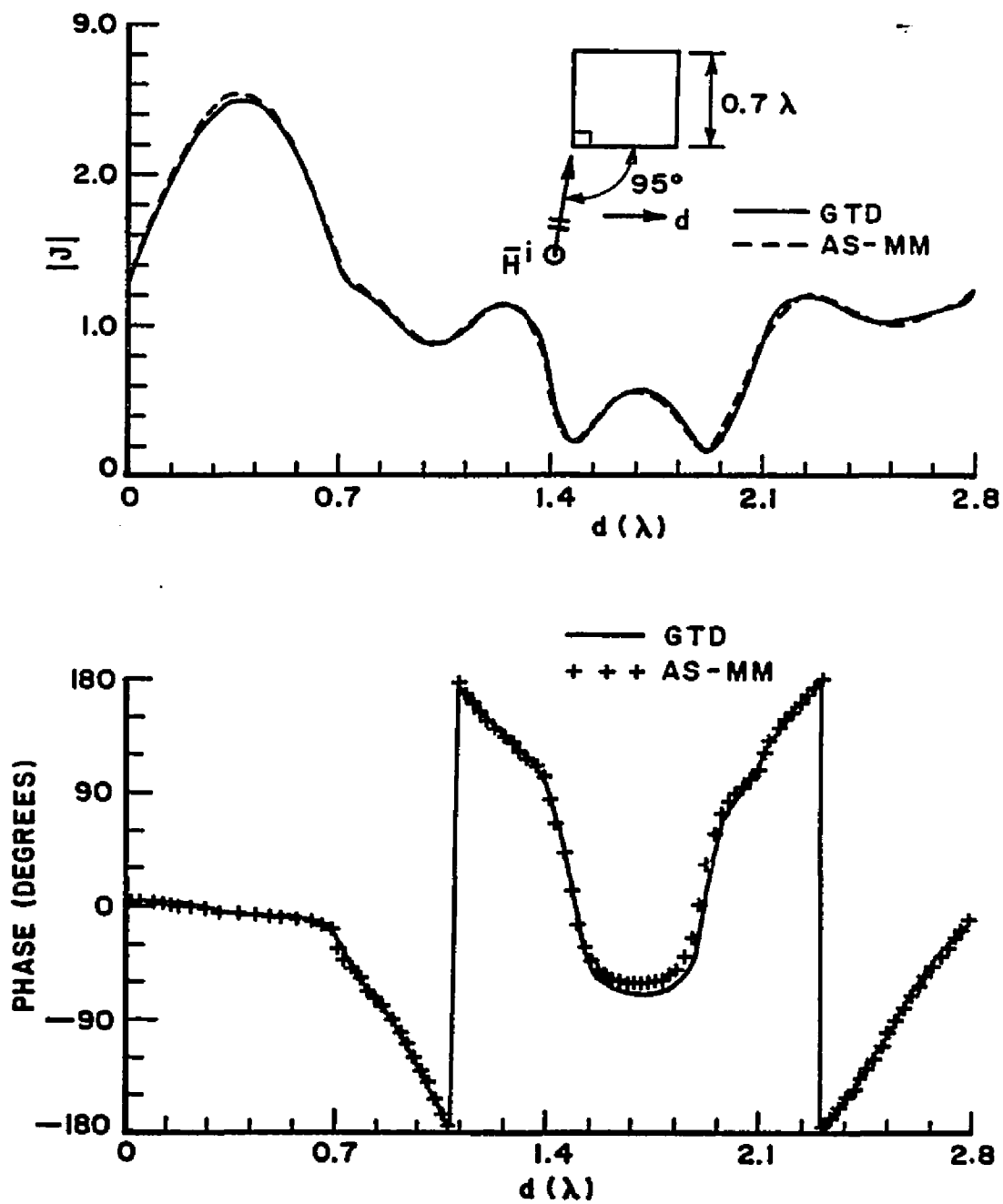
Figure 4.2. Current on a square cylinder for
$W=0.7\lambda$, $\theta_i=95^o$, and $C_{MM}=0.5W$.
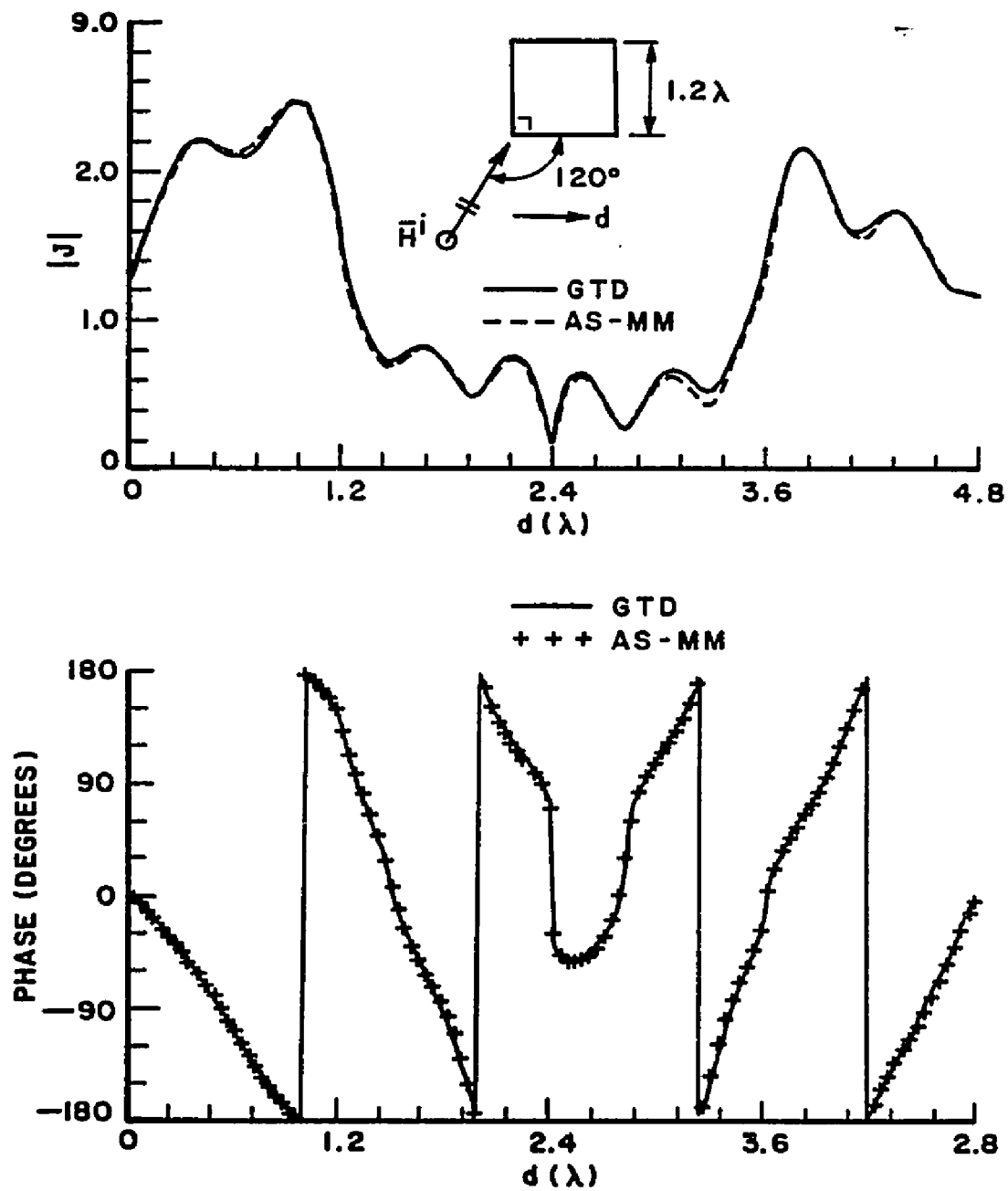
Figure 4.3. Current on a square cylinder for
$W=1.2\lambda$, $\theta_i=120^o$, and $C_{MM}=0.5W$.
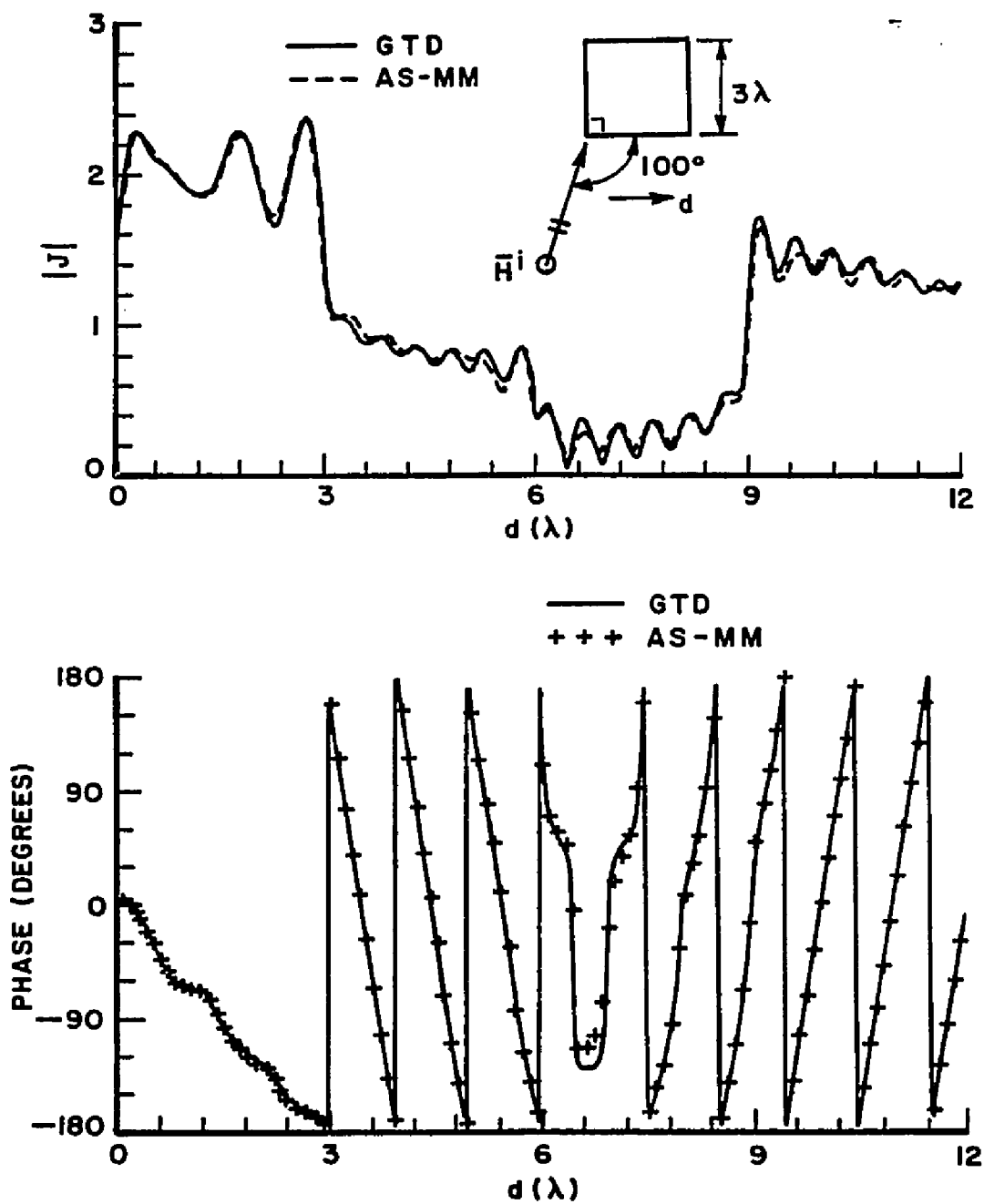
Figure 4.4. Current on a square cylinder for
$W=3.0\lambda$, $\theta_i=100^o$, and $C_{MM}=0.5W$.
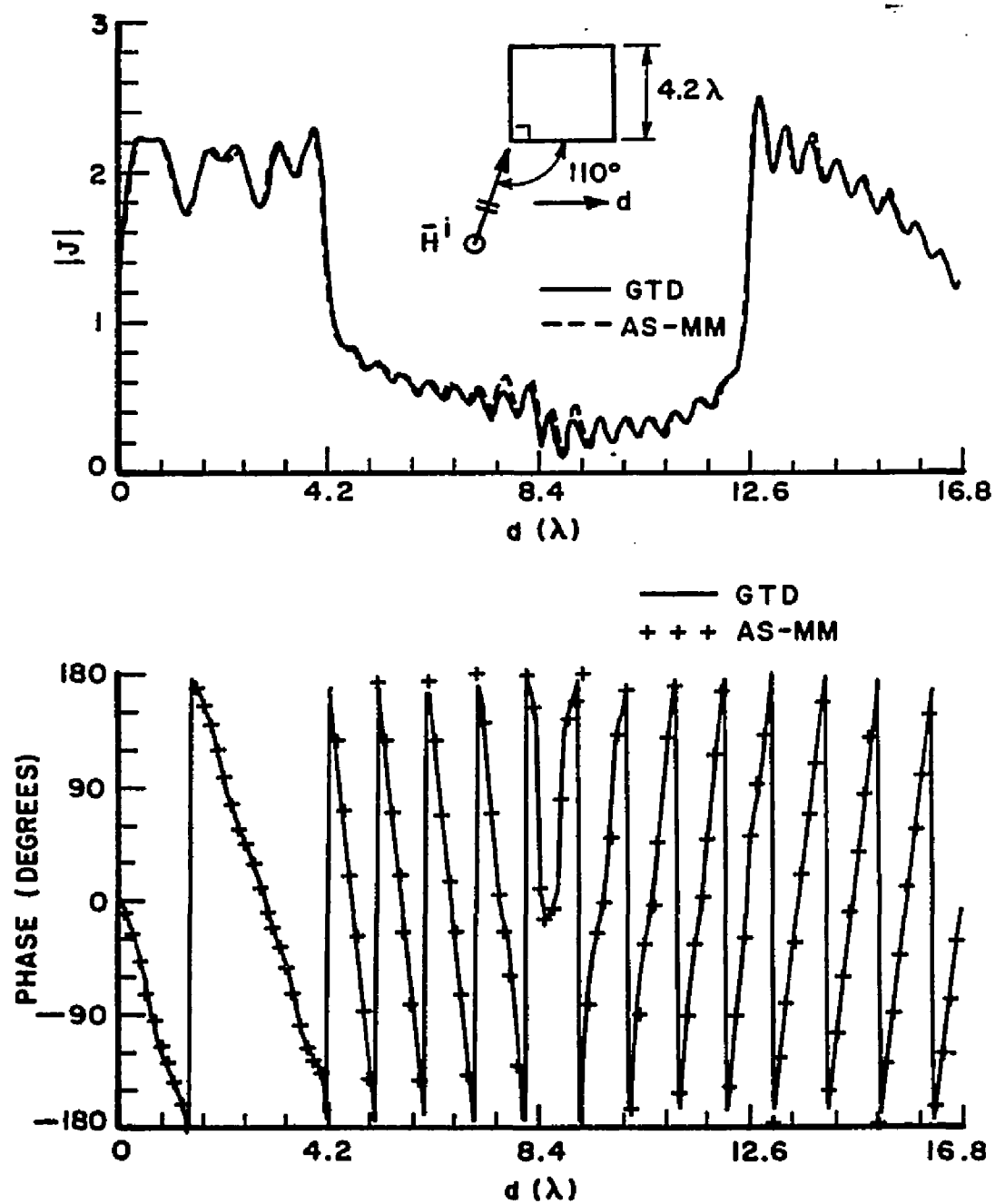
Figure 4.5. Current on a square cylinder for
$W=4.2\lambda$, $\theta_i=110^O$, and $C_{MM}=0.5W$.
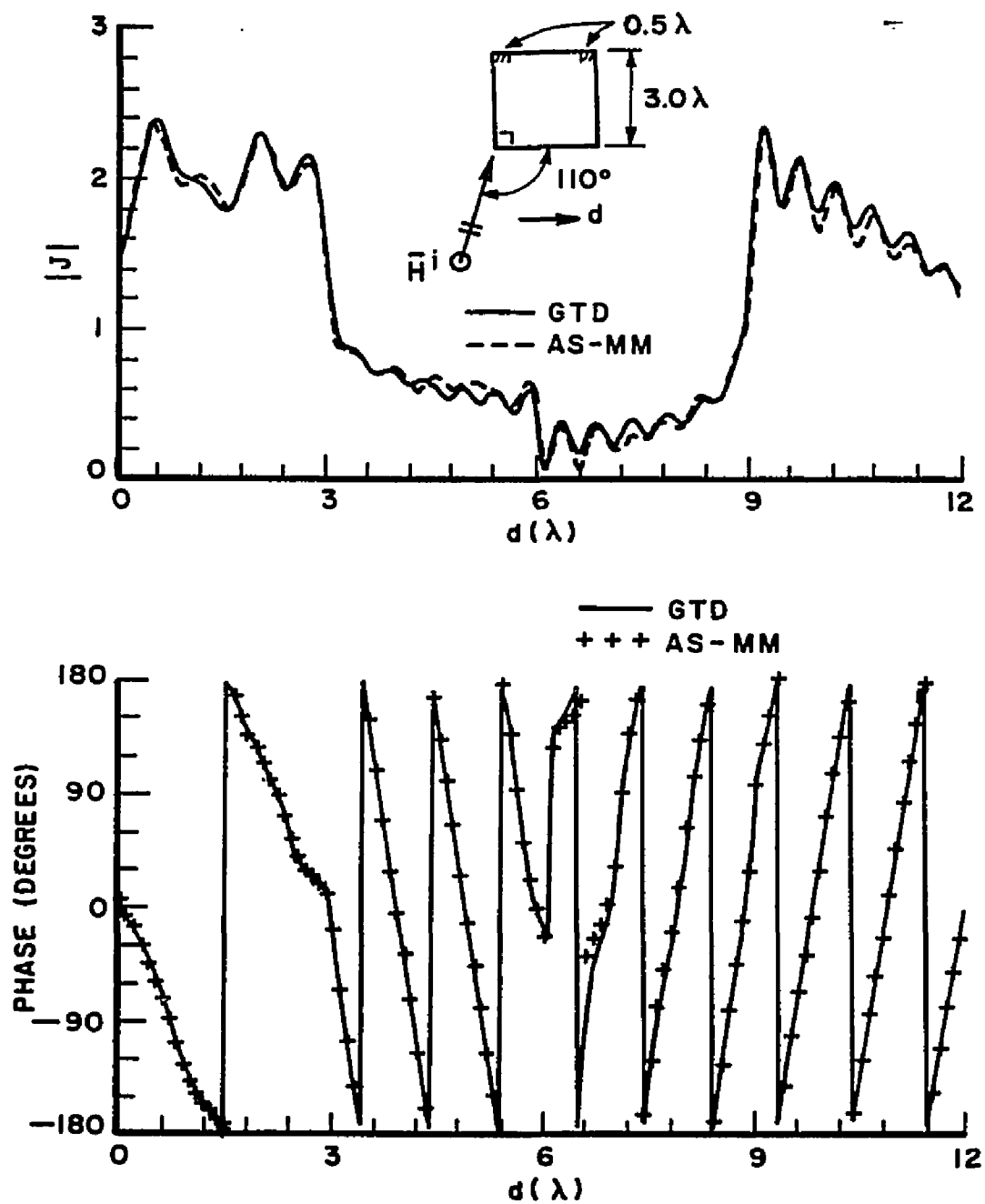
Figure 4.6. Current on a square cylinder for
$W=3.0\lambda$, $\theta_i=110^{\circ}$, and $C_{MM}=0.5\lambda$.
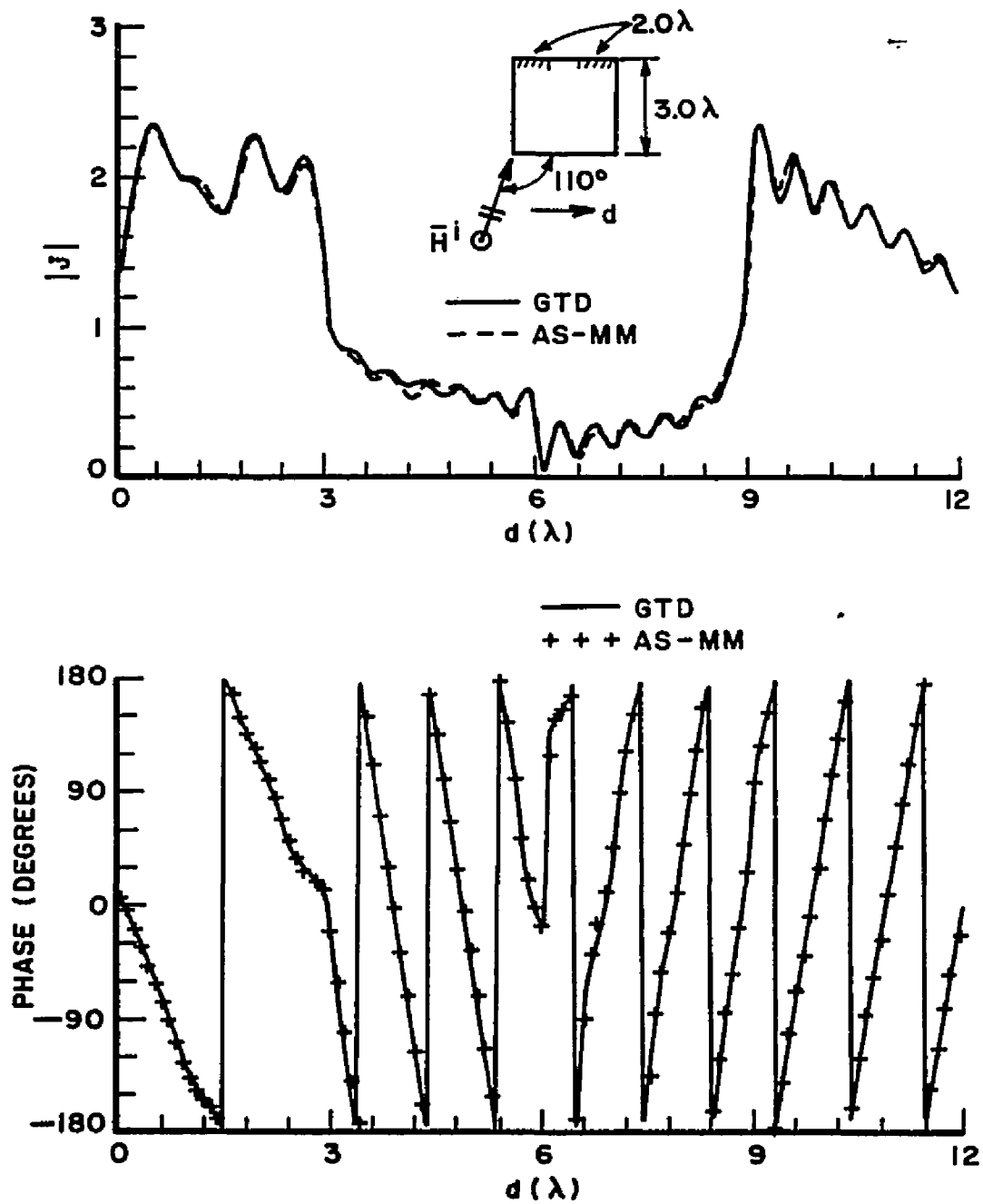
Figure 4.7. Current on a square cylinder for $W=3.0\lambda$, $\theta_i=110^\circ$, and $C_{MM}=2.0\lambda$.
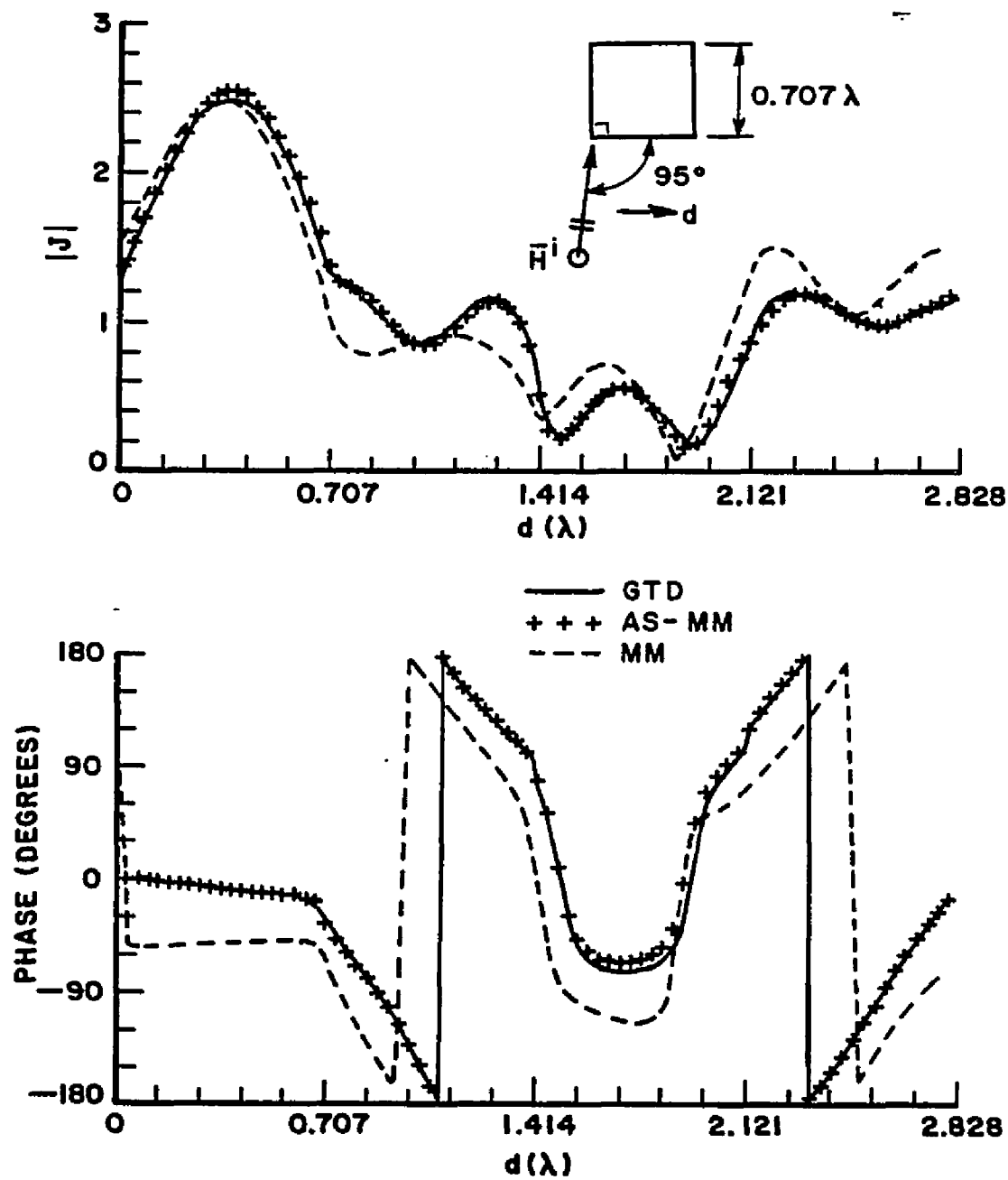
Figure 4.8. Current on a square cylinder for $W=0.707\lambda$ (resonance case), $\theta_i=95^\circ$, and $C_{MM}=0.5W$.
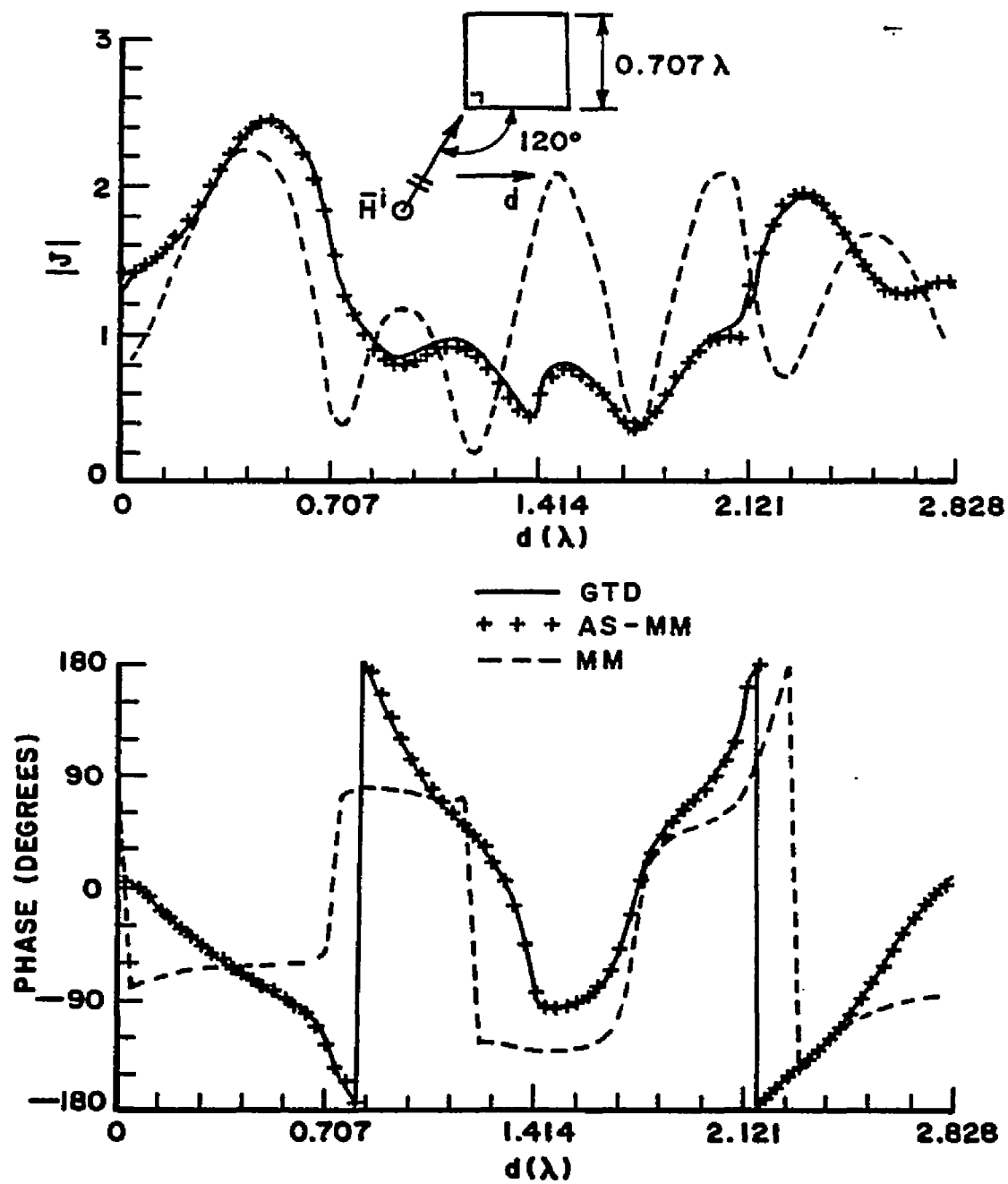
Figure 4.9. Current on a square cylinder for W=0.707λ (resonance case), $\theta_i=120^o$, and $C_{MM}=0.5W$.
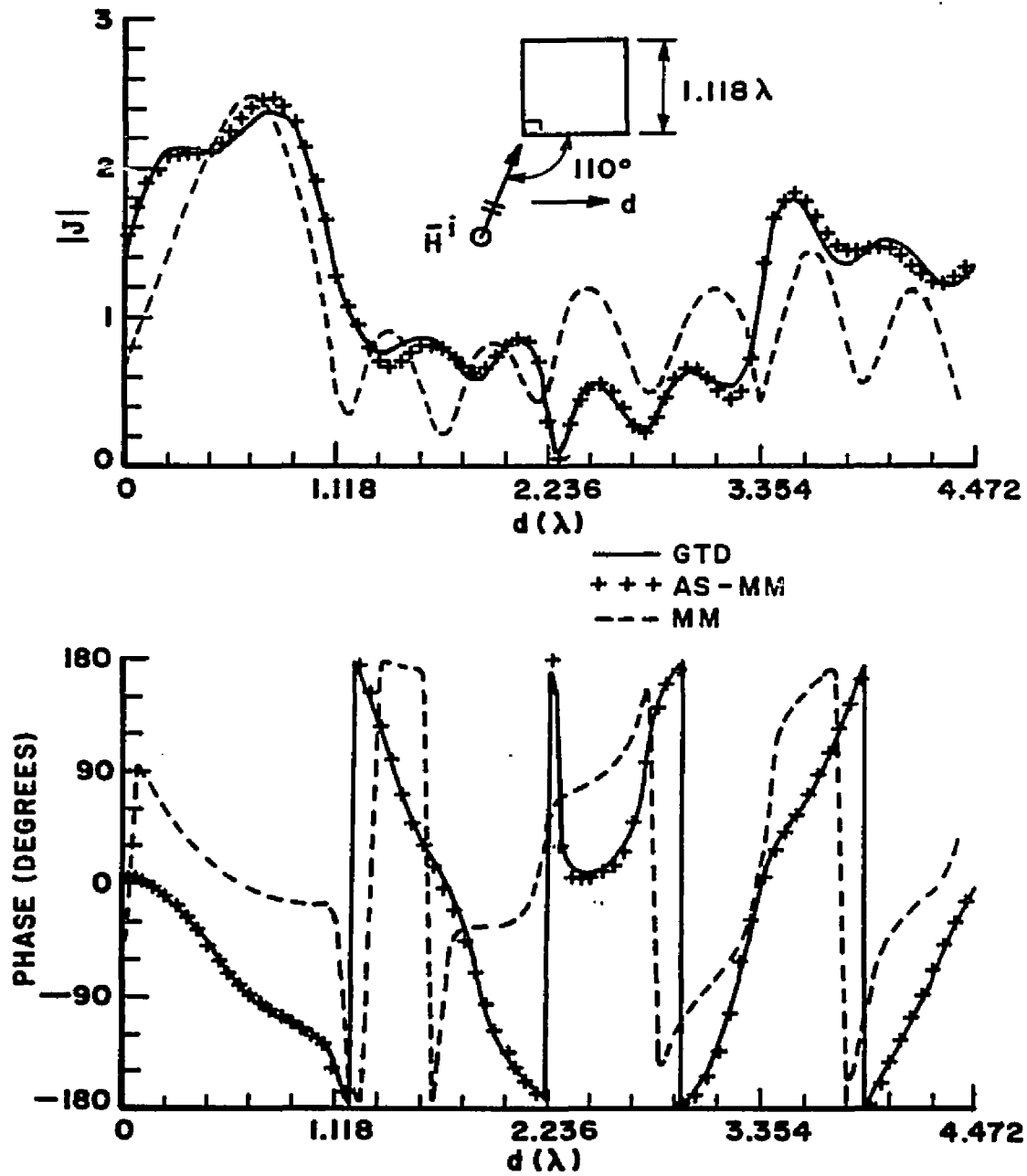
Figure 4.10. Current on a square cylinder for W=1.118λ (resonance case), θ_i=110°, and C_{MM}=0.5W.
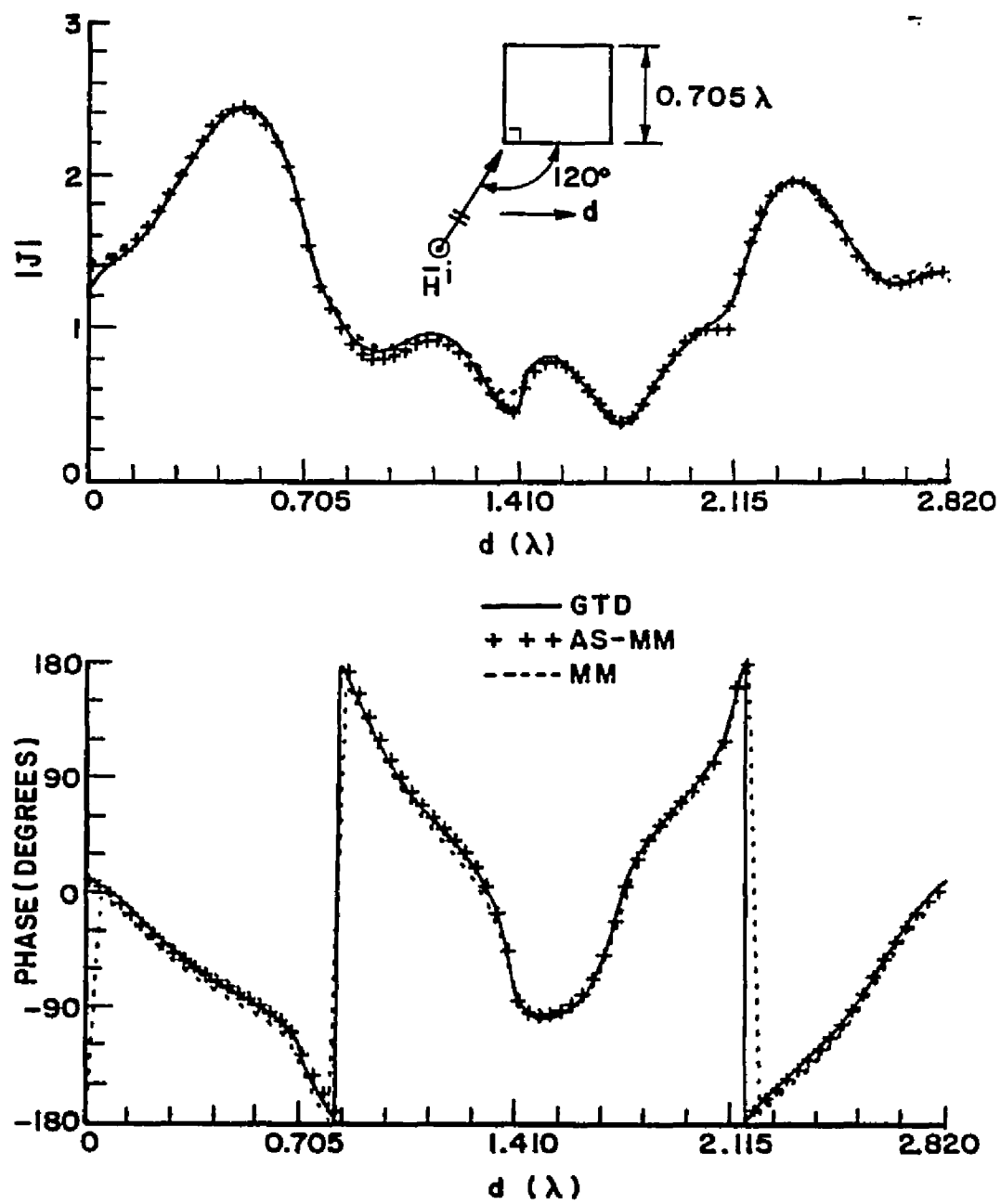
Figure 4.11. Current on a square cylinder for
$W=0.705\lambda$, $\theta_i=120^o$, and $C_{MM}=0.5W$.

CHAPTER V
CIRCULAR CYLINDER

5.1 Integral Equations

We will consider a perfectly conducting circular cylinder which is illuminated by a TE plane wave as shown in Figure 5.1. The moment method regions which are represented by C_{MM}^{ℓ} and C_{MM}^{s}, respectively in the lit and shadowed regions, are located in the regions near the shadow boundary.
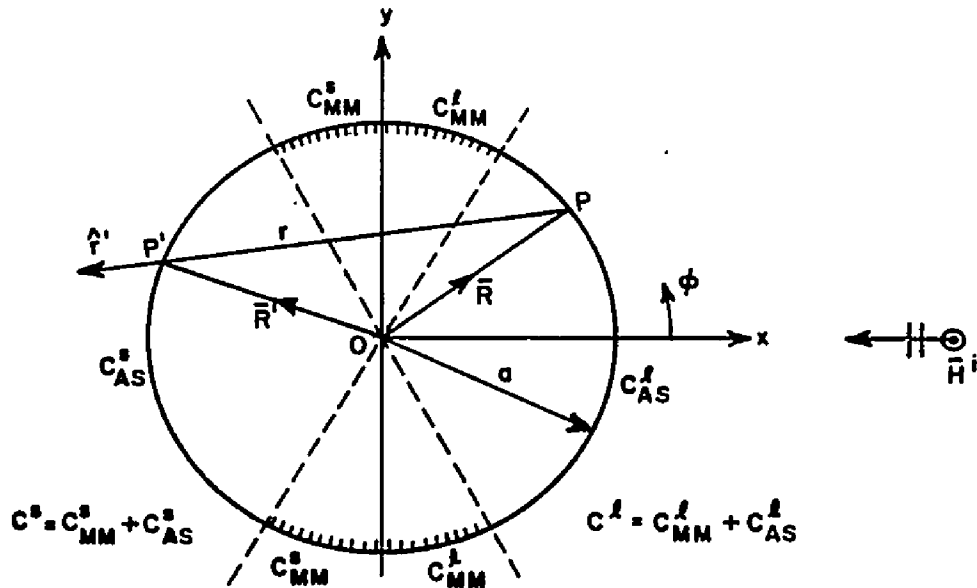
Figure 5.1. Surface divisions in a circular cylinder in two dimensions.

The equations for the surface currents on a circular cylinder will have the same forms as the general equations except for the integration regions. Therefore we can write the following equations directly from the general equations:

$$\bar{J}_{op}^{\ell}(\bar{R}) = 2\hat{n}x\bar{H}^{i}(\bar{R}) + 2\hat{n} \times \int_{C^{\ell}} \bar{J}_{op}^{\ell}(\bar{R}')x\nabla'G(r)d\ell' \tag{5.1}$$

$$\bar{J}_{op}^{S}(\bar{R}) = 2\hat{n}x\bar{H}^{i}(\bar{R}) + 2\hat{n} \times \int_{C^{\ell}} \bar{J}_{op}^{\ell}(\bar{R}')x\nabla'G(r)d\ell'$$

$$+ 2\hat{n} \times \int_{C^{S}} \bar{J}_{op}^{S}(\bar{R}')x\nabla'G(r)d\ell' \tag{5.2}$$

$$\bar{I}_{MM}^{\ell}(\bar{R}) = 2\hat{n} \times \int_{C_{MM}^{\ell}} \bar{I}_{MM}^{\ell}(\bar{R}')x\nabla'G(r)d\ell' + 2\hat{n} \times \int_{C_{MM}^{S}} \bar{I}_{MM}^{S}(\bar{R}')x\nabla'G(r)d\ell'$$

$$+ 2\hat{n} \times \int_{C^{S}} \bar{J}_{op}^{S}(\bar{R}')x\nabla'G(r)d\ell' \tag{5.3}$$

$$\bar{I}_{MM}^{S}(\bar{R}) = 2\hat{n} \times \int_{C_{MM}^{\ell}} \bar{I}_{MM}^{\ell}(\bar{R}')x\nabla'G(r)d\ell' + 2\hat{n} \times \int_{C_{MM}^{S}} \bar{I}_{MM}^{S}(\bar{R}')x\nabla'G(r)d\ell'$$

$$\tag{5.4}$$

G(r) is defined in Equation (2.6). The expressions for the currents on the asymptotic regions have the same forms as Equations (5.3) and (5.4) except the observation points are moved from the moment method regions to the asymptotic regions.

64

5.2 Consideration of the Singularity Patch

As we mentioned before, the equations for the curved surface have as many singular points as observation points. Therefore Equations (5.1) to (5.4) may not be useful for practical numerical calculations because we have to skip some finite areas containing the singular point instead of one point for the evaluation of the principle value of integration.

Let us consider the exaggerated part of the curved surface shown in Figure 5.2. The points A, B, C and D are the boundaries of division, and P_0, P_1 and P_2 represent observation points which are located at the center of each division. Thus, the currents at the points P_1, P_0 and P_2 represent the currents on the subintervals AB, BC and CD, respectively.
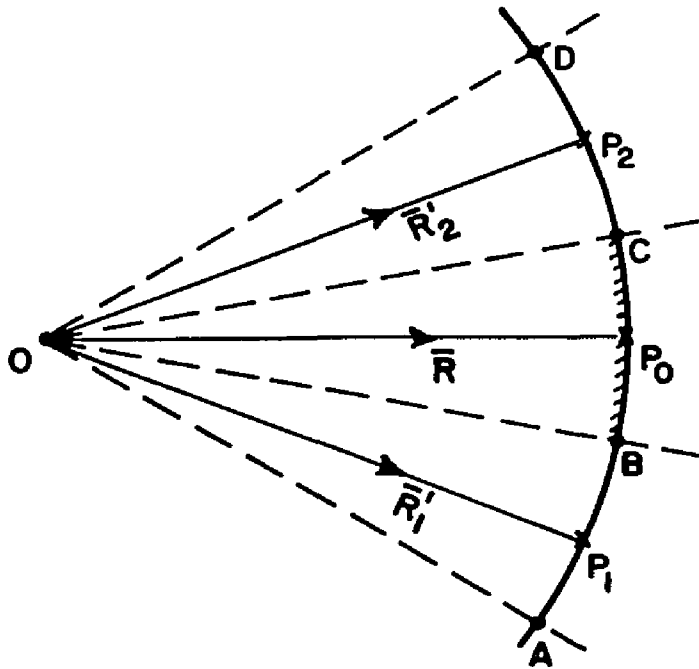
Figure 5.2. Source points around the singular point P_0.

When we perform numerical integration with the observation point at P_O, the contribution of the source currents which are located in the interval BC will be disregarded, and thus, the errors will be increased. If we subdivide the interval BC into many subintervals, then the resulting errors will be decreased. However, this way of solving the problem may not be efficient when we consider limits of computer memory storage and running time. Therefore we will derive the magnetic field integral equation which will be useful for practical calculations in general and then derive the specific result for the circular cylinder problem.

Just inside the surface of a perfectly conducting body, the following boundary condition will be satisfied.

$$\hat{n} \times \overline{H}^i(\overline{R}) + \hat{n} \times \overline{H}^s(\overline{R}) = 0 \qquad \text{just inside S} \qquad (5.5)$$

where $\overline{H}^i(\overline{R})$ is the incident magnetic field, and $\overline{H}^s(\overline{R})$ is the magnetic field due to the electric surface current on S and is given by

$$\overline{H}^s(\overline{R}) = \nabla \times \int_S \overline{J}(\overline{R}') \ G(r) \ ds' \qquad (5.6)$$

From Equations (5.5) and (5.6), we have

$$\hat{n} \times \overline{H}^i(\overline{R}) + \hat{n} \times \nabla \times \int_S \overline{J}(\overline{R}')G(r)ds' = 0 \ . \qquad (5.7)$$

Using the vector identity $\nabla \times (A\overline{B}) = (\nabla A) \times \overline{B} + A(\nabla \times \overline{B})$ and noting that $\nabla \times \overline{J}(\overline{R}')=0$, we have

$$\hat{n} \times \overline{H}^i(\overline{R}) + \hat{n} \times \int_S \overline{J}(\overline{R}') \times \nabla' G(r) ds' = 0 \qquad (5.8)$$

where we used the relationship $\nabla G(r) = -\nabla' G(r)$, and $\nabla' G(r)$ represents gradient of $G(r)$ in the source coordinate system. If we divide the surface S into two surfaces, $S-S_f$ and S_f which is finite and includes a singular point at the center of it, we can write Equation (5.8) as

$$\hat{n} \times \overline{H}^i(\overline{R}) + \hat{n} \times \int_{S-S_f} \overline{J}(\overline{R}') \times \nabla' G(r) ds' + \hat{n} \times \int_{S_f} \overline{J}(\overline{R}') \times \nabla' G(r) ds' = 0.$$

$$(5.9)$$

Since the third term of Equation (5.9) still has an r^{-1} singularity as $\overline{R}$ approaches $\overline{R}'$, we will consider a hemispherical surface S_ϵ which is mounted over the singular point P_0 with radius r_c as shown in Figure 5.3. Then Equation (5.9) can be rewritten as

$$\hat{n} \times \overline{H}^i(\overline{R}) + \hat{n} \times \int_{S-S_f} \overline{J}(\overline{R}') \times \nabla' G(r) ds'$$

$$+ \lim_{S_\epsilon \to 0} \left\{ \hat{n} \times \int_{S_f-S_\epsilon} \overline{J}(\overline{R}') \times \nabla' G(r) ds' + \hat{n} \times \int_{S_\epsilon} \overline{J}(\overline{R}') \times \nabla' G(r) ds' \right\} = 0$$

$$(5.10)$$

Let

$$\overline{J}_1(\overline{R}) = \lim_{S_\epsilon \to 0} \hat{n} \times \int_{S_\epsilon} \overline{J}(\overline{R}') \times \nabla' G(r) ds' \qquad (5.11)$$

67
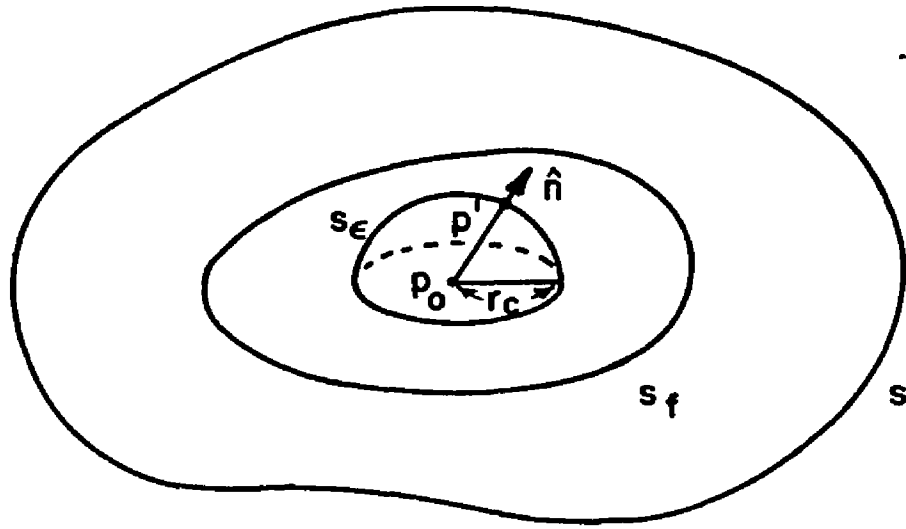
Figure 5.3. Surface divisions around the singular point P_o.

and

$$\overline{J}_2(\overline{R}) = \lim_{S_\epsilon \to 0} \hat{n} \times \int_{S_f - S_\epsilon} \overline{J}(\overline{R}') \times \nabla' G(r) ds' \quad . \tag{5.12}$$

Then Equation (5.10) becomes

$$\hat{n} \times \overline{H}^i(\overline{R}) + \hat{n} \times \int_{S - S_f} \overline{J}(\overline{R}') \times \nabla' G(r) ds' + \overline{J}_1(\overline{R}) + \overline{J}_2(\overline{R}) = 0 \quad . \tag{5.13}$$

Using a small argument approximation for $H_0^{(2)}(\beta r)$, $\overline{J}_1(\overline{R})$ can be easily obtained as (see Appendix A)

$$\overline{J}_1(\overline{R}) = -\frac{1}{2} \overline{J}(\overline{R}) \quad . \tag{5.14}$$

Although this result is obtained for the two dimensional problem, the same result can be obtained for the three dimensional sphere problem which we will consider in Chapter VI.

Next we will consider $\overline{J}_s(\overline{R})$ in Equation (5.12). Let $\overline{J}(\overline{R})$ be in the direction of $\hat{t}$ on the surface, then we can write

$$\overline{J}(\overline{R}) = \hat{t}\ J(\overline{R})\ \ .\tag{5.15}$$

The unit vector $\hat{t}$ will be $-\hat{\phi}$ for the geometry in Figure 5.1. Also let

$$\nabla'G(r) = \hat{r}'\ G_c(r)\tag{5.16}$$

where

$$G_c(r) = -\frac{\beta}{4j}\ H_1^{(2)}(\beta r)\tag{5.17}$$

and $\quad \hat{r}' = \dfrac{\overline{R}'-\overline{R}}{|\overline{R}-\overline{R}'|}$

Since $\hat{n} \times (\hat{t}'x\hat{r}') = \hat{t}\ \cos\theta$, where θ is the angle between the unit vectors $\hat{n}'$ and $\hat{r}'$, Equation (5.12) can be rewritten as

$$\overline{J}_2(\overline{R}) = \lim_{S_\epsilon \to 0}\ \hat{t}\ \int_{S_f - S_\epsilon} \cos\theta\ J(\overline{R}')G_c(r)ds'\tag{5.18}$$

or since $\hat{n}' \cdot \hat{r}' = \cos\theta$, we can write Equation (5.18) as

$$\overline{J}_2(\overline{R}) = \lim_{S_\epsilon \to 0} \oint_{S_f - S_\epsilon} \hat{n}' \cdot \hat{r}' \, J(\overline{R}')G_c(r)ds' \qquad (5.19)$$

where $\hat{n}'$ is the unit normal vector to the surface at the source point. To obtain the approximation for $\overline{J}_2(\overline{R})$, we assume that

$$J(\overline{R}') \simeq J(\overline{R}) \qquad (5.20)$$

for the small finite area S_f. Then Equation (5.19) becomes

$$\overline{J}_2(\overline{R}) \simeq J(\overline{R}) \lim_{S_\epsilon \to 0} \int_{S_f - S_\epsilon} \hat{n}' \cdot \hat{r}' \, G_c(r)ds' \quad . \qquad (5.21)$$

From Equations (5.13), (5.14) and (5.21) we have expression for $\overline{J}(\overline{R})$, which is given by

$$\overline{J}(\overline{R}) = C_0 \left[2\hat{n} \times \overline{H}^i(\overline{R}) + 2\hat{n} \times \int_{S - S_f} \overline{J}(\overline{R}') \times \nabla' G(r)ds' \right] \qquad (5.22)$$

where the constant C_0 is

$$C_0 = \frac{1}{1 - 2 \lim_{S_\epsilon \to 0} \int_{S_f - S_\epsilon} \hat{n}' \cdot \hat{r}' \, G_c(r)ds'} \quad . \qquad (5.23)$$

Now let us calculate C_0 explicitly for a circular cylinder. Consider an exaggerated part of the circular surface shown in Figure 5.4. Points A and B are the boundaries of the finite surface S_f, and the observation point P is located at the center of AB. The value of $\hat{n}'\cdot\hat{r}'$ can be obtained from Figure 5.4 as

$$\hat{n}'\cdot\hat{r}' = \cos\theta = \frac{r}{2a} \ .$$

(5.24)
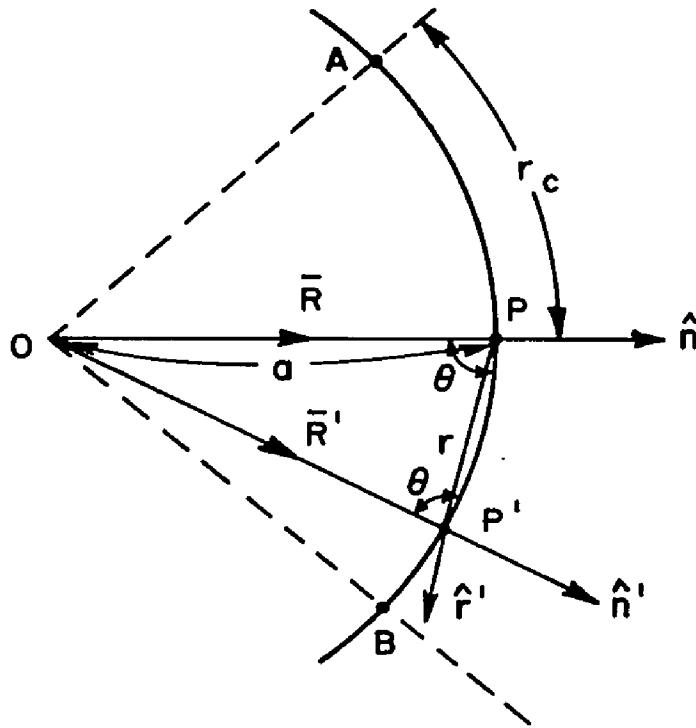
Figure 5.4. Surface around the singular point P to give relationship between a, r, and θ.

Also the small argument approximation for $G_c(r)$ is given by

71

$$G_c(r) \simeq -\frac{\beta}{4j}\left(\frac{\beta r}{2} + j\frac{2}{\pi\beta r}\right) \qquad \text{for small } \beta r. \qquad (5.25)$$

Substituting Equations (5.24) and (5.25) into Equation (5.23), we obtain

$$C_0 \simeq \frac{1}{1-4 \lim_{r_0\to 0} \int_{r_0}^{r_c} \left(\frac{r}{2a}\right)\left(-\frac{\beta}{4j}\right)\left(\frac{\beta r}{2} + j\frac{2}{\pi\beta r}\right)dr} \qquad . \qquad (5.26)$$

Evaluating the integration in Equation (5.26), we obtain

$$C_0 \simeq \frac{1}{1 + \frac{r_c}{2a}\left(\frac{2}{\pi} - j\frac{\beta^2 r_c^2}{6}\right)} \qquad . \qquad (5.27)$$

Notice that for very small r_c, C_0 becomes one, and thus, Equation (5.22) becomes the usual magnetic field integral equation.

The Equation (5.22) will be useful for practical numerical integration because the finite area S_f is removed instead of just a point for evaluation of the principle value of integration. The constant C_0 will supplement the contribution which is lost by removing the finite area S_f. Although the result in Equation (5.27) is obtained for a circular cylinder, the same result may be used as an approximation for an arbitrary smooth surface in two dimensions.

5.3 Impedance Matrix

To solve for $\overline{I}_{MM}^{\ell}(\overline{R})$ and $\overline{I}_{MM}^{S}(\overline{R})$, we use the moment method. For the sake of simplicity, we will derive the approximate form of the impedance matrix by ignoring all possible terms that make a minor contribution. Expressing Equations (5.3) and (5.4) in the scalar forms, we have

$$
I_{MM}^{\ell}(\overline{R}) = 2 \int_{C_{MM}^{\ell}} I_{MM}^{\ell}(\overline{R}')G_d(\overline{R},\overline{R}')d\ell' + 2 \int_{C_{MM}^{S}} I_{MM}^{S}(\overline{R}')G_d(\overline{R},\overline{R}')d\ell'
$$

$$
+ 2 \int_{C^S} J_{op}^{S}(\overline{R}')G_d(\overline{R},\overline{R}')d\ell' \quad (5.28)
$$

and

$$
I_{MM}^{S}(\overline{R}) = 2 \int_{C_{MM}^{\ell}} I_{MM}^{\ell}(\overline{R}')G_d(\overline{R},\overline{R}')d\ell' + 2 \int_{C_{MM}^{S}} I_{MM}^{S}(\overline{R}')G_d(\overline{R},\overline{R}')d\ell' \quad (5.29)
$$

where

$$
G_d(\overline{R},\overline{R}') = - \frac{\beta}{4j} \frac{|\overline{R}-\overline{R}'|}{2a} H_1^{(2)}(\beta|\overline{R}-\overline{R}'|) \quad . \quad (5.30)
$$

Substitution of Equation (5.29) in Equation (5.28) leads to

$$
I_{MM}^{\ell}(\overline{R}) = 2 \int_{C_{MM}^{\ell}} I_{MM}^{\ell}(\overline{R}')G_d(\overline{R},\overline{R}')d\ell'
$$

$$+ 4 \int_{C_{MM}^S} \int_{C_{MM}^{\ell}} I_{MM}^{\ell}(\overline{R}')G_d(\overline{R}'',\overline{R}')G_d(\overline{R},\overline{R}'')d\ell'd\ell''$$

$$+ 4 \int_{C_{MM}^S} \int_{C_{MM}^S} I_{MM}^S(\overline{R}')G_d(\overline{R}'',\overline{R}')G_d(\overline{R},\overline{R}'')d\ell'd\ell''$$

$$+ 2 \int_{C^S} J_{op}^S(\overline{R}')G_d(\overline{R},\overline{R}')d\ell' \quad . \tag{5.31}$$

If we substitute Equation (5.29) into Equation (5.31) repeatedly, we will have an infinite number of multiple integral terms. For an approximation, we ignore all multiple integrals higher than double integrals. This approximation can be justified by noting that the dominant terms in Equation (5.31) are the first and last terms. Therefore Equation (5.31) can be reduced to

$$I_{MM}^{\ell}(\overline{R}) \simeq 2 \int_{C_{MM}^{\ell}} I_{MM}^{\ell}(\overline{R}')G_d(\overline{R},\overline{R}')d\ell'$$

$$+ 4 \int_{C_{MM}^S} \int_{C_{MM}^{\ell}} I_{MM}^{\ell}(\overline{R}')G_d(\overline{R}'',\overline{R}')G_d(\overline{R},\overline{R}'')d\ell'd\ell''$$

$$+ 2 \int_{C^S} J_{op}^S(\overline{R}')G_d(\overline{R},\overline{R}')d\ell' \quad . \tag{5.32}$$

74

$$= 2 \int_{C^S} J_{op}^S(\overline{R}')G_d(\overline{R}_m,\overline{R}')d\ell'$$

$$m=1,2,3,\ldots,N. \hspace{3cm} (5.36)$$

If we represent Equation (5.36) in the form of

$$[Z_{mn}^\ell][I_n^\ell] = [V_m^\ell] \hspace{1cm} m,n,=1,2,\ldots,N, \hspace{2cm} (5.37)$$

we have the impedance matrix $[Z_{mn}^\ell]$ whose elements are given by

$$Z_{mn}^\ell = P(\overline{R}_m-\overline{R}_n) - 2\, G_d(\overline{R}_m,\overline{R}_n)\,\Delta\ell$$

$$- 4 \int_{C_{MM}^S} G_d(\overline{R}',\overline{R}_n)G_d(\overline{R}_m,\overline{R}')\Delta\ell d\ell' \quad . \hspace{1.5cm} (5.38)$$

Also the elements of $[V_m^\ell]$ are determined from

$$V_m^\ell = 2 \int_{C^S} J_{op}^S(\overline{R}')G_d(\overline{R}_m,\overline{R}')d\ell' \quad . \hspace{2cm} (5.39)$$

5.4 Numerical Results

We divide the circumference of the cylinder into 120 sub-intervals for the various numerical calculations which follow. The total extent of the MM-region on the lit surface, C_{MM}^ℓ, was 60° in angle, and 20 pulse basis functions in the point-matching technique were used

to obtain the current in the MM-region. Our results (marked by + in all data) were compared with the exact solutions (marked by the solid lines). Usually the second or the third order approximations were enough for acceptable results. Also all results were obtained with the constant C_0 given in Equation (5.27), which was noted by $C_0 \neq 1$ in the figures to follow.

Figures 5.5 to 5.8 show the magnitude and phase of the surface currents on the circular cylinders of 0.2λ to 5.7λ radii. It is seen that agreement with the exact currents are quite good regardless of the cylinder size. By comparing Figure 5.9 with Figure 5.10, which show the current results on a 5.2λ circular cylinder, respectively with $C_{MM}^{\ell}=30^0$ and $C_{MM}^{\ell}=120^0$, we can see the effect of the extent of the MM-region on the surface currents. It is shown that the surface currents are affected very little by the size of C_{MM}^{ℓ}, which is a very desirable feature of this method. However, it will be seen that as C_{MM}^{ℓ} is increased, a slightly better result is obtained.

The effect of the constant C_0 is shown by Figures 5.11 to 5.14. The results in Figures 5.11 and 5.12 were obtained with a circular cylinder of the 4.8λ radius. We see that a little improvement was made with the constant C_0. However, for the radius of 3.0λ, the ninth order approximation gave the results in Figures 5.13 and 5.14, where it is clearly seen that the constant C_0 provides a great improvement in the magnitude and a little improvement in the phase of the surface current. We realize that the radius of 4.8λ corresponds to a non-resonant frequency and that the radius of 3.0λ is near a resonance

77

mode. For the geometries corresponding to the resonant frequencies, the higher order approximations are shown to be needed to obtain acceptable results.

Recently, several methods such as the combined source, combined field, and hybrid methods have been presented to solve the interior resonance problem. However, it seems that any of these methods are difficult to apply to our method because we use the iteration technique for $\overline{J}_{op}^{\ell}(\overline{R})$ and $\overline{J}_{op}^{S}(\overline{R})$, which needs a proper initial starting current.

Actually the interior resonance does not affect the surface current on a circular cylinder so seriously. Although we obtained the results for the cylinders of up to the radius of 5.7λ, the method does not have difficulties for the larger cylinders. Also there are no difficulties in this method for the cylinders of radii smaller than 0.2λ.

Figure 5.5.   Current on a circular cylinder for
a=0.2λ, C_{MM}^{ℓ}=60^0,   and $C_0 \neq 1$.

Figure 5.6. Current on a circular cylinder for
$a=1.2\lambda$, $C^{\ell}_{MM}=60^{0}$, and $C_{0}\neq 1$.

80

Figure 5.7. Current on a circular cylinder for
$a=3.2\lambda$, $C_{MM}^{\ell}=60^{\circ}$, $C_{o}\neq 1$.

Figure 5.8. Current on a circular cylinder for $a=5.7\lambda$, $C_{MM}^{\ell}=60°$, and $C_o \neq 1$.
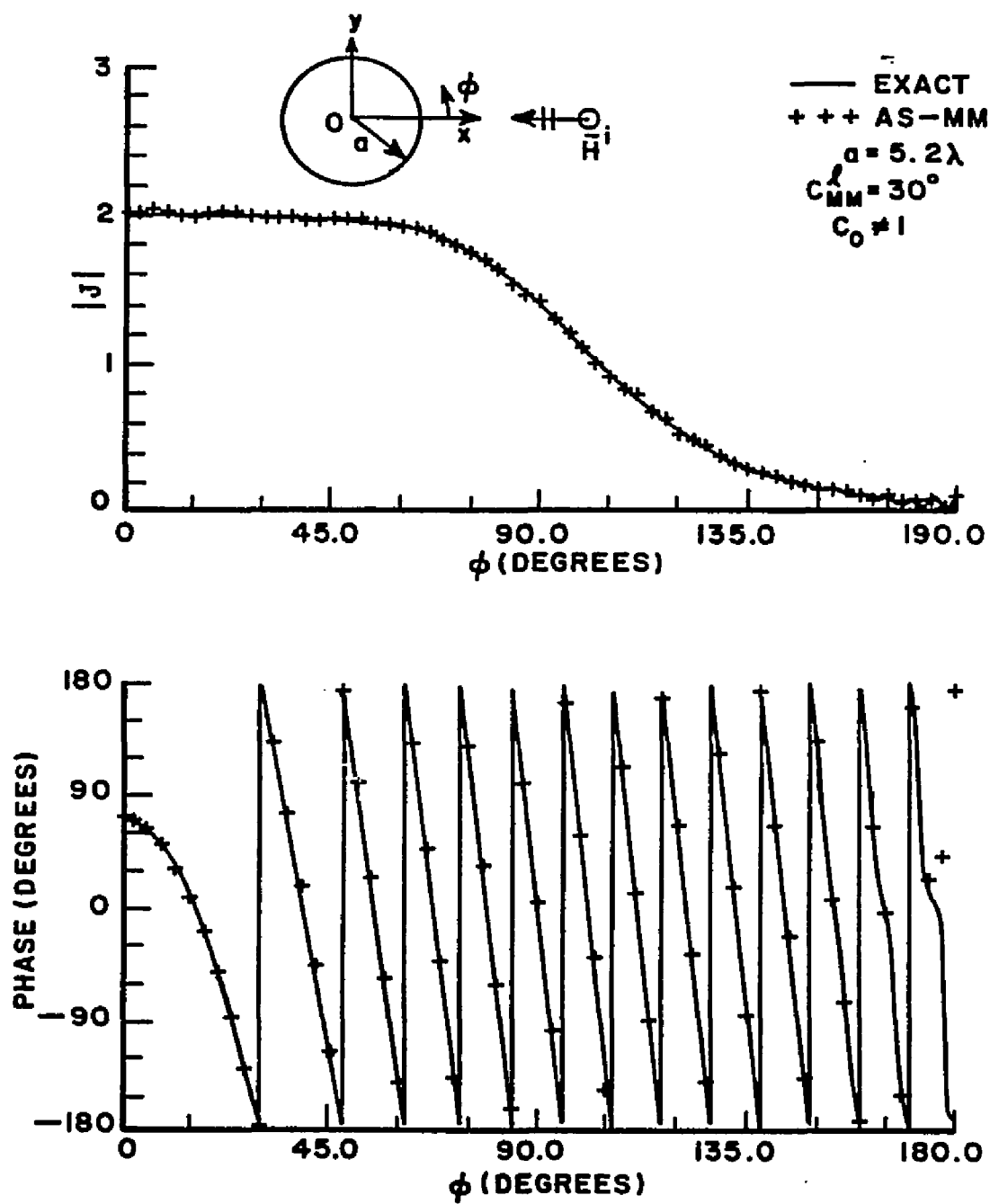
Figure 5.9. Current on a circular cylinder for
a=5.2λ, $C_{MM}^{\ell}=30°$, and $C_0 \neq 1$.
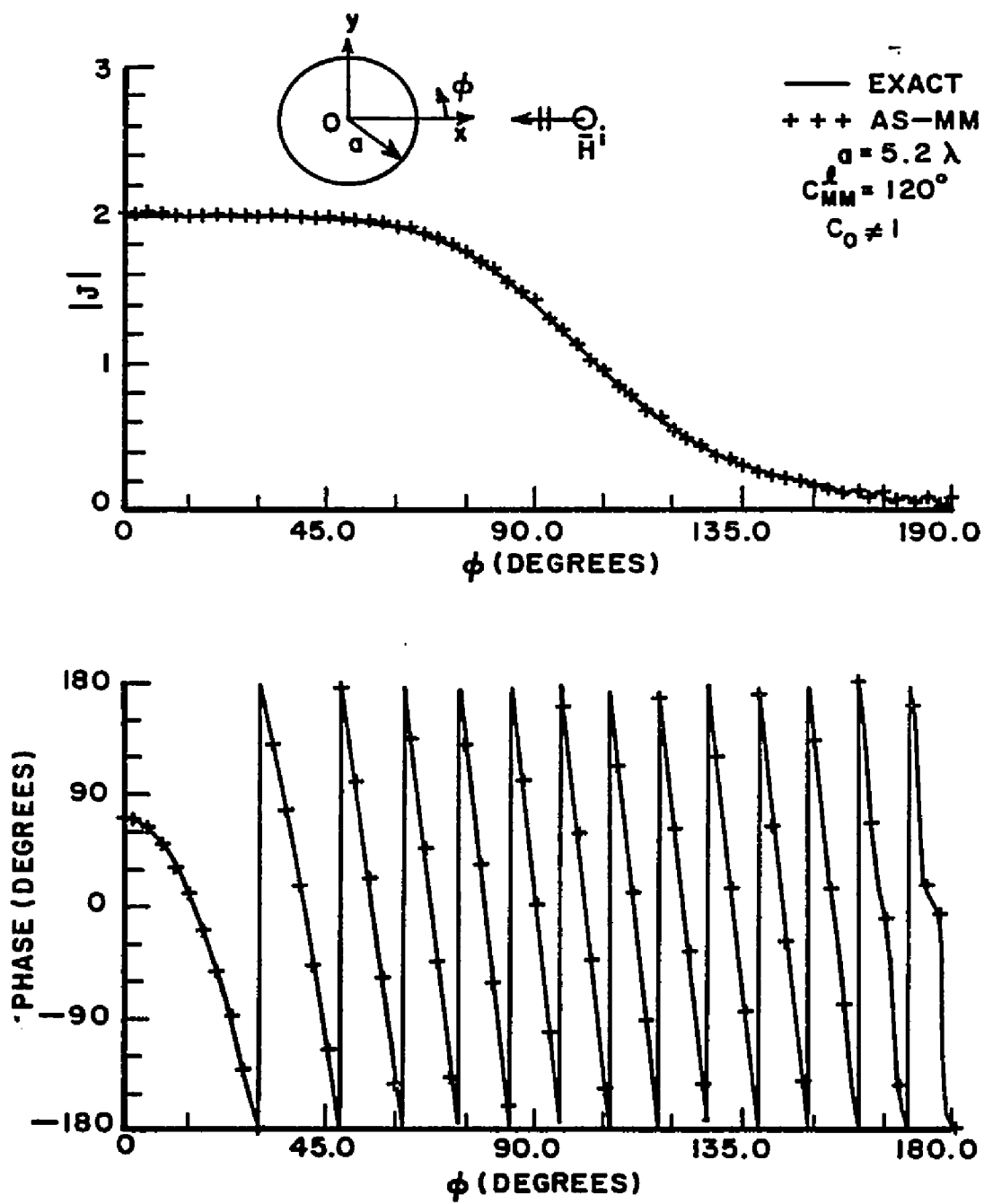
Figure 5.10. Current on a circular cylinder for
$a=5.2\lambda$, $C^{\ell}_{MM}=120^{o}$, and $C_{o}\neq1$.

84
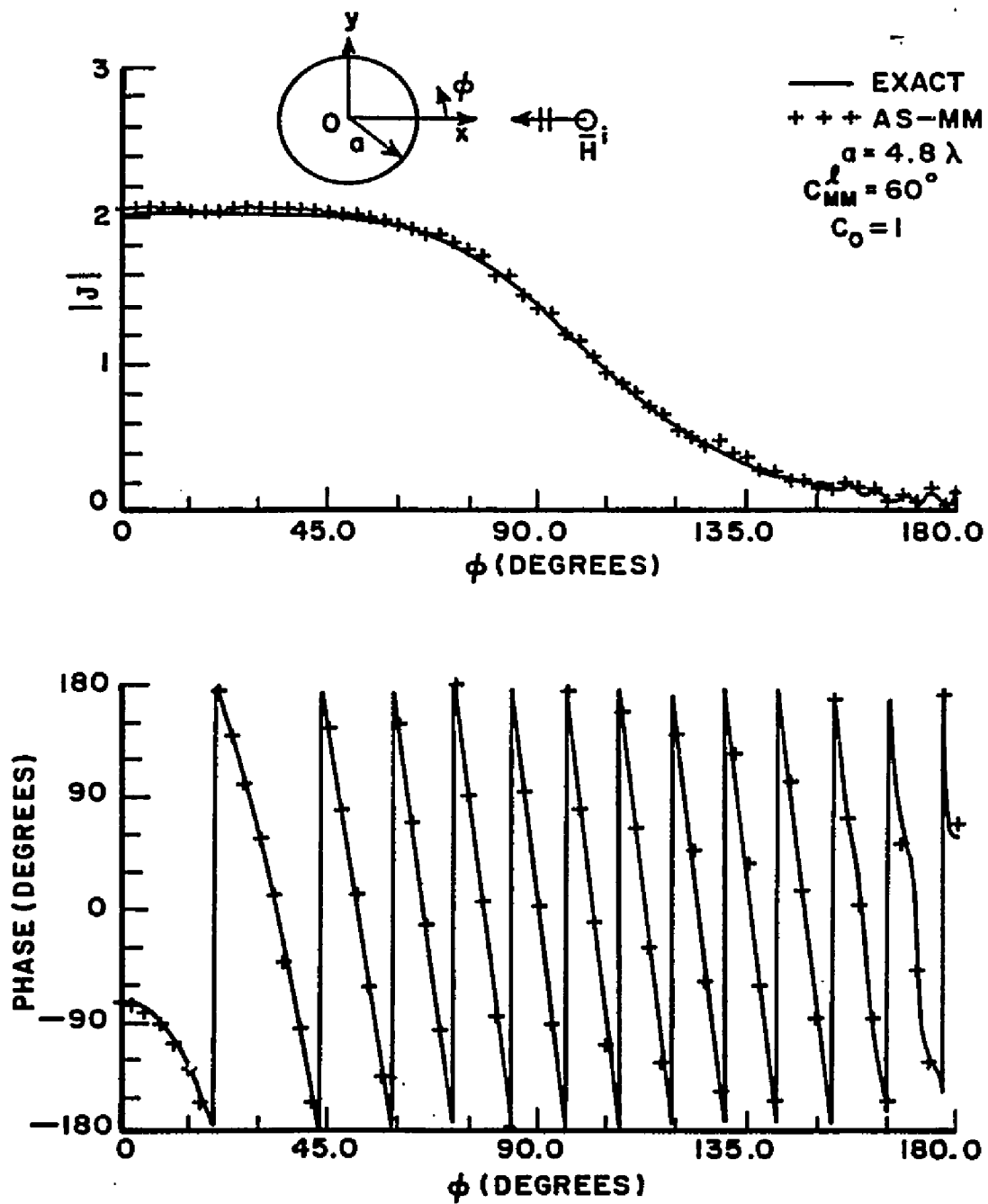
Figure 5.11. Current on a circular cylinder for
$a=4.8\lambda$, $C_{MM}^{\ell}=60^{o}$, and $C_{o}=1$.
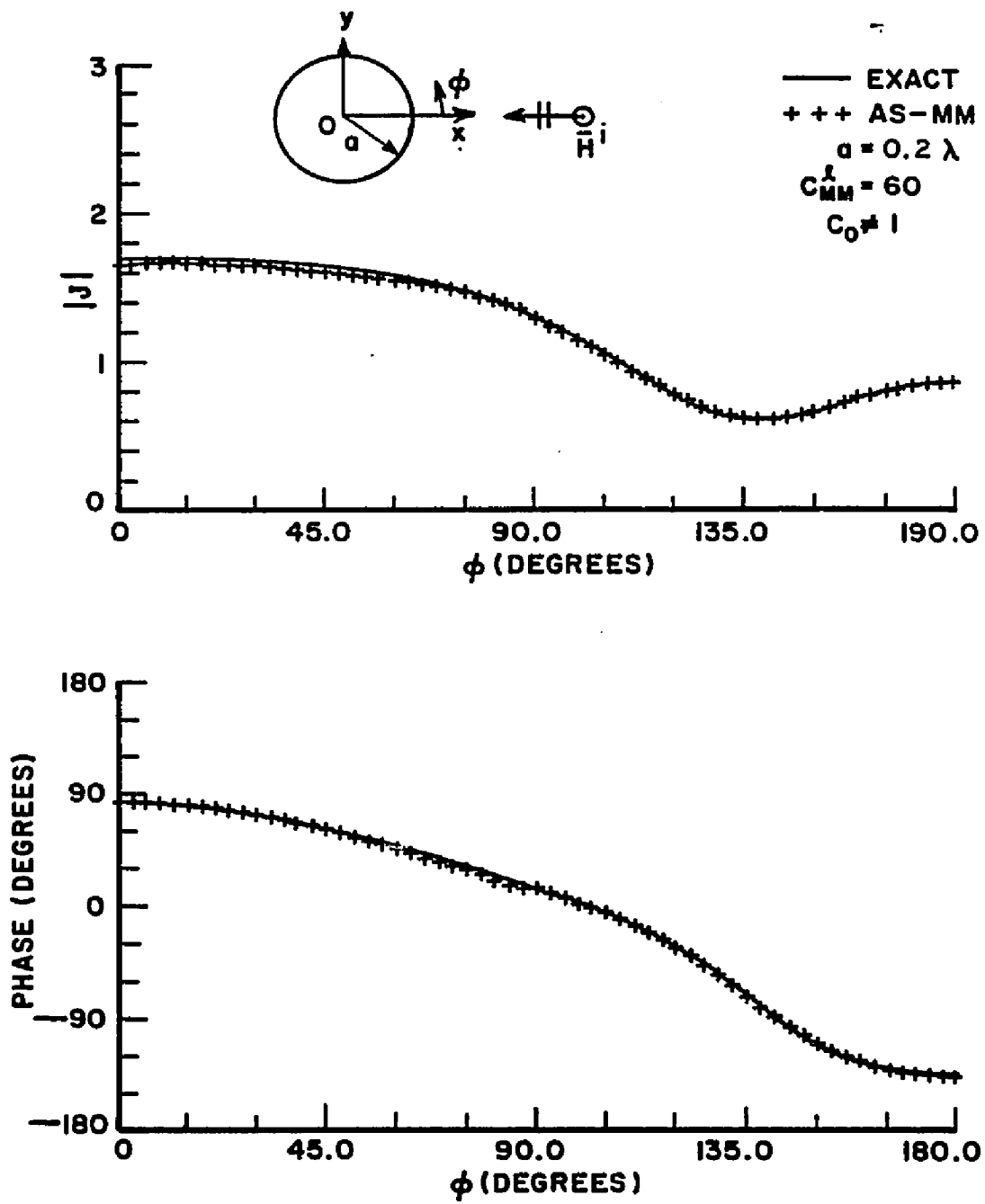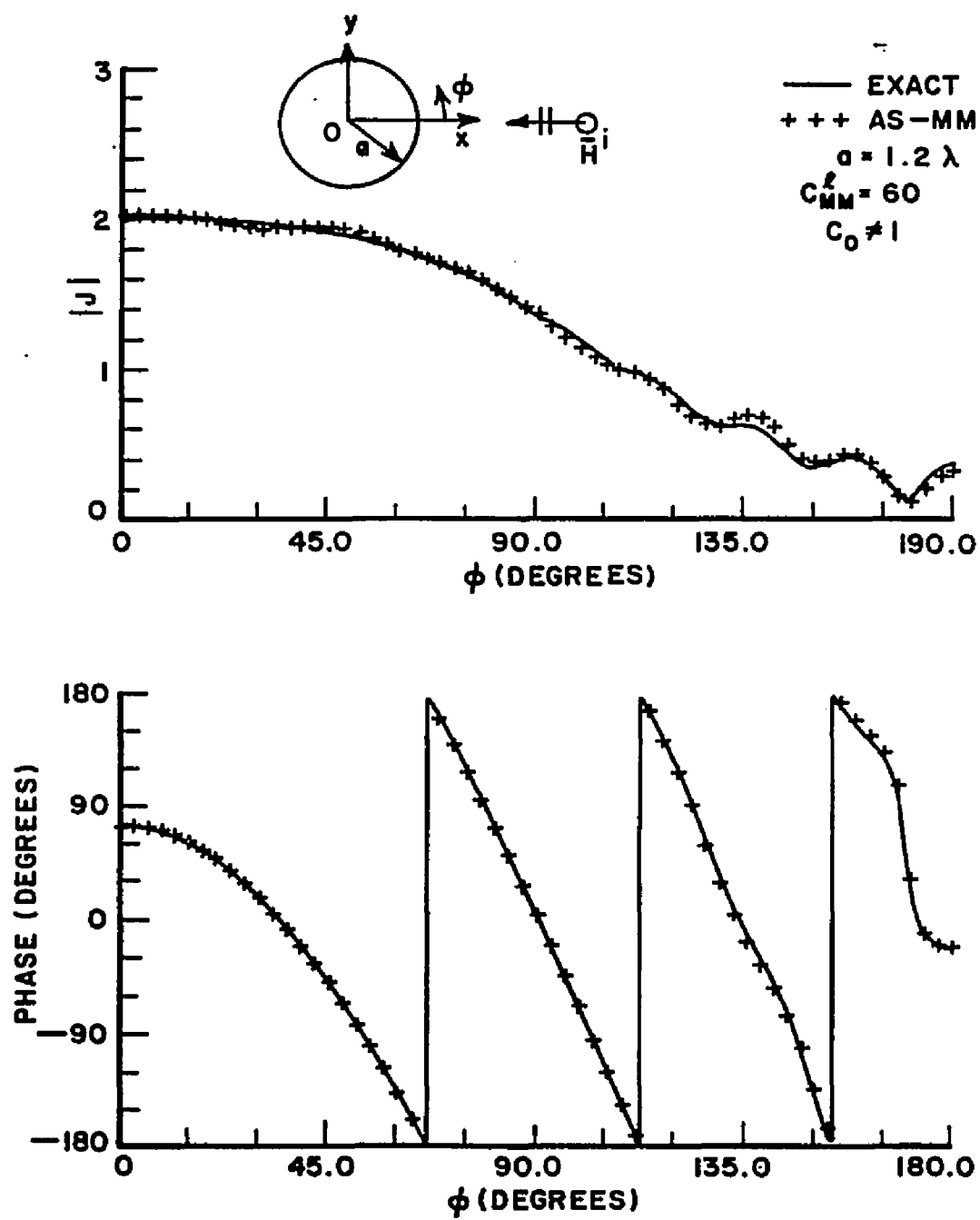
85
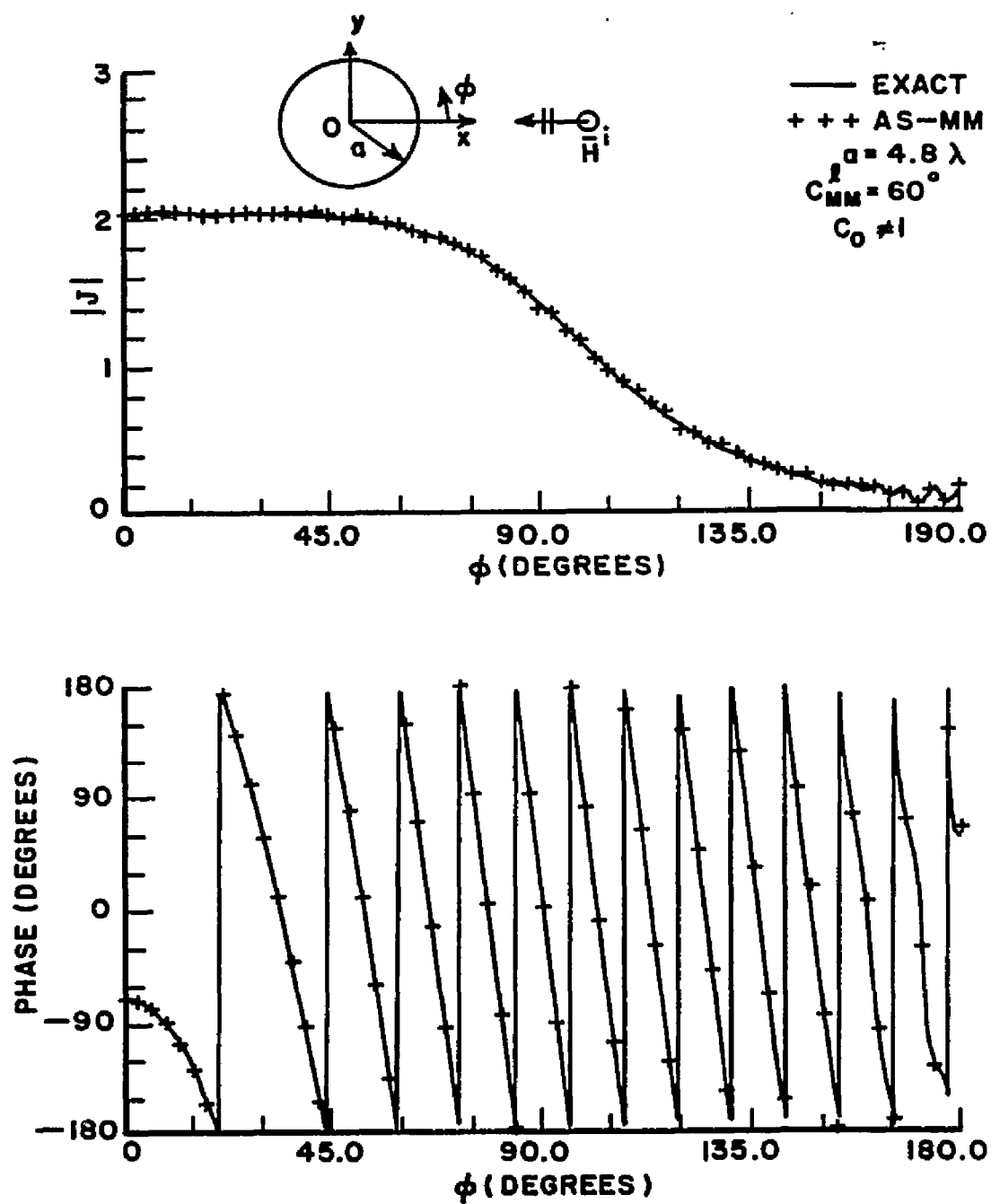
Figure 5.12. Current on a circular cylinder for
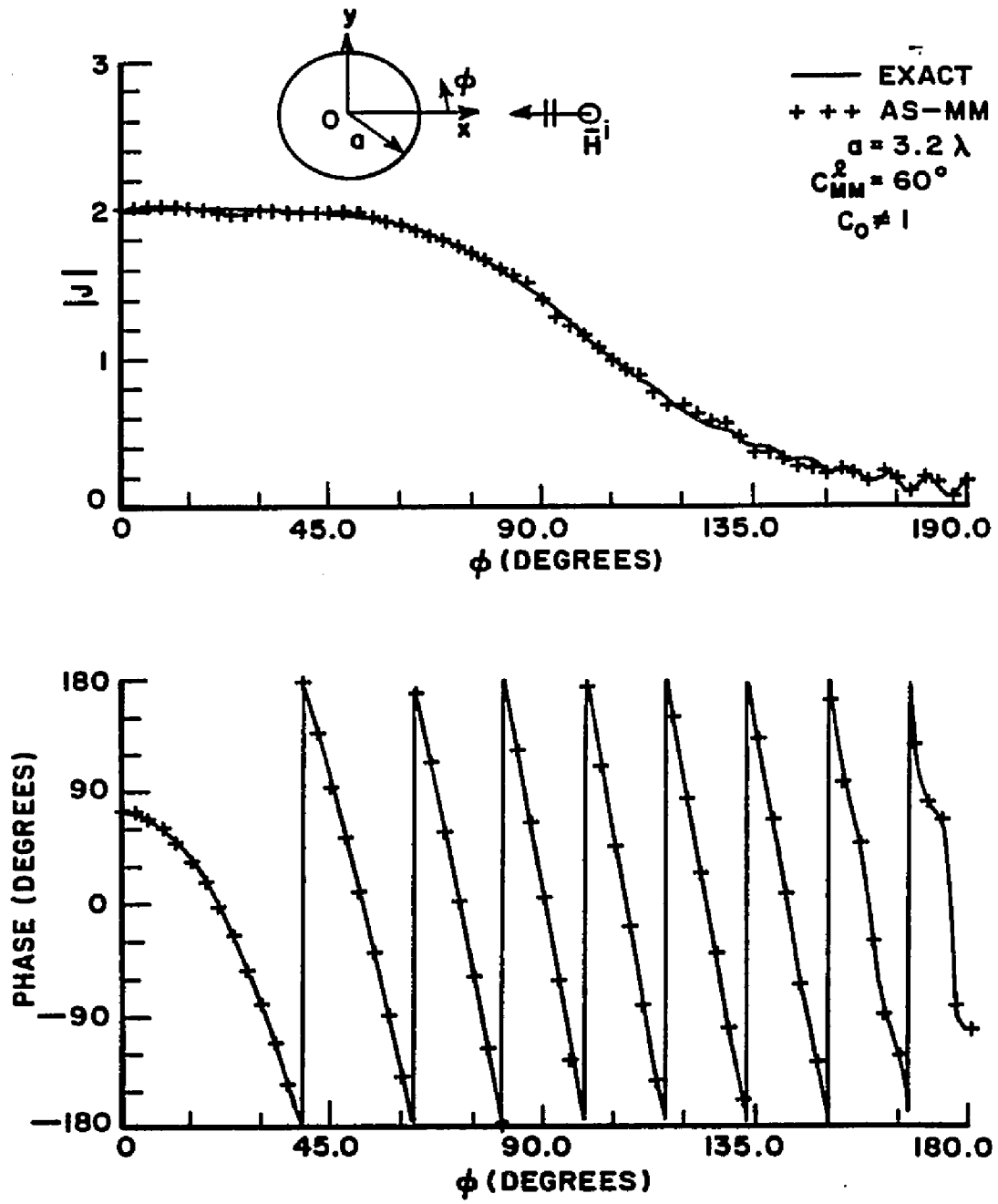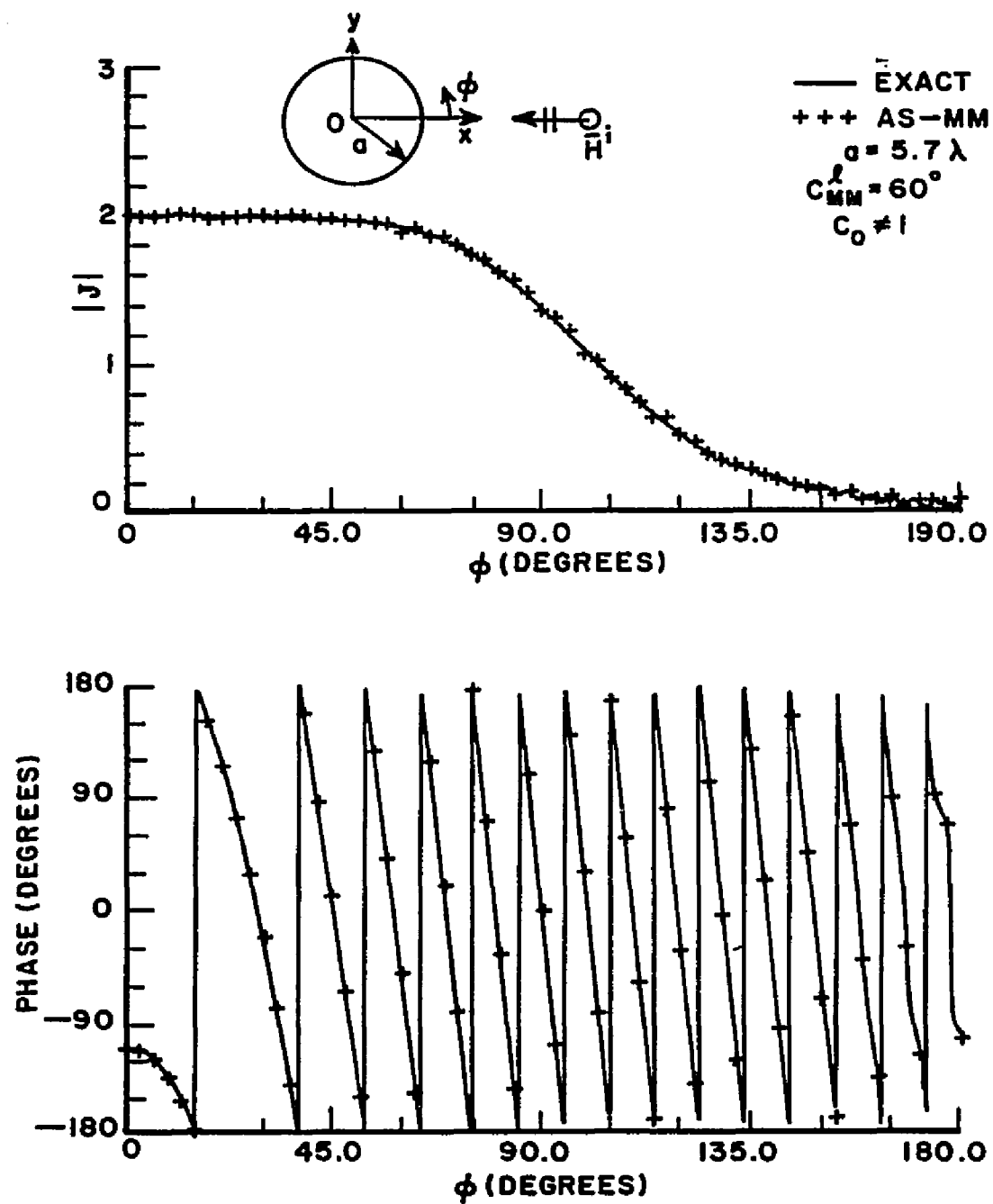$a=4.8\lambda$, $C_{MM}^{\ell}=60^{O}$, and $C_{o}\neq1$.
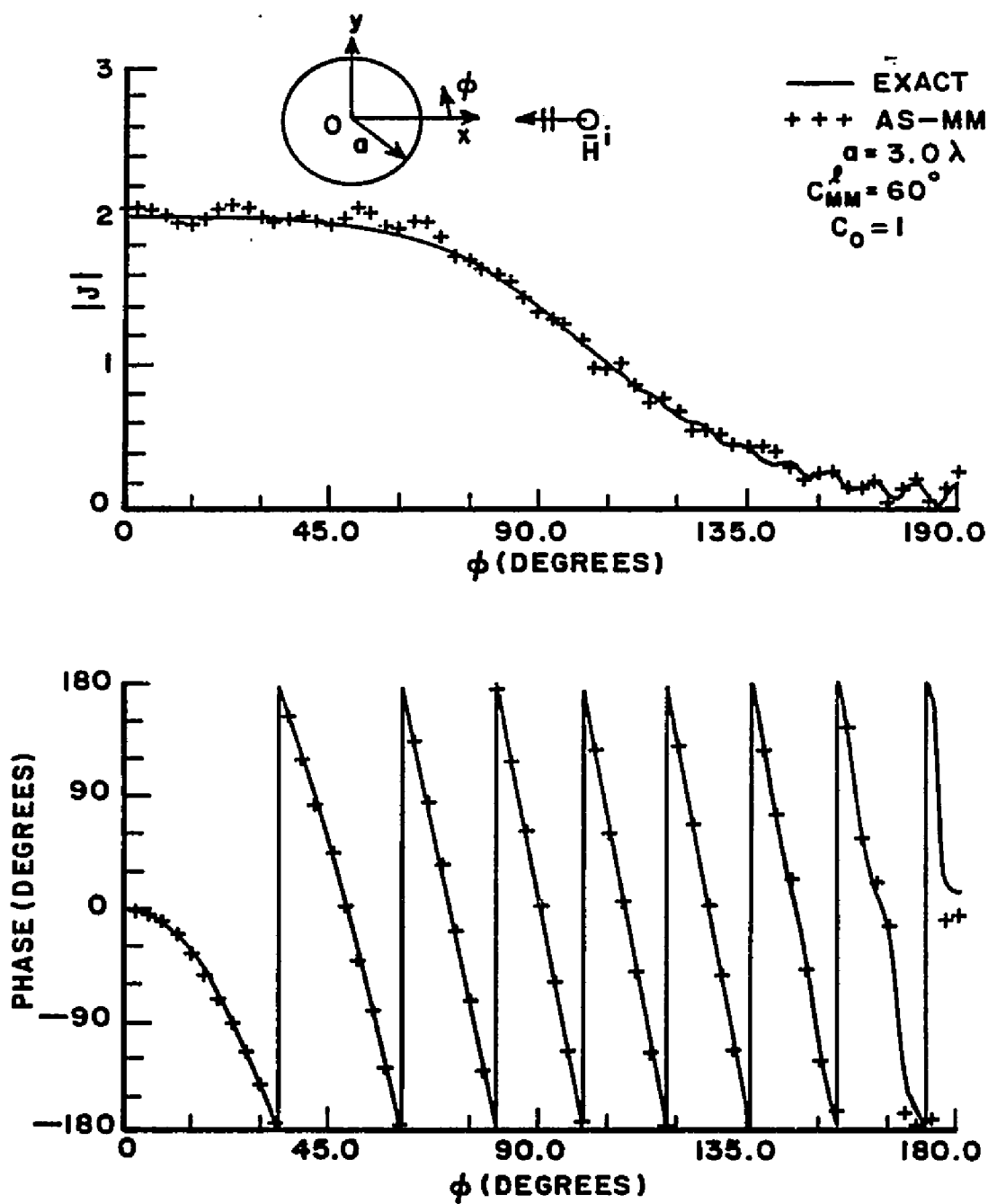
Figure 5.13. Current on a circular cylinder for $a=3.0\lambda$, $C_{MM}^{\ell}=60^{\circ}$, and $C_o=1$.
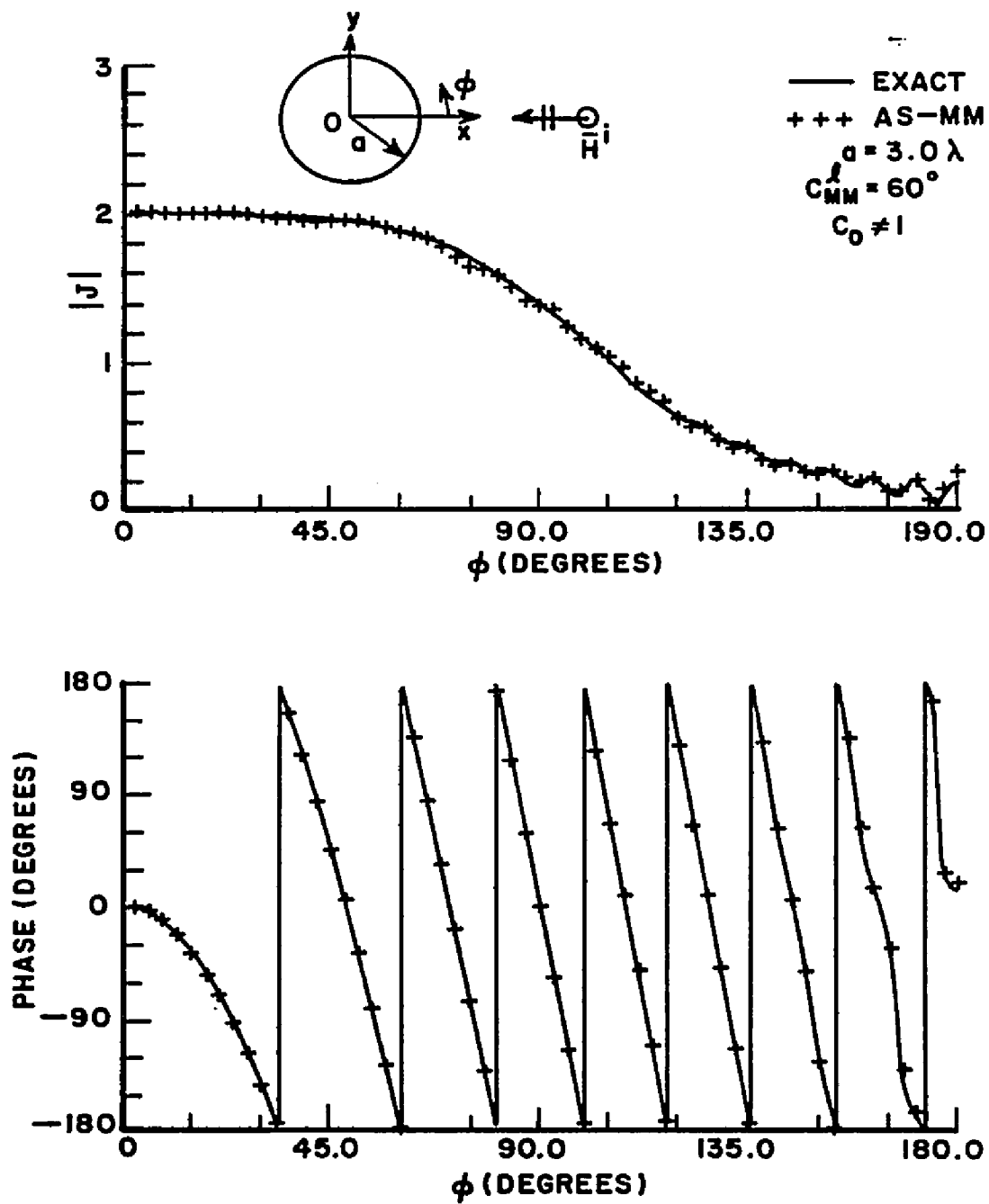
Figure 5.14.   Current on a circular cylinder for
a=3.0λ, C_{MM}^{ℓ}=60°, and C_o≠1.

CHAPTER VI
SPHERE

6.1 Integral Equations

So far, we have considered conductors only in two-dimensions where integrals over the surface reduced to line integrals. In this chapter, we will consider a three dimensional problem, that of a perfectly conducting sphere.

Since the integration must be performed over the surface of the sphere, a longer computer running time and increased memory storage will be needed for the three-dimensional problem than for the two-dimensional one. However, by using the symmetric property which a body of revolution has, we can decrease the computing time very greatly and also the computer memory storage needed.

The general equations we derived in Chapter II cannot be reduced to a simpler form for a sphere, but instead it will be useful to derive integral equations for the surface currents in the E- and H-planes. The geometry in which a sphere is illuminated by a plane wave is shown in Figure 6.1. Let the incident magnetic field be xpolarized and traveling to the negative z direction as shown in Figure 6.1. At an observation point P the induced surface current $\vec{J}(\vec{R})$ can be separated into two components $\hat{\theta}J_\theta(\vec{R})$ and $\hat{\phi}J_\phi(\vec{R})$, where $\hat{\theta}$ and $\hat{\phi}$ represent the unit vectors in the directions of θ and ϕ, respectively.
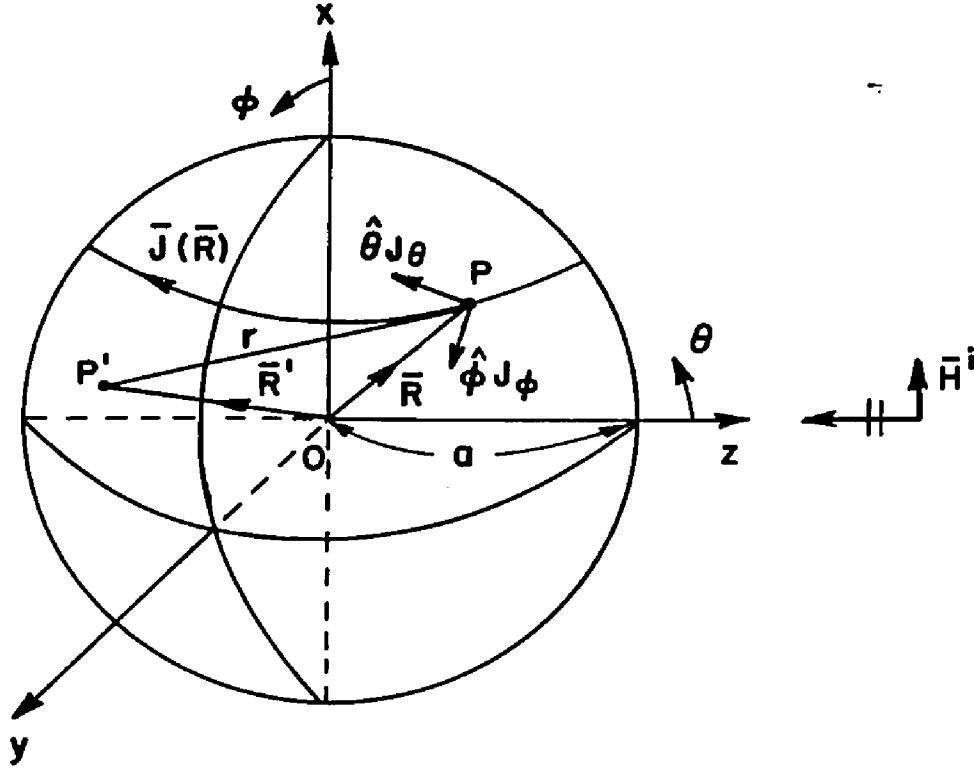
Figure 6.1   Geometry of a sphere illuminated by the x-polarized
plane wave.

Consider the magnetic field integral equation given by

$$\bar{J}(\bar{R}) = \bar{J}^i(\bar{R}) + 2\hat{n}x \int_S \bar{J}(\bar{R}')x\nabla'G(r)ds' \tag{6.1}$$

where

$$\bar{J}^i(\bar{R}) = 2\hat{n}x\bar{H}^i(\bar{R}) \quad . \tag{6.2}$$

Since $\bar{J}^i(\bar{R})$ and $\bar{J}(\bar{R})$ are composed of the $\hat{\theta}$ and $\hat{\phi}$ components, they can be written as

$$\vec{J}^i(\vec{R}) = \hat{\theta} \; J^i_\theta(\vec{R}) + \hat{\phi} \; J^i_\phi(\vec{R}) \tag{6.3}$$

and

$$\vec{J}(\vec{R}) = \hat{\theta} J_\theta(\vec{R}) + \hat{\phi} J_\phi(\vec{R}) \quad . \tag{6.4}$$

The currents $J_\theta(\vec{R})$ and $J_\phi(\vec{R})$ can be obtained, respectively by $\hat{\theta}\cdot\vec{J}(\vec{R})$ and $\hat{\phi}\cdot\vec{J}(\vec{R})$, which are given by

$$J_\theta(\vec{R}) = J^i_\theta(\vec{R}) + 2\hat{\theta}\cdot\hat{n} \; x \; \oint_S \vec{J}(\vec{R}')x\nabla'G(r)ds' \tag{6.5}$$

$$J_\phi(\vec{R}) = J^i_\phi(\vec{R}) + 2\hat{\phi}\cdot\hat{n} \; x \; \oint_S \vec{J}(\vec{R}')x\nabla'G(r)ds' \tag{6.6}$$

By using the vector identity $\vec{A}\cdot\vec{B}x\vec{C} = \vec{C}\cdot\vec{A}x\vec{B}$ and noting that $\hat{\theta}x\hat{n}=-\hat{\phi}$ and $\hat{\phi}x\hat{n}=\hat{\theta}$ on the spherical surface, we can rewrite Equations (6.5) and (6.6) as

$$J_\theta(\vec{R}) = J^i_\theta(\vec{R}) - 2 \oint_S \hat{\phi}\cdot\vec{J}(\vec{R}')x\nabla'G(r)ds' \tag{6.7}$$

$$J_\phi(\vec{R}) = J^i_\phi(\vec{R}) + 2 \oint_S \hat{\theta}\cdot\vec{J}(\vec{R}')x\nabla'G(r)ds' \tag{6.8}$$

Substituting Equation (6.4) into Equations (6.7) and (6.8), we obtain

$$J_\theta(\vec{R}) = J^i_\theta(\vec{R}) -2 \oint_S \left[\hat{\phi}\cdot\hat{\theta}'J_\theta(\vec{R}')+\hat{\phi}\cdot\hat{\phi}'J_\phi(\vec{R}') \right] x\nabla'G(r)ds' \tag{6.9}$$

$$J_\phi(\overline{R}) = J_\phi^i(\overline{R}) + 2 \oint_S \left[\hat{\theta} \cdot \hat{\theta}' J_\theta(\overline{R}') + \hat{\theta} \cdot \hat{\phi}' J_\phi(\overline{R}') \right] \times \nabla' G(r) ds' \qquad (6.10)$$

where $\hat{\theta}'$ and $\hat{\phi}'$ are the unit vectors, respectively in the θ and ϕ directions at a source point P'. Let

$$\nabla' G(r) = \hat{r}' G_s(r) \qquad (6.11)$$

and

$$G_s(r) = - \left(j\beta + \frac{1}{r} \right) \frac{e^{-j\beta r}}{4\pi r} . \qquad (6.12)$$

Using the notations given by

$$C_{\theta\theta}(r) = \hat{\phi} \cdot \hat{\theta}' \times \hat{r}' \, G_s(r) \qquad (6.13)$$

$$C_{\theta\phi}(r) = \hat{\phi} \cdot \hat{\phi}' \times \hat{r}' \, G_s(r) \qquad (6.14)$$

$$C_{\phi\theta}(r) = \hat{\theta} \cdot \hat{\theta}' \times \hat{r}' \, G_s(r) \qquad (6.15)$$

$$C_{\phi\phi}(r) = \hat{\theta} \cdot \hat{\phi}' \times \hat{r}' \, G_s(r) \qquad (6.16)$$

we can express Equations (6.9) and (6.10) as

$$J_\theta(\overline{R}) = J_\theta^i(\overline{R}) - 2 \oint_S \left[C_{\theta\theta}(r) J_\theta(\overline{R}') + C_{\theta\phi}(r) J_\phi(\overline{R}') \right] ds' \qquad (6.17)$$

and

$$J_\phi(\overline{R}) = J_\phi^i(\overline{R}) + 2 \oint_S \left[C_{\phi\theta}(r) J_\theta(\overline{R}') + C_{\phi\phi}(r) J_\phi(\overline{R}') \right] ds' \quad . \qquad (6.18)$$

92

After calculating the vectors in Equations (6.13) to (6.16), we can obtain the following results

$$C_{\theta\theta}(r) = C_{\phi\phi}(r) = \frac{a}{r}\left[\sin\theta'\sin\theta+\cos(\phi-\phi')(\cos\theta\cos\theta'-1)\right]G_s(r)$$

(6.19)

and

$$C_{\theta\phi}(r) = -C_{\phi\theta}(r) = \frac{a}{r}(\cos\theta-\cos\theta')\sin(\phi-\phi')G_s(r).$$

(6.20)

where r is given by

$$r = a\sqrt{2\left[1-\sin\theta\sin\theta'\cos(\phi-\phi')-\cos\theta\cos\theta'\right]}$$

(6.21)

and a is the sphere radius.

Since $\overline{H}^i(\overline{R})$ is x-polarized, $J_\theta^i(\overline{R})$ and $J_\phi^i(\overline{R})$ are given by

$$J_\theta^i(\overline{R}) = 2\sin\phi\ e^{j\beta a\cos\theta}$$

(6.22)

$$J_\phi^i(\overline{R}) = 2\cos\theta\cos\phi\ e^{j\beta a\cos\theta}.$$

(6.23)

Equations (6.17) to (6.20) are not very useful for practical numerical calculations since so many observation points are involved in them. Therefore we will derive integral equations having only the E- and H-plane currents as unknowns. For this purpose, if we represent the E- and H-plane currents of $\overline{J}^i(\overline{R})$ as $J_\theta^i(\theta)$ and $J_\phi^i(\theta)$, respectively, Equations (6.22) and (6.23) can be expressed as

93

$$J_\theta^i(\overline{R}) = J_\theta^i(\theta)\sin\phi \tag{6.24}$$

$$J_\phi^i(\overline{R}) = J_\phi^i(\theta)\cos\phi \tag{6.25}$$

where $J_\theta^i(\theta)$ and $J_\phi^i(\theta)$ are independent on the angle ϕ and are given by

$$J_\theta^i(\theta) = 2 \, e^{j\beta a\cos\theta} \tag{6.26}$$

$$J_\phi^i(\theta) = 2 \cos\theta \, e^{j\beta a\cos\theta} \tag{6.27}$$

Also the relationships of Equations (6.24) and (6.25) are valid for $J_\theta(\overline{R})$ and $J_\phi(\overline{R})$. Thus,

$$J_\theta(\overline{R}) = J_\theta(\theta) \, \sin\phi \tag{6.28}$$

$$J_\phi(\overline{R}) = J_\phi(\theta) \, \cos\phi \, . \tag{6.29}$$

Equations (6.28) and (6.29) are useful properties which can be applied to an arbitrary conducting body of revolution when $\overline{H}^i(\overline{R})$ is x-polarized. Using Equations (6.24), (6.25), (6.28) and (6.29) in Equations (6.17) and (6.18), we can obtain

$$J_\theta(\theta) = J_\theta^i(\theta) - 2 \int_S \left[C_1(r_1)J_\theta(\theta') + C_2(r_1)J_\phi(\theta') \right] ds' \tag{6.30}$$

and

$$J_\phi(\theta) = J_\phi^i(\theta) + 2 \int_S \left[D_1(r_2)J_\theta(\theta') + D_2(r_2)J_\phi(\theta') \right] ds' \tag{6.31}$$

94

where

$$C_1(r_1) = \frac{aG_s(r_1)}{r_1}\left[\sin\theta\sin\theta'+\sin\phi'(\cos\theta\cos\theta'-1)\right]\sin\phi' \qquad (6.32)$$

$$C_2(r_1) = \frac{aG_s(r_1)}{r_1}(\cos\theta-\cos\theta')\cos^2\phi' \qquad (6.33)$$

$$D_1(r_2) = \frac{aG_s(r_2)}{r_2}(\cos\theta-\cos\theta')\sin^2\phi' \qquad (6.34)$$

$$D_2(r_2) = \frac{aG_s(r_2)}{r_2}\left[\sin\theta\sin\theta'+\cos\phi'(\cos\theta\cos\theta'-1)\right]\cos\phi' \quad . \qquad (6.35)$$

Also r_1 and r_2 are given by

$$r_1 = a\sqrt{2\,(1-\sin\theta\sin\theta'\sin\phi'-\cos\theta\cos\theta')} \qquad (6.36)$$

$$r_2 = a\sqrt{2\,(1-\sin\theta\sin\theta'\cos\phi'-\cos\theta\cos\theta')} \quad . \qquad (6.37)$$

If the currents $J_\theta(\theta)$ and $J_\phi(\theta)$ are known, the surface currents at any arbitrary point on the sphere can be readily determined from Equations (6.28) and (6.29). Equations (6.30) and (6.31) can be applied directly to any equations we derived in Chapter II by adding proper subscript and superscript.

If we look at Equations (6.32) to (6.37), we can easily see that $D_1(r_2)$ and $D_2(r_2)$ can be obtained, respectively from $C_2(r_1)$ and $C_1(r_1)$ just replacing ϕ' by $90^\circ \pm \phi'$. This characteristic will make the computer program simple.

95

6.2 Consideration of the Singularity Patch

For reasons we discussed in Section 5.2 of Chapter V, we need to consider the singularity problem. We will use a part of the result of Section 5.2 to derive the proper constants for the sphere. If we rewrite Equation (5.13) here again with the different definition of $\nabla'G(r)$ given by Equation (6.11), the equation will be

$$\hat{n}\times\bar{H}^i(\bar{R}) + \hat{n} \times \int_{S-S_f} \bar{J}(\bar{R}')\times\nabla'G(r)ds' + \bar{J}_1(\bar{R}) + \bar{J}_2(\bar{R}) = 0 \qquad (6.38)$$

where $\bar{J}_1(\bar{R})$ and $\bar{J}_2(\bar{R})$ are given in Equations (5.11) and (5.12), respectively.

By the similar procedure as done in Section 5.2, we can easily find $\bar{J}_1(\bar{R})$ in the three dimensional case, which is given by (see Appendix B)

$$\bar{J}_1(\bar{R}) = -\frac{1}{2} \bar{J}(\bar{R}) \quad . \qquad (6.39)$$

Now let us derive $\bar{J}_2(\bar{R})$ for the $\hat{\theta}$ and $\hat{\phi}$ components. Using the results of Equations (6.30) and (6.31), we can write $J_{2\theta}(\theta)$ and $J_{2\phi}(\phi)$ as

$$J_{2\theta}(\theta) = -2 \lim_{S_\epsilon \to 0} \int_{S_f-S_\epsilon} \left[C_1(r_1)J_\theta(\theta') + C_2(r_1)J_\phi(\theta') \right] ds' \qquad (6.40)$$

and

$$J_{2\phi}(\theta) = 2 \lim_{S_\epsilon \to 0} \int_{S_f-S_\epsilon} \left[D_1(r_2)J_\theta(\theta') + D_2(r_2)J_\phi(\theta') \right] ds' \qquad (6.41)$$

96

where $J_{2\theta}(\theta)$ and $J_{2\phi}(\theta)$ are the currents observed on the $\phi=90^O$ and $\phi=0^O$ lines, respectively.

Since the surface area S_f is small, we can make the following approximations for $J_{2\theta}(\theta)$ and $J_{2\phi}(\theta)$

$$\phi' \simeq \frac{\pi}{2} \qquad \text{on } S_f \qquad \text{for } J_{2\theta}(\theta) \tag{6.42}$$

$$\phi' \simeq 0 \qquad \text{on } S_f \qquad \text{for } J_{2\phi}(\theta) \quad . \tag{6.43}$$

Then using Equations (6.42) and (6.43), the approximations for $C_1(r_1)$, $C_2(r_1)$, $D_1(r_2)$, and $D_2(r_2)$ on S_f can be obtained as

$$C_1(r_1) \simeq -\frac{r_a}{2a} G_s(r_a) \qquad \text{on } S_f \tag{6.44}$$

$$C_2(r_1) \simeq 0 \qquad \text{on } S_f \tag{6.45}$$

and

$$D_1(r_2) \simeq 0 \qquad \text{on } S_f \tag{6.46}$$

$$D_2(r_2) \simeq -\frac{r_a}{2a} G_s(r_a) \qquad \text{on } S_f. \tag{6.47}$$

where

$$r_a \simeq a\sqrt{2(1-\sin\theta\sin\theta'-\cos\theta\cos\theta')} \qquad \text{on } S_f \qquad (6.48)$$

Substitutions of Equations (6.44) and (6.45) in Equation (6.40) and Equations (6.46) and (6.47) in Equation (6.41) yield

$$J_{2\theta}(\theta) \simeq -2 \lim_{S_\epsilon \to 0} \int_{S_f - S_\epsilon} (-\frac{r_a}{2a}) G_s(r_a) J_\theta(\theta') ds' \qquad (6.49)$$

$$J_{2\phi}(\theta) \simeq 2 \lim_{S_\epsilon \to 0} \int_{S_f - S_\epsilon} (-\frac{r_a}{2a}) G_s(r_a) J_\phi(\theta') ds' \quad . \qquad (6.50)$$

Also for the small surface area S_f, we can make the following approximations.

$$J_\theta(\theta') \simeq J_\theta(\theta) \qquad \text{on } S_f \qquad (6.51)$$

$$J_\phi(\theta') \simeq J_\phi(\theta) \qquad \text{on } S_f \quad . \qquad (6.52)$$

Then by substituting Equations (6.51) and (6.52) into Equations (6.49) and (6.50), we obtain

$$J_{2\theta}(\theta) \simeq -2 J_\theta(\theta) \lim_{S_\epsilon \to 0} \int_{S_f - S_\epsilon} (\frac{-r_a}{2a}) G_s(r_a) ds' \qquad (6.53)$$

98

$$J_{2\phi}(\theta) \simeq 2 J_\phi(\theta) \lim_{S_\epsilon \to 0} \int_{S_f - S_\epsilon} (\frac{-r_a}{2a}) G_s(r_a) ds' \quad . \tag{6.54}$$

Assuming that the patch S_f is a circular surface with the radius r_s, then we can obtain the following results from Equations (6.53) and (6.54).

$$J_{2\theta}(\theta) \simeq - S_0 J_\theta(\theta) \tag{6.55}$$

$$J_{2\phi}(\theta) \simeq S_0 J_\phi(\theta) \tag{6.56}$$

where

$$S_0 = \frac{1}{2j a \beta} \left[2 - (2 + j\beta r_s) e^{-j\beta r_s} \right] \quad . \tag{6.57}$$

Then from Equations (6.38), (5.11), (5.12), (6.55) and (6.56) we can obtain the following integral equations.

$$J_\theta(\theta) = S_\theta \ \hat{\theta} \cdot \left[2\hat{n} \times \overline{H}^i(\overline{R}) + 2\hat{n} \times \int_{S-S_f} \overline{J}(\overline{R}') \times \nabla' G(r) ds' \right]_{\phi = \frac{\pi}{2}} \tag{6.58}$$

$$J_\phi(\theta) = S_\phi \ \hat{\phi} \cdot \left[2\hat{n} \times \overline{H}^i(\overline{R}) + 2\hat{n} \times \int_{S-S_f} \overline{J}(\overline{R}') \times \nabla' G(r) ds' \right]_{\phi = 0} \tag{6.59}$$

99

or by using the results of Equations (6.30) and (6.31), we can express Equations (6.58) and (6.59) as

$$J_\theta(\theta) = S_\theta \left\{ J_\theta^i(\theta) - 2 \int_{S-S_f} \left[C_1(r_1) J_\theta(\theta') + C_2(r_1) J_\phi(\theta') \right] ds' \right\} \quad (6.60)$$

$$J_\phi(\theta) = S_\phi \left\{ J_\phi^i(\theta) + 2 \int_{S-S_f} \left[D_1(r_2) J_\theta(\theta') + D_2(r_2) J_\phi(\theta') \right] ds' \right\} \quad (6.61)$$

where

$$S_\theta = \frac{1}{1+S_0} \quad (6.62)$$

$$S_\phi = \frac{1}{1-S_0} \quad . \quad (6.63)$$

We see that as r_s approaches zero, S_θ and S_ϕ approach one. This means that if the sphere surface is divided into very many subpatches then the constants S_θ and S_ϕ will not affect the integral equations significantly. However, dividing the surface into many divisions may not be efficient for numerical calculations. By using the constants S_θ and S_ϕ we can provide the same effect as using a large number of divisions for numerical integration.

6.3   Impedance Matrix

In calculating the impedance matrix, the moment method region is set up around the shadow boundary making a ring form as shown in Figure 6.2. If we consider all points on S_{MM} as unknowns, the computer

storage may not handle the matrix because of too many unknowns. There-
fore we will use the results we have derived in Section 6.2 to obtain
the impedance matrix.
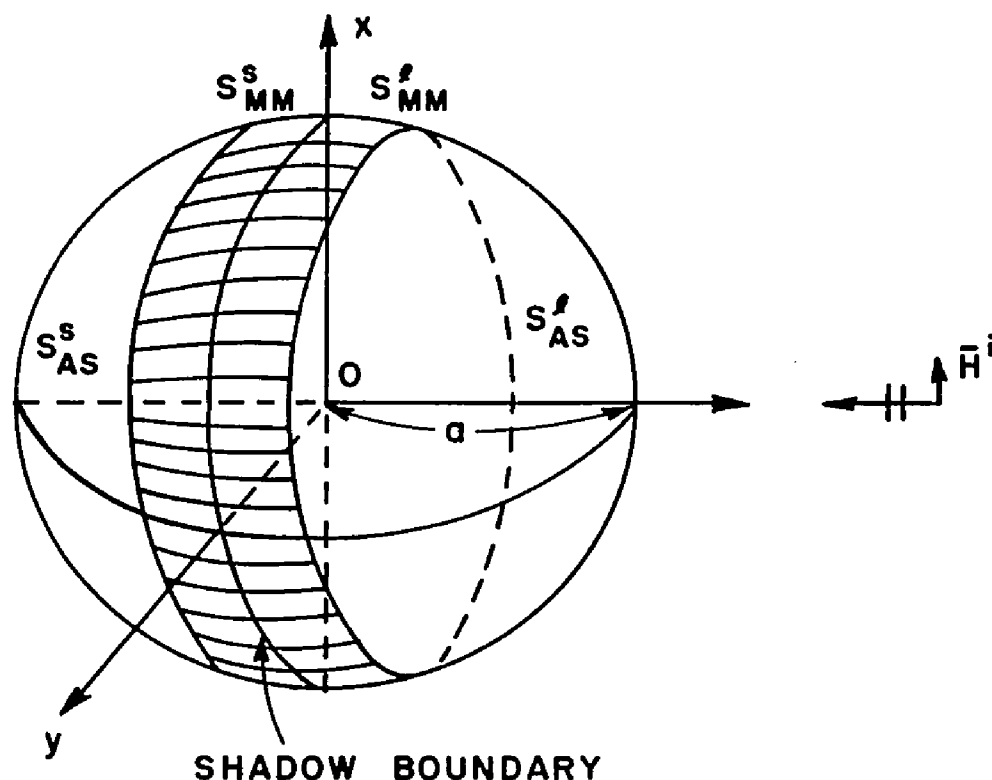
Figure 6.2. Surface divisions in a sphere.

Also since the equations for currents are involved with two
currents $J_\theta(\theta)$ and $J_\phi(\theta)$, the expressions for the impedance matrices
$Z_{\theta mn}$ and $Z_{\phi mn}$ will be very complicated and may not be useful for nu-
merical calculations. Therefore we will derive comparatively simple
approximate forms by ignoring all the terms that contribute insignif-
icantly to calculations. Let

$$I_{M\phi}^{\ell}(\theta) = 2 \int_{S_{MM}^{\ell}} \left[D_1(\theta;\theta',\phi')I_{M\theta}^{\ell}(\theta')+D_2(\theta;\theta',\phi')I_{M\phi}^{\ell}(\theta') \right]ds'$$

$$+ 2 \int_{S_{MM}^{S}} \left[D_1(\theta;\theta',\phi')I_{M\theta}^{S}(\theta')+D_2(\theta;\theta',\phi')I_{M\phi}^{S}(\theta') \right]ds'$$

$$+ F_{\phi}(\theta) \qquad\qquad (6.67)$$

$$I_{M\theta}^{S}(\theta) = - 2 \int_{S_{MM}^{\ell}} \left[C_1(\theta;\theta',\phi')I_{M\theta}^{\ell}(\theta')+C_2(\theta;\theta',\phi')I_{M\phi}^{\ell}(\theta') \right]ds'$$

$$- 2 \int_{S_{MM}^{S}} \left[C_1(\theta;\theta',\phi')I_{M\theta}^{S}(\theta)+C_2(\theta;\theta',\phi')I_{M\phi}^{S}(\theta') \right]ds' \quad (6.68)$$

$$I_{M\phi}^{S}(\theta) = 2 \int_{S_{MM}^{\ell}} \left[D_1(\theta;\theta',\phi')I_{M\theta}^{\ell}(\theta')+D_2(\theta;\theta',\phi')I_{M\phi}^{\ell}(\theta') \right]ds'$$

$$+ 2 \int_{S_{MM}^{S}} \left[D_1(\theta;\theta',\phi')I_{M\theta}^{S}(\theta')+D_2(\theta;\theta',\phi')I_{M\phi}^{S}(\theta') \right]ds' \quad (6.69)$$

where

$$F_\theta(\theta) = -2 \int_{S^S} \left[C_1(\theta; \theta', \theta') J_{p\theta}^S(\theta') + C_2(\theta; \theta', \phi') J_{p\phi}^S(\theta') \right] ds' \quad (6.70)$$

and

$$F_\phi(\theta) = 2 \int_{S^S} \left[D_1(\theta; \theta', \phi') J_{p\theta}^S(\theta') + D_2(\theta; \theta', \phi') J_{p\phi}^S(\theta') \right] ds' \quad (6.71)$$

$J_{p\theta}^S(\theta')$ and $J_{p\phi}^S(\theta')$ represent the $\hat{\theta}$ and $\hat{\phi}$ components of $J_{op}^S(\theta')$, respectively. Substituting Equations (6.68) and (6.69) into Equations (6.66) and (6.67) repeatedly, and ignoring the third and the higher multiple integrals, we obtain

$$I_{M\theta}^\ell(\theta) \approx -2\int_{S_{MM}^\ell} \left[C_1(\theta; \theta', \phi') I_{M\theta}^\ell(\theta') + C_2(\theta; \theta', \phi') I_{M\phi}^\ell(\theta') \right] ds'$$

$$+ 4\int_{S_{MM}^S} \int_{S_{MM}^\ell} I_{M\theta}^\ell(\theta') \left[C_1(\theta''; \theta', \phi') C_1(\theta; \theta'', \phi'') - D_1(\theta''; \theta', \phi') C_2(\theta; \theta'', \phi'') \right] ds' ds''$$

$$+ 4\int_{S_{MM}^S} \int_{S_{MM}^\ell} I_{M\phi}^\ell(\theta') \left[C_2(\theta''; \theta', \phi') C_1(\theta; \theta'', \phi'') - D_2(\theta''; \theta', \phi') C_2(\theta; \theta'', \phi'') \right] ds' ds''$$

$$+ F_\theta(\theta) \quad (6.72)$$

$$I_{M\phi}^\ell(\theta) \approx 2\int_{S_{MM}^\ell} \left[D_1(\theta; \theta', \phi') I_{M\theta}^\ell(\theta') + D_2(\theta; \theta', \phi') I_{M\phi}^\ell(\theta') \right] ds'$$

$$+ 4\int_{S_{MM}^S} \int_{S_{MM}^\ell} I_{M\theta}^\ell(\theta') \left[-C_1(\theta''; \theta', \phi') D_1(\theta; \theta'', \phi'') + D_1(\theta''; \theta', \phi') D_2(\theta; \theta'', \phi'') \right] ds' ds''$$

104

$$+4 \int_{S_{MM}^S} \int_{S_{MM}^\ell} I_{M\phi}(\theta') \left[-C_2(\theta'';\theta',\phi')D_1(\theta;\theta'',\phi'')+D_2(\theta'';\theta',\phi')D_2(\theta;\theta'',\phi'') \right] ds'ds''$$

$$+ F_\phi(\theta) \tag{6.73}$$

Substituting Equation (6.73) into Equation (6.72) repeatedly, and then ignoring the triple or the higher multiple integrals containing $I_\theta^\ell(\theta')$ and the double or the higher multiple integrals containing $F_\phi(\theta)$, we obtain the following approximation for $I_{M\theta}^\ell(\theta)$.

$$I_{M\theta}^\ell(\theta) \simeq - 2 \int_{S_{MM}^\ell} I_{M\theta}^\ell(\theta')C_1(\theta;\theta',\phi')ds'$$

$$- 4 \int_{S_{MM}} \int_{S_{MM}^\ell} I_{M\theta}^\ell(\theta')D_1(\theta'';\theta',\phi')C_2(\theta;\theta'',\phi'')ds'ds''$$

$$+ 4 \int_{S_{MM}^S} \int_{S_{MM}^\ell} I_{M\theta}^\ell(\theta')C_1(\theta'';\theta',\phi')C_1(\theta;\theta'',\phi'')ds'ds''$$

$$+ F_\theta(\theta) - 2 \int_{S_{MM}^\ell} F_\phi(\theta')C_2(\theta;\theta',\phi')ds' \quad . \tag{6.74}$$

Also by a similar procedure we can obtain an expression for $I_{M\phi}^\ell(\theta)$ as

105

$$I_{M\phi}^{\ell}(\theta) \simeq 2 \int\limits_{S_{MM}^{\ell}} I_{M\phi}^{\ell}(\theta')D_2(\theta;\theta',\phi')ds'$$

$$- 4 \int\limits_{S_{MM}} \int\limits_{S_{MM}^{\ell}} I_{M\phi}^{\ell}(\theta')C_2(\theta'';\theta',\phi')D_1(\theta;\theta'',\phi'')ds'ds''$$

$$+ 4 \int\limits_{S_{MM}^{S}} \int\limits_{S_{MM}^{\ell}} I_{M\phi}^{\ell}(\theta')D_2(\theta'';\theta',\phi')D_2(\theta;\theta'',\phi'')ds'ds''$$

$$+ F_\phi(\theta) + 2 \int\limits_{S_{MM}^{\ell}} F_\theta(\theta')D_1(\theta;\theta',\phi')ds'. \qquad (6.75)$$

Assume that $I_{M\theta}^{\ell}(\theta)$ and $I_{M\phi}^{\ell}(\theta)$ can be approximated by

$$I_{M\theta}^{\ell}(\theta) = \sum_{n=1}^{N} I_{\theta n}^{\ell} \, P(\theta-\theta_n) \qquad (6.76)$$

$$I_{M\phi}^{\ell}(\theta) = \sum_{n=1}^{N} I_{\phi n}^{\ell} \, P(\theta-\theta_n) \qquad (6.77)$$

where

$$P(\theta) = \begin{cases} 1 & \text{for } |\theta-\theta_n| < \frac{\Delta\theta}{2} \\ 0 & \text{elsewhere.} \end{cases} \qquad (6.78)$$

and $\Delta\theta = \frac{2\pi}{N}$, where N is a number of divisions.

106

Substituting Equations (6.76) and (6.77) into Equation (6.74), and rearranging terms, we have

$$\sum_{n=1}^{N} I_{\theta n}^{\ell} \left\{ P(\theta-\theta_n) + 2 \int_{\phi_{MM}^{\ell}} C_1(\theta;\theta_n,\phi')d\phi' \right.$$

$$+ 4 \int_{S_{MM}} \int_{\phi_{MM}^{\ell}} D_1(\theta'';\theta_n,\phi')C_2(\theta;\theta'',\phi'')d\phi'ds''$$

$$\left. - 4 \int_{S_{MM}^{S}} \int_{\phi_{MM}^{\ell}} C_1(\theta'';\theta_n,\phi')C_1(\theta;\theta'',\phi'')d\phi'ds'' \right] a^2 \sin\theta_n \Delta\theta \right\}$$

$$= F_\theta(\theta) - 2 \int_{S_{MM}^{\ell}} F_\phi(\theta')C_2(\theta;\theta',\phi')ds' \qquad (6.79)$$

where the integration region ϕ_{MM}^{ℓ} represents the lit moment method region for the angle ϕ.

Multiplying both sides of Equation (6.79) by $\delta(\theta-\theta_m)$, m=1,2,...,N, integrating them over θ_{MM}^{ℓ}, and then dividing both sides by $\Delta\theta$, we obtain

$$\sum_{n=1}^{N} I_{\theta n}^{\ell} \left\{ P(\theta_m-\theta_n) + \left[2 \int_{\phi_{MM}^{\ell}} C_1(\theta_m;\theta_n,\phi')d\phi' \right. \right.$$

107

$$+ 4 \int_{S_{MM}} \int_{\phi_{MM}^{\ell}} D_1(\theta'';\theta_n,\phi')C_2(\theta_m;\theta'',\phi'')d\phi'ds''$$

$$- 4 \int_{S_{MM}^S} \int_{\phi_{MM}^{\ell}} C_1(\theta'';\theta_n,\phi')C_1(\theta_m;\theta'',\phi'')d\phi'ds'' \Bigg] a^2 \sin\theta_n \Delta\theta \Bigg\}$$

$$= F_\theta(\theta_m) - 2 \int_{S_{MM}^{\ell}} F_\phi(\theta')C_2(\theta_m;\theta',\phi')ds' \tag{6.80}$$

Representing Equation (6.80) in the matrix form of

$$[Z_{\theta mn}^{\ell}][I_{\theta n}^{\ell}] = [V_{\theta m}^{\ell}] \qquad m,n=1,2,\ldots,N \tag{6.81}$$

means that the elements of the impedance matrix $[Z_{\theta mn}^{\ell}]$ are given by

$$Z_{\theta mn}^{\ell} = P(\theta_m-\theta_n) + \Bigg\{ 2 \int_{\phi_{MM}^{\ell}} C_1(\theta_m;\theta_n,\phi')d\phi'$$

$$+ 4 \int_{S_{MM}} \int_{\phi_{MM}^{\ell}} D_1(\theta'';\theta_n,\phi')C_2(\theta_m;\theta'',\phi'')d'ds''$$

$$- 4 \int_{S_{MM}^S} \int_{\phi_{MM}^{\ell}} C_1(\theta'';\theta_n,\phi')C_1(\theta_m;\theta'',\phi'')d\phi'ds'' \Bigg\} a^2 \sin\theta_n \Delta\theta . \tag{6.82}$$

Also the elements of $[V_{\theta m}^{\ell}]$ can be obtained from

$$V_{\theta m}^{\ell} = F_\theta(\theta_m) - 2 \int_{S_{MM}^{\ell}} F_\phi(\theta')C_2(\theta_m;\theta',\phi')ds' \ . \qquad (6.83)$$

By the same procedure we can obtain the impedance matrix and the voltage matrix for the $\hat{\phi}$ component of the surface current, whose elements are given by

$$Z_{\phi mn}^{\ell} = P(\theta_m-\theta_n) + \left\{ - 2 \int_{\phi_{MM}^{\ell}} D_2(\theta_m;\theta_n,\phi')d\phi' \right.$$

$$+ 4 \int_{S_{MM}} \int_{\phi_{MM}^{\ell}} C_2(\theta'';\theta_n,\phi')D_1(\theta_m;\theta'',\phi'')d\phi'ds''$$

$$\left. - 4 \int_{S_{MM}^{s}} \int_{\phi_{MM}^{\ell}} D_2(\theta'';\theta_n,\phi')D_2(\theta_m;\theta'',\phi'')d\phi'ds'' \right\} a^2\sin\theta_n\Delta\theta$$

$$\qquad (6.84)$$

and

$$V_{\phi m}^{\ell} = F_\phi(\theta_m) + 2 \int_{S_{MM}^{\ell}} F_\theta(\theta')D_1(\theta_m;\theta',\phi')ds' \ . \qquad (6.85)$$

The dominant terms in Equations (6.82) and (6.84) are the first two ones. Therefore if we want the simpler forms for computer programs, we may ignore the last two terms in those equations.

109

6.4 Numerical Results

Two possible segmentation schemes for numerical integration over the sphere surface are shown in Figures 6.3 and 6.4. In the uniform segmentation shown in Figure 6.3, the surface is divided into equal angles in the θ and ϕ directions. Therefore the patch areas around $\theta=0^{o}$ will be very small compared to those around $\theta=90^{o}$.
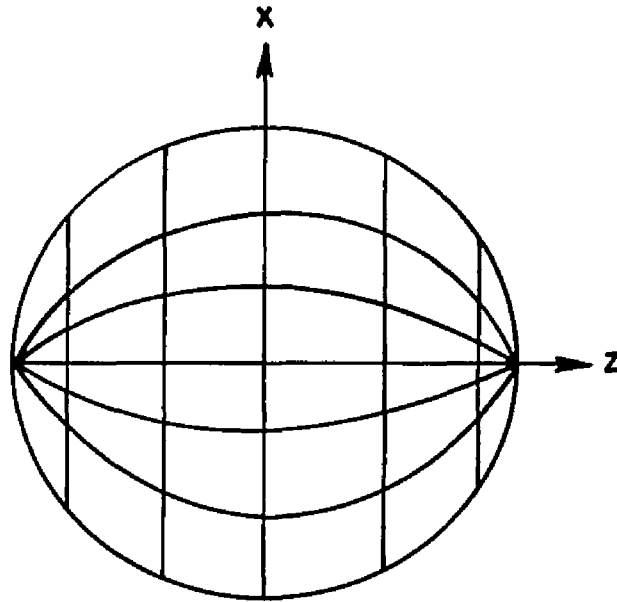
Figure 6.3. Uniform segmentation scheme.

On the other hand, in the variable ϕ segmentation shown in Figure 6.4, we divide the surface equally in the θ direction and proportional to $\sin\theta$ in the ϕ direction so that all patch areas are almost equal. Experience shows that the better numerical results are obtained with the variable ϕ segmentation scheme. All numerical results for a sphere were obtained with the variable ϕ segmentation scheme, where we divided
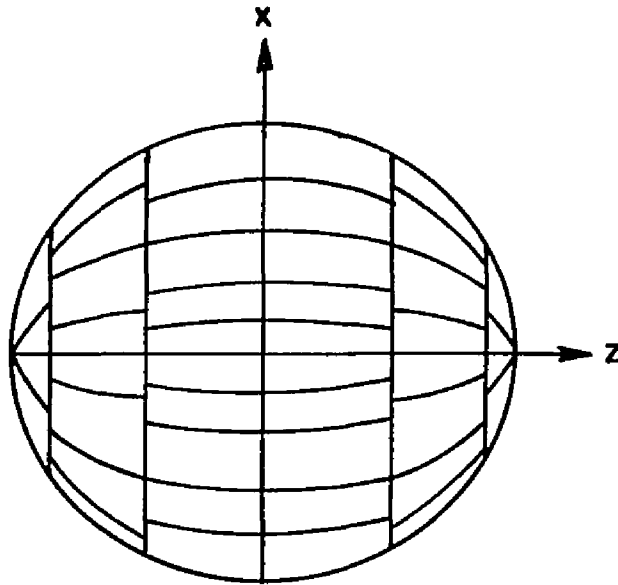
110

Figure 6.4.   Variable φ segmentation scheme.

the surface of the interval θ=0 to π/2 into twenty four bands (we call the number of this division N) and each band starting at the pole (θ=0) in the interval φ=0 to π/2 was divided into subpatches as follows; 1,2,4,5,7,8,10,11,13,14,15,16,18,19,20,20,21,22,22,23,23,24, 24,24. With the larger number of N, better results can be obtained, but also the resulting computational time will be increased significantly. For example, the computer* running time with N=24 is about twenty six minutes for the seventh order approximation, but if we increase the number N by two times, the computing time will be increased by approximately six times for the same order approximation.

_____

*Modified Datacraft model 6024.

111

This example shows that there is the upper limit on the sphere size which can be handled practically by this method.

The interior resonance appears to affect the surface current more seriously on a sphere than on a circular cylinder. This seems to be due to the interaction of the two currents $J_\theta(\theta)$ and $J_\phi(\theta)$. Also it is observed that the resonance problem becomes more severe for the larger spheres. Therefore this resonance phenomenon limits the numerical calculations for arbitrary sizes of a sphere but may not be of any consequence for other 3-dimensional geometries.

We obtained acceptable numerical results for conducting spheres of radii 0.25λ to 2.3λ using N=24. Compared to a circular cylinder, higher order approximation were needed for a sphere. The surface current on a sphere was obtained with the seventh to the eleventh order approximations. Also in the moment method region, whose size was 30° in angle for all data, eight pulse basis and delta weighting functions were used. All results were compared with the exact eigenfunction solutions which were denoted by solid lines in the figures.

In Figures 6.5 and 6.6 the H-plane and E-plane currents, which are denoted by J_ϕ and J_θ, respectively, are shown for a sphere of radius $a=0.25\lambda$. The agreements with the exact solutions are remarkably good in both the E-plane and H-plane currents. Also the results for $a=0.5\lambda$ are in good agreement with the exact solutions as shown in Figures 6.7 and 6.8.

112

Figures 6.9 and 6.10 show the surface currents for the 1.0λ sphere, where we can see that the differences from the exact solutions are larger in both the magnitude and phase for the surface current compared to the results obtained for the smaller spheres.

It seems that the surface current on a sphere is affected not only at the resonance frequency but also the frequencies around it. Therefore we cannot find many sizes of spheres with which we can obtain numerical results by this method. For example, although a=1.5λ and 2.0λ are not the exact geometries that have the interior resonance, the surface currents on those spheres are much different from the exact currents. The radii of the spheres which are in the interior resonance modes around a=1.5λ and 2.0λ are a 1.48λ and 1.98λ, respectively. The surface current results for the sphere of 1.7λ are shown in Figures 6.11 and 6.12 and are in fairly good agreement with the exact results. However, it is obvious that they are not that good compared to the results for the spheres of 0.5λ or 1.0λ radius.

The largest radius of a sphere for which we obtained numerical results was 2.3λ, and the results are shown in Figures 6.13 and 6.14. We can observe that even though the results are acceptable, the magnitude curves show many oscillations compared to other sizes of spheres. The greatest departure from the exact solutions is shown in the phase of the H-plane current in the shadow region. The oscillations shown on the magnitude curves can be decreased a little, but not significantly by increasing the number of divisions. However, as it has

113

been mentioned before, by increasing the number of divisions the computing time will be greatly increased. Therefore instead of increasing N, it will be more efficient to use the constants S_θ and S_ϕ which are given in Equations (6.62) and (6.63) to make improvement in the results. Notice that the results in Figures 6.13 and 6.14 were obtained with those constants.

If we examine the results shown in Figures 6.15 and 6.16, where we used N=24 without the constants S_θ and S_ϕ, we can realize that those constants, which were derived on the basis of very careful approximations, make the magnitude curves considerably smoother.

Although we obtained numerical results for spheres of up to the 2.3λ radius, it will be possible to obtain the surface currents for larger spheres by using a larger number of divisions with the constants S_θ and S_ϕ.
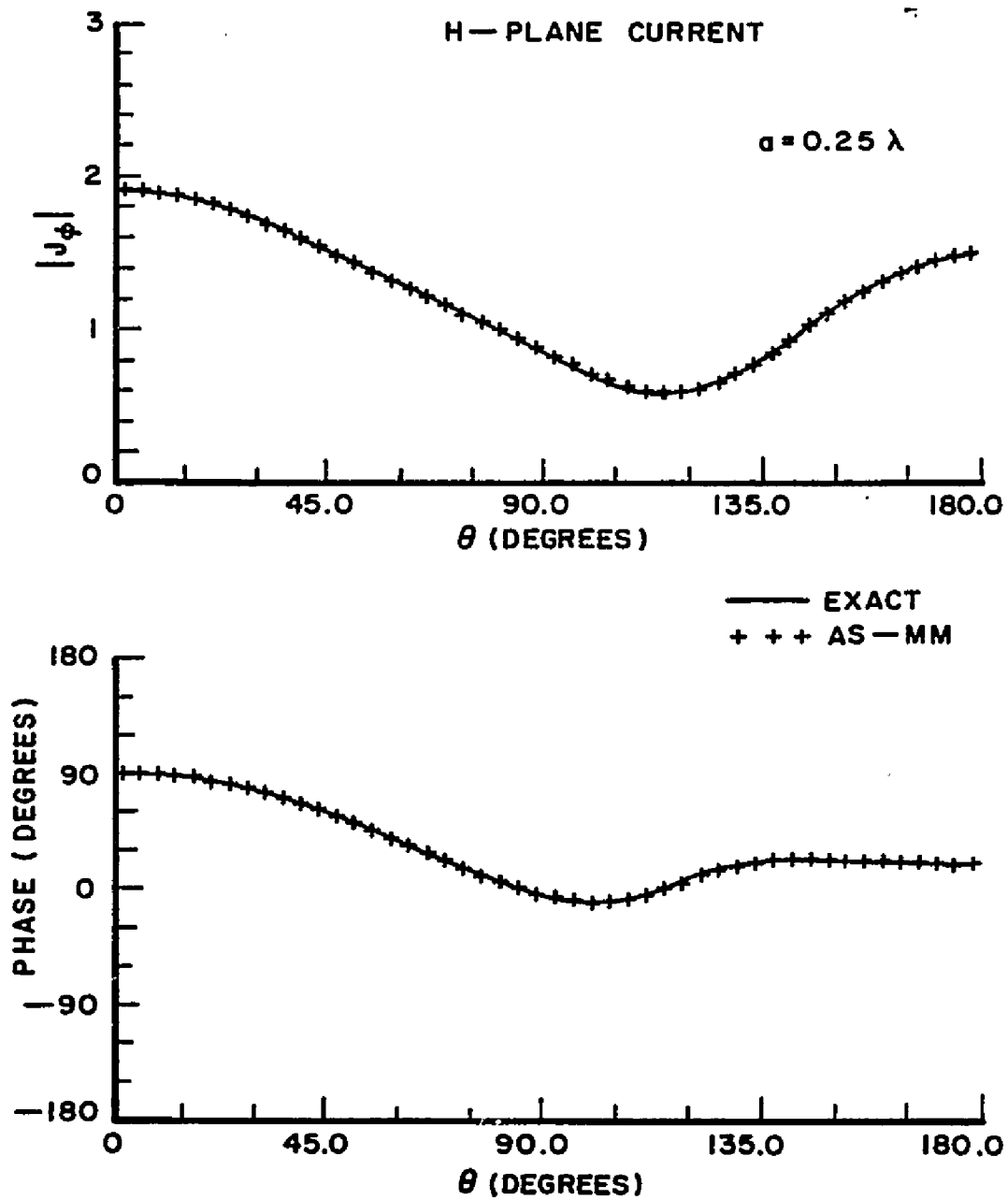
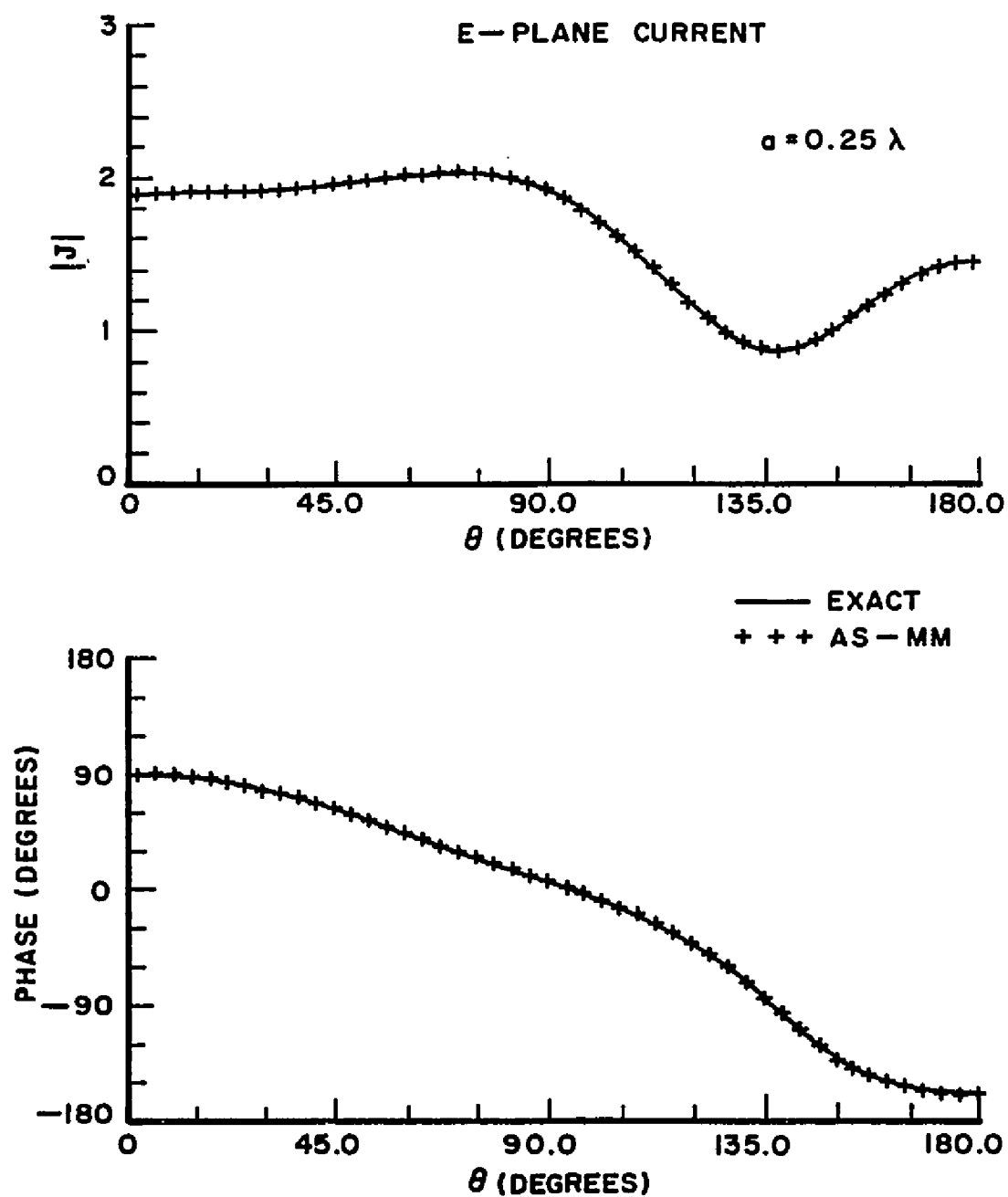Figure 6.5. The H-plane current on a sphere for
a=0.25λ, N=24, and S_{MM}=30°.

Figure 6.6. The E-plane current on a sphere for
a=0.25λ, N=24, and S_{MM}=30°.

Figure 6.7. The H-plane current on a sphere for
a=0.5λ, N=24, and $S_{MM}=30^0$.

Figure 6.8. The E-plane current on a sphere for
a=0.5λ, N=24, and S_{MM}=30°.

Figure 6.10. The E-plane current on a sphere for
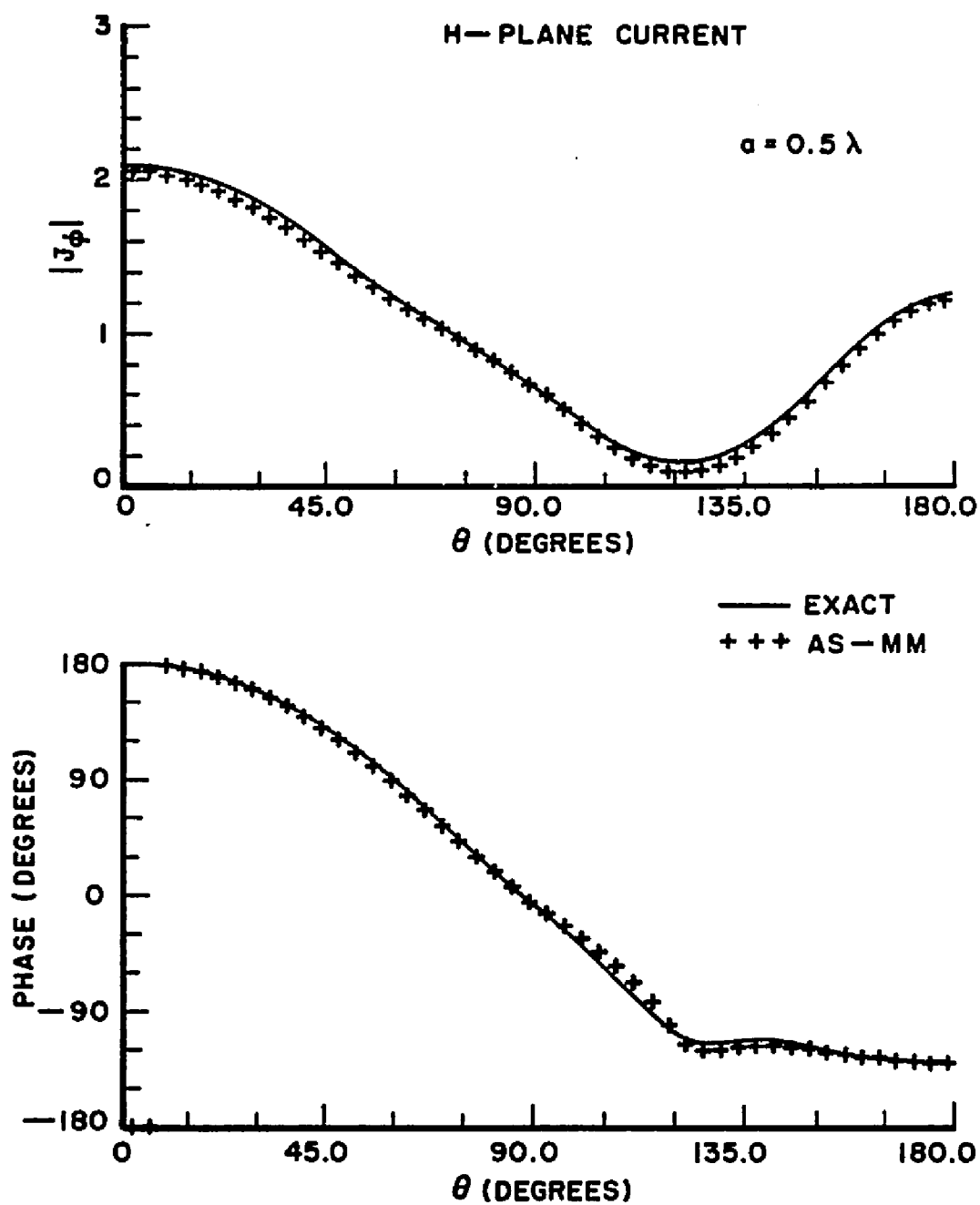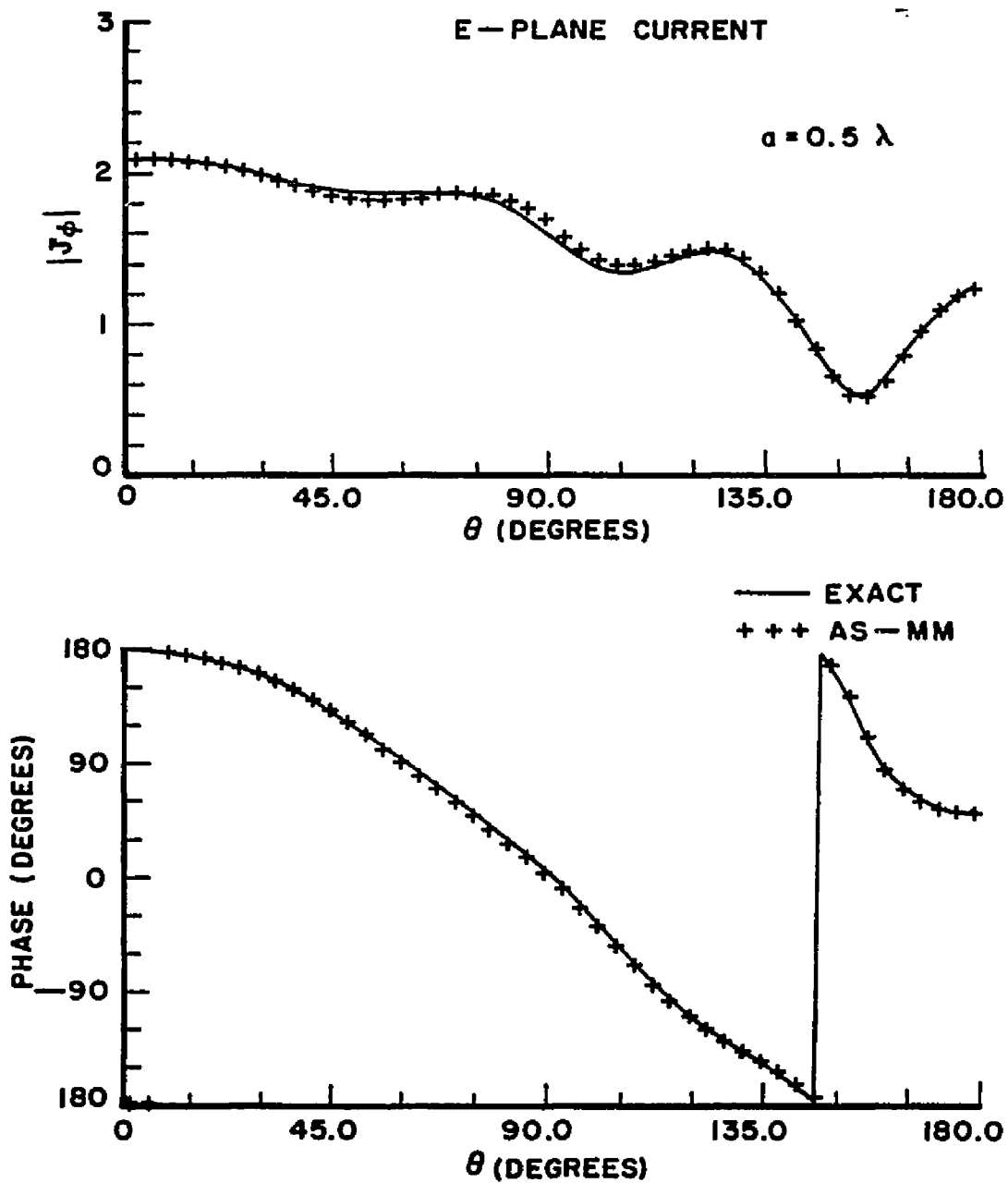a=1.0λ, N=24, and S_{MM}=30°.
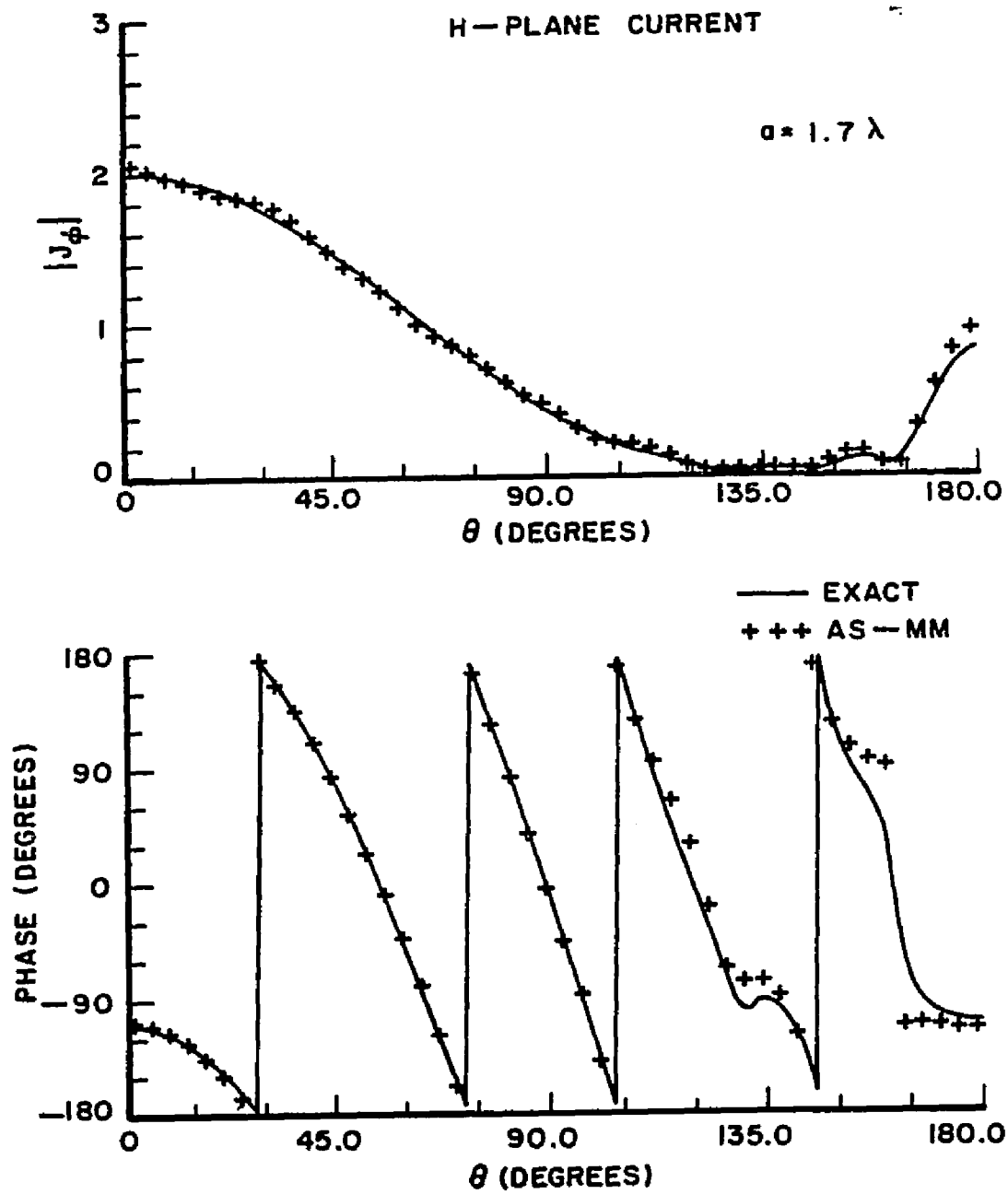
Figure 6.11. The H-plane current on a sphere for
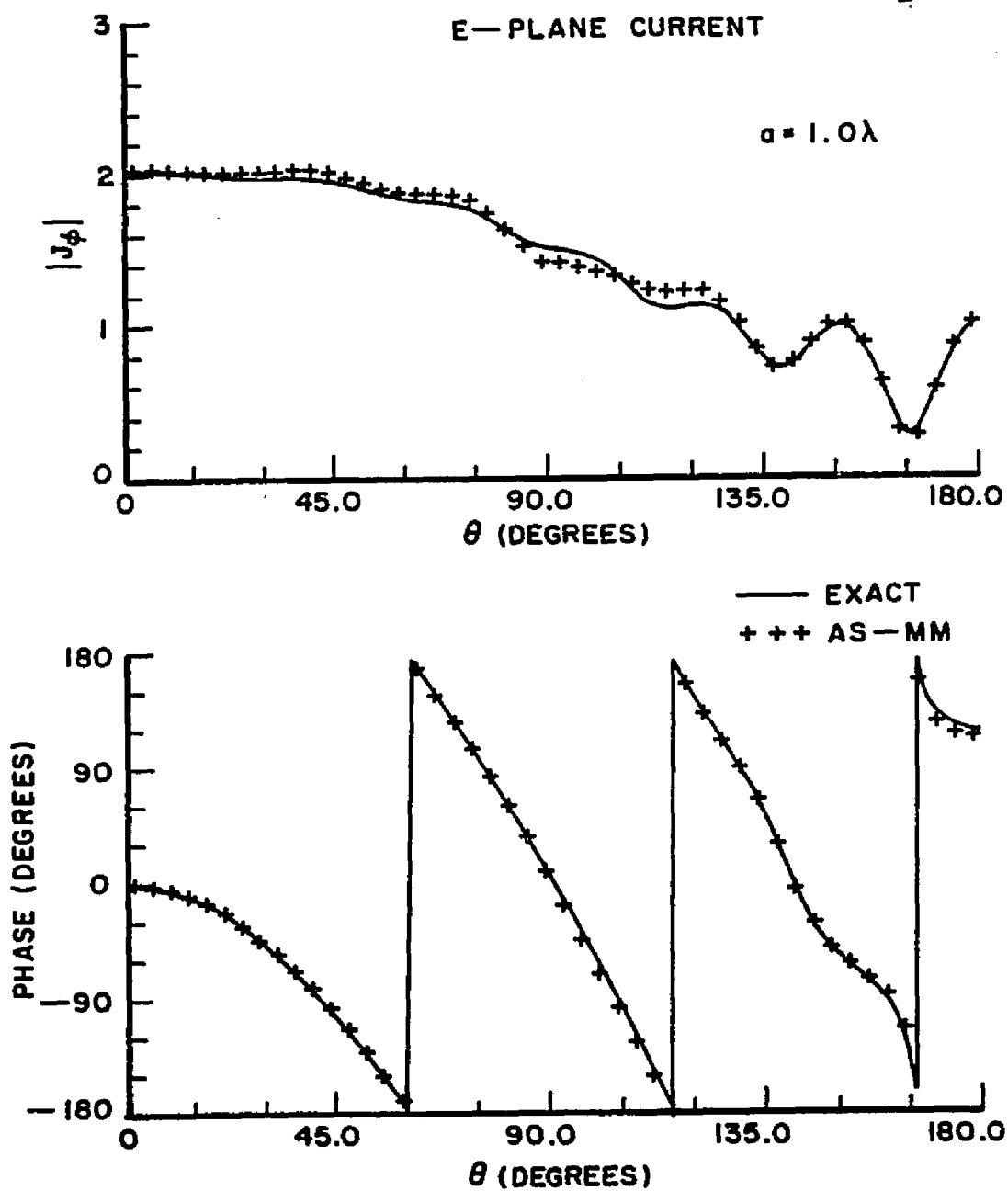$a=1.7\lambda$, $N=24$, and $S_{MM}=30^{\circ}$.
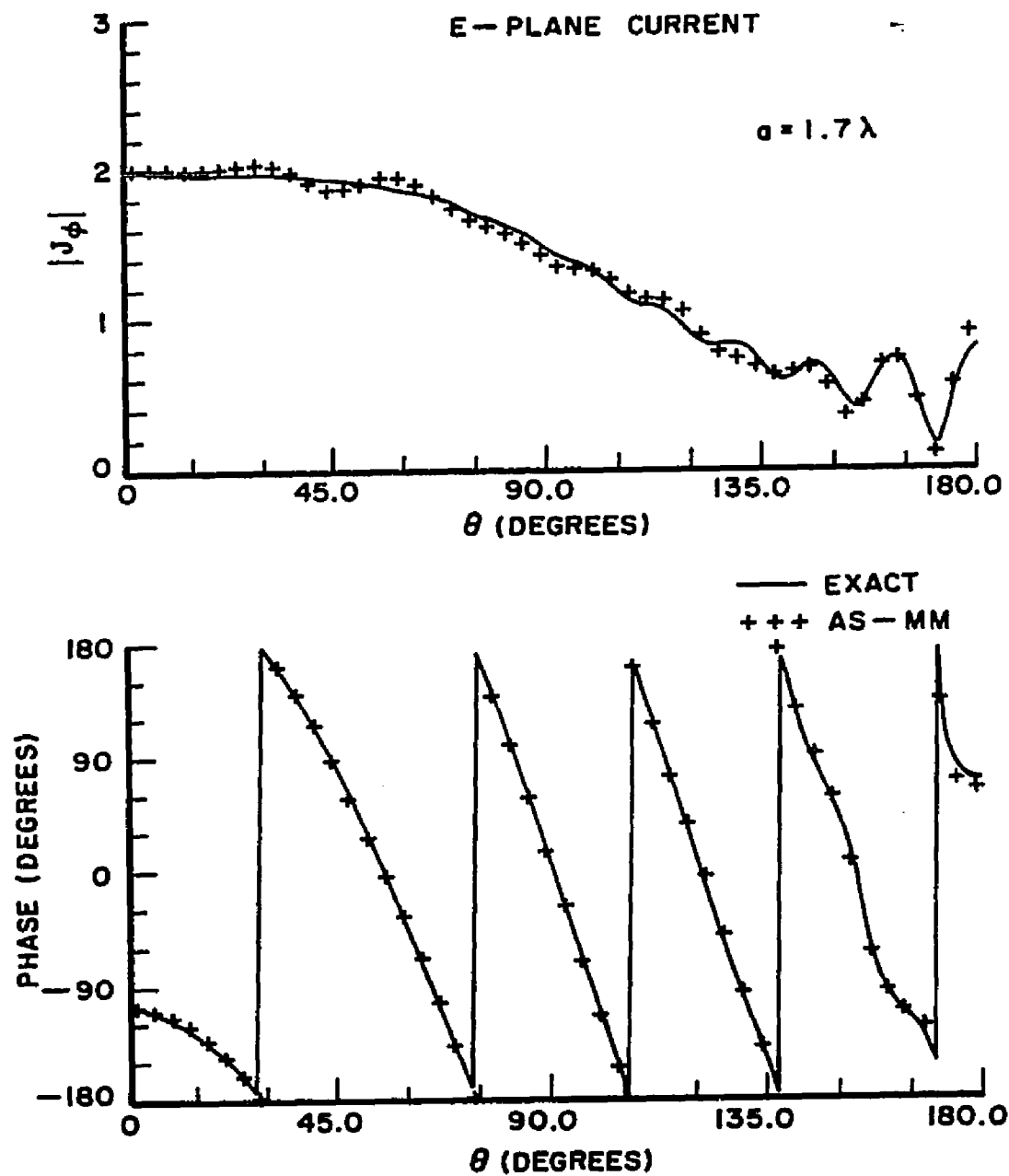
Figure 6.12. The E-plane currents on a sphere for
a=1.7λ, N=24, and $S_{MM}=30^\circ$.

Figure 6.13. The H-plane current on a sphere for
a=2.3λ, N=24, S_{MM}=30°, and S_{θ}, S_{ϕ}≠1.

Figure 6.14. The E-plane current on a sphere for
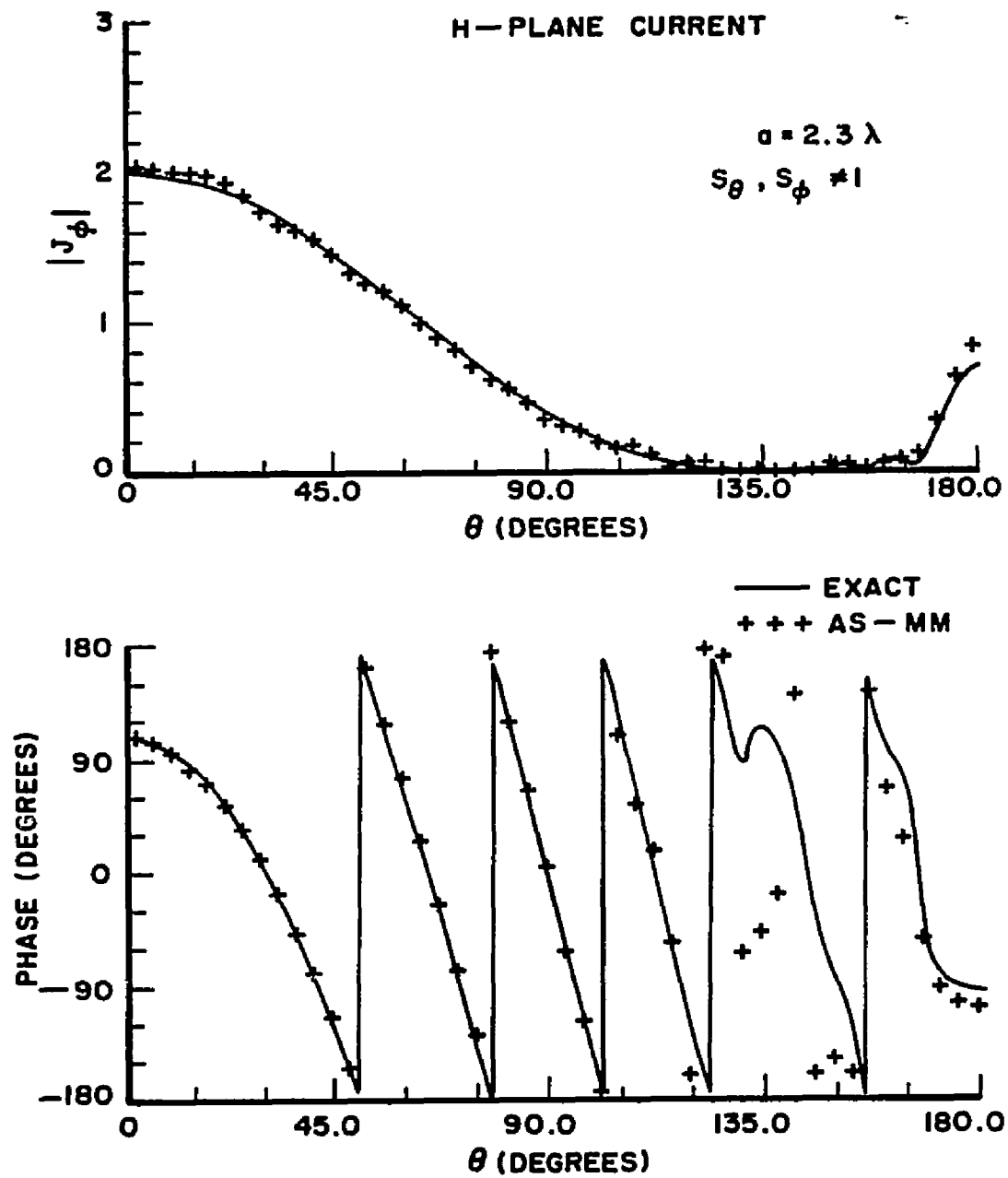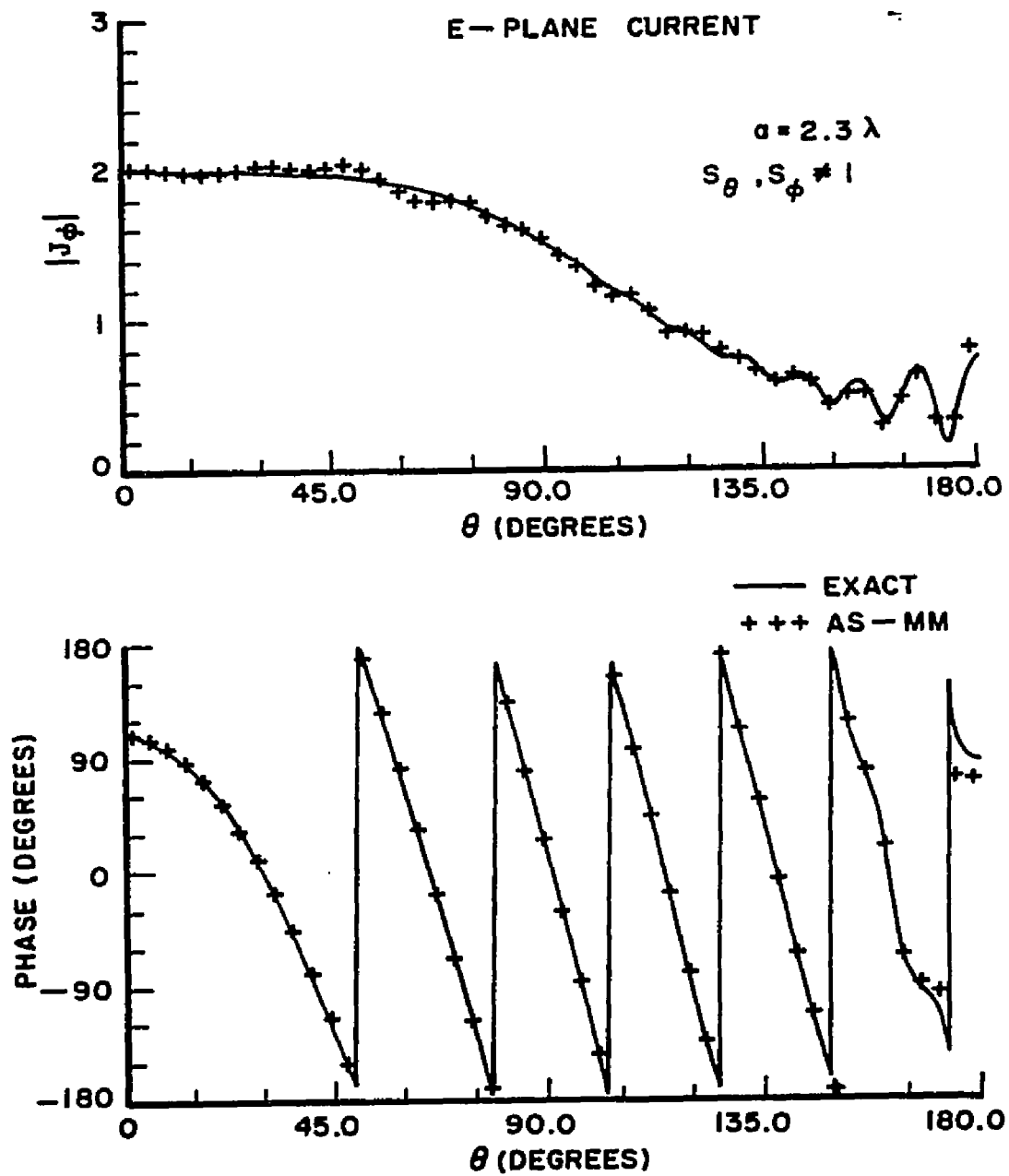a=2.3λ, N=24, $S_{MM}=30^{o}$, and $S_\theta, S_\phi \neq 1$.
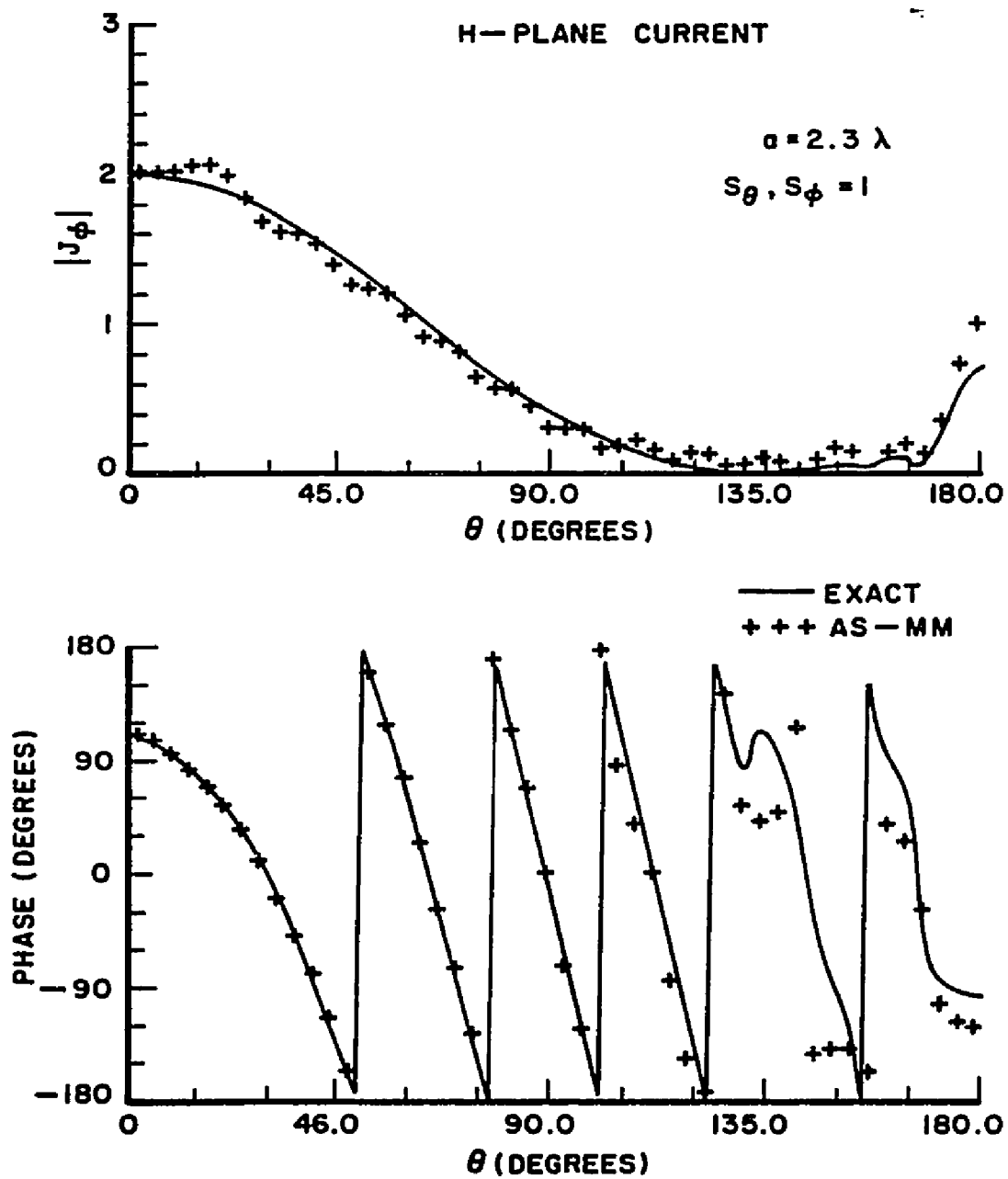
Figure 6.15. The H-plane current on a sphere for
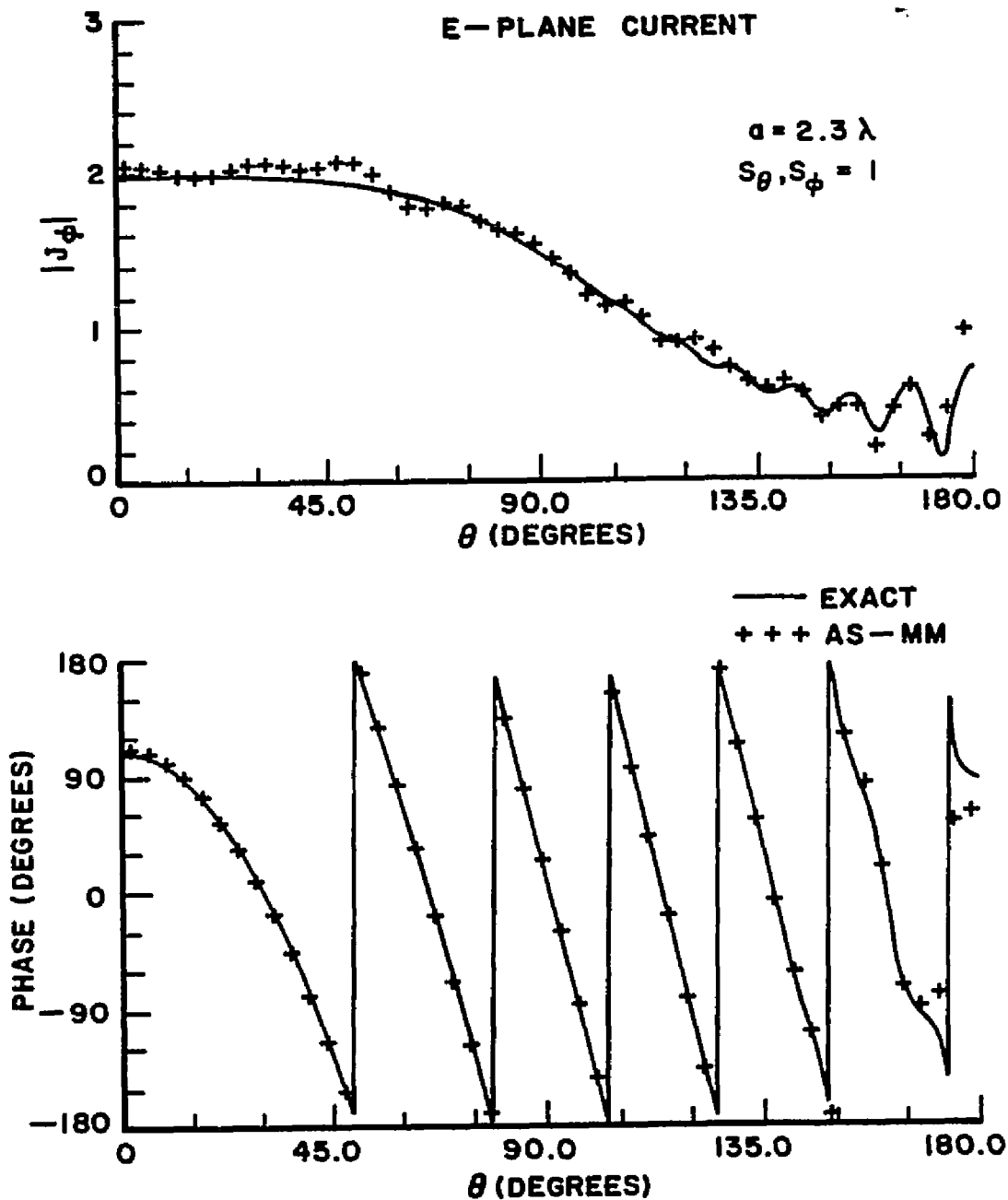a=2.3λ, N=24, $S_{MM}=30°$, and $S_{\theta},S_{\phi}=1$.

Figure 6.16. The E-plane current on a sphere for
a=2.3λ, N=24, $S_{MM}=30^{\circ}$, and $S_{\theta}, S_{\phi}=1$.

126

CHAPTER VII

SUMMARY AND CONCLUSIONS

We have derived the necessary integral equations for the hybrid AS-MM method and applied them to four different shaped perfectly conducting bodies, namely a wedge, square and circular cylinders and a sphere.

The modified geometrical optics current terms which were denoted by $\overline{J}_{op}^{\ell}(\overline{R})$ and $\overline{J}_{op}^{S}(\overline{R})$, respectively in the lit and shadow regions were obtained by an iterative technique in numerical calculations. The currents in the moment method regions, which were denoted by $T_{MM}^{\ell}(\overline{R})$ and $T_{MM}^{S}(\overline{R})$, respectively in the lit and shadow regions were solved by a matrix technique (i.e., the moment method). For this purpose, we derived the impedance matrix for each conducting body. The currents in other than the moment method region were determined by using the currents in the MM-region in the magnetic field integral equation for the first order approximation. For the higher order approximation, the iterative method was used to obtain both the moment method and asymptotic region currents. The extent of the moment method region did not affect the surface current significantly. Usually the second or the third order approximation produced good results for the wedge, square and circular cylinders, but for the sphere higher than the fifth

order approximations were required to give acceptable results. This is maybe due to the interior resonance problem.

The singularity patch problem in the curved surface geometries was considered and some constants were derived on the basis of approximations to make up some of the contribution lost by excluding the patch area instead of just the singular point in the calculations. It was seen that the constants made possible good improvement in the results of the surface current and that they were useful for practical numerical calculations.

In this study we considered a technique for combining a moment method current and an asymptotic current in both two and three dimensions. From the formulations for the surface current on a conducting body, we see that the method does not need any a priori knowledge of the current form away from the moment method region. Also we don't have to follow ray paths on the surface of a conductor as we do in the GTD method. Therefore these advantages of this method tend to make it relatively easy to obtain the surface current on arbitrarily shaped bodies.

As we have seen from the several examples, this method does not have difficulties in its application to the arbitrary sizes of bodies. However, this method usually requires relatively large computing time and memory storage especially for bodies having many surfaces. This disadvantage may limit the method in practical numerical calculations.

As we have seen in the wedge problem in Chaper III, this method cannot provide us acceptable results for the surface current on the wedge if the magnetic incident field is grazing to the lit surface or if the wedge angle is small. Of course these limitations are of no consequence in bodies whose dimensions are finite.

Also it was shown that this method could not eliminate what appears to be spurious resonances appearing in the large sizes of a sphere. However, this method was not affected by the resonance in its applications to the square and circular cylinders.

In spite of these disadvantages and limitations, this method provides generally good results for the surface currents on the perfectly conducting bodies. Extension of this method to more complex bodies should be possible. Future work should study ways to reduce the computer running time by making appropriate approximations in the integrals. Future work should also consider the possibility of combining this hybrid method with the GTD. Thus, one would treat areas far removed from shadow boundaries and/or sharp discontinuities in geometry by the GTD thereby eliminating numerical integration time. The hybrid method of this paper could then be used to handle a wide variety of discontinuities in geometry for which diffraction coefficients are unknown.

REFERENCES

1. F. A. Molinet, "On the Methods Which Combine the Moment Method with Asymptotic Technique," 1978 URSI General Assembly Symposium Abstracts, pp. 133.

2. G. A. Thiele and T. H. Newhouse, "A Hybrid Technique for Combining Moment Methods with the Geometrical Theory of Diffraction," IEEE Trans. Ant. and Prop., Vol. AP-23, pp. 62-69, January 1975.

3. W. D. Burnside, C. L. Yu, and R. J. Marhefka, "A Technique to Combine the Geometrical Theory of Diffraction and the Moment Method," IEEE Trans. Ant. and Prop., Vol. AP-23, pp. 551-558, July 1975.

4. T. J. Kim and G. A. Thiele, "A Hybrid Technique Which Combines the Moment Method with a Physical Optics Type Current," URSI Symposium, 1980.

5. R. G. Kouyoumjian and P. H. Pathak, "A Uniform Geometrical Theory of Diffraction for an Edge in a Perfectly Conducting Surface," IEEE Proc., Vol. 62, pp. 1448-1461, November 1974.

6. M. G. Anderson, "Scattering from Bodies of Revolution," IEEE Trans. Ant. and Prop., Vol. AP-13, pp. 303-310, March 1965.

7. Wai Lee Ko and Raj Mittra, "A New Approach Based on a Combination of Integral Equation and Asymptotic Techniques for Solving Electromagnetic Scattering Problems," IEEE Trans. Ant and Prop., Vol. AP-25, pp. 187-197, March 1977.

8. Raj Mittra and Wai Lee Ko, "An Approach to High-Frequency Scattering From Smooth Convex Surfaces," IEEE Trans. Ant. and Prop., Vol. AP-25, No. 6, pp. 781-788, November 1977.

9. William A. Davis and Raj Mittra, "A New Approach to the Thin Scatterer Problems Using the Hybrid Equations," IEEE Trans. Ant. and Prop., Vol. AP-23, No. 3, pp. 402-406, May 1977.

10. A. J. Poggio and E. K. Miller, "Integral Equation Solutions for Three Dimensional Scattering Problems," in Computer Techniques for Electromagnetics, Edited by R. Mittra, Oxford; Pergamon, 1973.

11. D. R. Wilton and S. Govind, "Incorporation of Edge Conditions in Moment Solutions," IEEE Trans. Ant. and Prop., Vol. AP-25, pp. 845-850, November 1977.

12. K. K. Mei and J. G. Van Bladel, "Scattering by Perfectly Conducting Rectangular Cylinders," IEEE Trans. Ant. and Prop., Vol. AP-11, pp. 185-192, March 1963.

13. M. A. Plonus, R. Williams, and S. Ch. Wang, "Radar Cross Section of Curved Plates Using Geometrical and Physical Diffraction Techniques," IEEE Trans. Ant. and Prop., Vol. Ap-26, pp. 488-493, May 1978.

14. C. R. Mullin, R. Sandburg, and C. O. Velline, "A Numerical Technique for the Determination of Scattering Cross Section of Infinite Cylinders of Arbitrary Geometrical Cross Section," IEEE Trans. Ant. and Prop., Vol. AP-13, pp. 141-149, January 1965.

15. J. H. Richmond, "A Computer Program for Physical-Optics Scattering by Convex Conducting Targets," Report 2430-7, May 1968, The Ohio State University ElectroScience Laboratory, Department of Electrical Engineering; prepared under Contract F19628-67-C-0308 for Department of the Air Force. (AD 669815)

16. J. H. Richmond, Note 201 "An Integral Equation Solution for TE Radiation and Scattering From Conducting Cylinders," April 1973, ElectroScience Laboratory, Department of Electrical Engineering.

17. Shung-Wu Lee, Johannes Boersma, Chak-Lam Law and Georges A. Deschamps, "Singularity in Green's Function and It's Numerical Evaluation," IEEE Trans. Ant. and Prop., Vol. AP-28, pp. 311-317, May 1980.

18. J. Van Bladel, "Some Remarks on Green's Dyadic for Infinite Space," IRE Trans. Ant. and Prop., Vol. AP-9, pp. 563-566, November 1961.

19. Jean-Charles Bolomey and Walid Tabbara, "Numerical Aspects on Coupling Between Complementary Boundary Value Problems," IEEE Trans. Ant. and Prop., Vol. AP-21, No. 3, pp. 356-363, May 1973.

20. Arthur D. Yaghijian, "Electric Dyadic Green's Functions in the Source Region," IRE Trans. Ant. and Prop., Vol. 68, No. 2, pp. 248-263, February 1980.

21. Joseph R. Mautz and Roger F. Harrington, "A Combined Source Solution for Radiation and Scattering from a Perfectly Conducting Body," IEEE Trans. Ant. and Prop., Vol. AP-21, No. 3, pp. 356-363, May 1973.

22. Joseph R. Mautz and Roger F. Harrington, "H-Field, E-Field and Combined Field Solutions for Bodies of Revolution," Technical Report TR-77-2, February 1977, Department of Electrical and Computer Engineering, Syracuse University, Syracuse, New York.

23. Arthur D. Yaghijian, "Augmented Electric- and Magnetic-Field Integral Equations Which Eliminate the Spurious Resonances," URSI Symposium, Munich, August 1980.

24. R. F. Harrington, Time Harmonic Electromagnetic Fields, New York; McGraw-Hill, 1961.

25. R. F. Harrington, Field Computation by Moment Methods, New York; McMillan, 1968.

26. D. L. SenGupta, Chapter 10, The Sphere, in Electromagnetic and Acoustic Scattering by Simple Shapes, Edited by J. J. Bowman, T. B. A, and P. L. E. Uslenghi, Amsterdam; North-Holland, 1969.

27. C. D. Green, Integral Equation Methods, New York; Barnes S. Noble, Inc., 1969.

28. U. V. Vorobyev, <u>Moment Method in Applied Mathematics</u>, New York; Gordon S. Breach Science Publishing Co., 1962.

29. Francis Scheid, <u>Numerical Analysis</u>, New York; McGraw-Hill, 1968.

30. L. M. Delves and J. Walsh, <u>Numerical Solution of Integral Equations</u>, Oxford, Clarendon Press, 1974.

31. John Sahalos and G. A. Thiele, "Bistatic Scattering by a Triangular Pyramid," Technical Report 4372-4, June 1977, The Ohio State University ElectroScience Laboratory, Department of Electrical Engineering; prepared under Contract N00014-76-C-0573 for Department of the Navy.

Appendix A

CURRENT CALCULATION AT A SINGULAR POINT FOR
TWO-DIMENSIONAL PROBLEMS

To derive Equation (5.14) from Equation (5.11), we consider a semicircular path ℓ_ϵ as shown in Figure A1. Let the Surface current $\bar{J}(\bar{R})$ be in the direction of $\hat{t}$, then Equation (5.11) can be expressed as

$$\bar{J}_1(\bar{R}) = \hat{t} \lim_{\epsilon \to 0} \int \bar{J}(\bar{R}') \, (\hat{n}' \cdot \hat{r}') \, \frac{\partial G(\epsilon)}{\partial \epsilon} \, d\ell \qquad (A1)$$

where

$$G(\epsilon) = -\frac{j}{4} H_0^{(2)}(\beta\epsilon) \quad . \qquad (A2)$$

For small $\beta\epsilon$, $H_0^{(2)}(\beta\epsilon)$ can be approximated as

$$H_0^{(2)}(\beta\epsilon) \approx 1 - j \frac{2}{\pi} \log_e \left(\frac{\gamma\beta\epsilon}{2}\right) \qquad (A3)$$

where γ is Euler's constant. Then $\frac{\partial G(\epsilon)}{\partial \epsilon}$ can be evaluated as

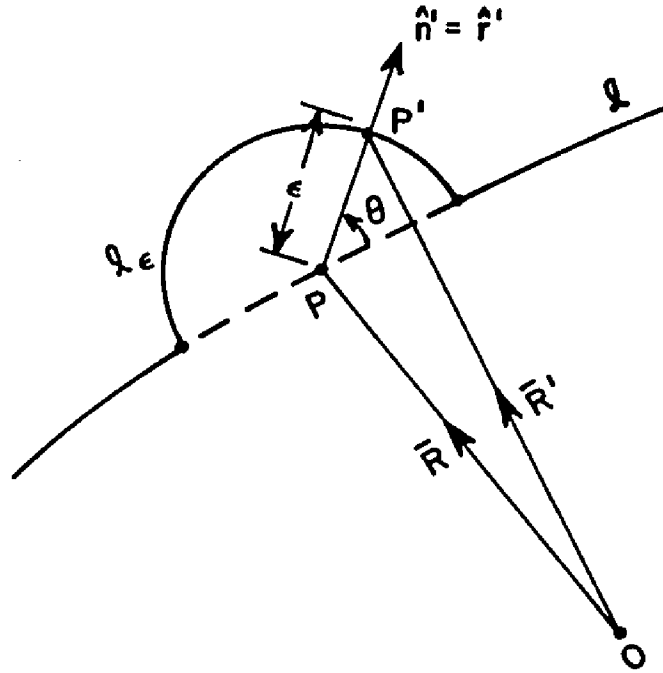$$\frac{\partial G(\epsilon)}{\partial \epsilon} = -\frac{1}{2\pi\epsilon} \quad . \qquad (A4)$$

Figure .A1.   Integration path around the singular point
P in two dimensional problems.

Also for small circular path ℓ_ϵ, $J(\overline{R}')$ can be approximated as $J(\overline{R})$.

Substituting Equation (A4) into Equation (A1), and noting that $\hat{n}' \cdot \hat{r}' = 1$

and $J(\overline{R}') \cong J(\overline{R})$, we obtain

$$\overline{J}_1(\overline{R}) = \hat{\ell}\ J(\overline{R})\ \lim_{\epsilon \to 0}\ \int_{\ell_\epsilon}\ (\ \frac{1}{2\pi\epsilon})\,d\ell$$

$$= \overline{J}(\overline{R})\ \lim_{\epsilon \to 0}\int_0^\pi\ (-\frac{1}{2\pi\epsilon})\,\epsilon\ d\theta$$

$$= -\frac{1}{2}\ \overline{J}(\overline{R}) \tag{A5}$$

which leads to Equation (5-14).

136

APPENDIX B

CURRENT CALCULATION AT A SINGULAR POINT FOR
THREE-DIMENSIONAL PROBLEMS

Consider a hemispherical surface S_ϵ with the radius shown in Figure B1. By the same way as done for Equation (A1), Equation (5.11) can be written as

$$\bar{J}_1(\bar{R}) = \hat{t} \lim_{\epsilon \to 0} \int_{S_\epsilon} J(\bar{R}')(\hat{n}' \cdot \hat{r}') \frac{\partial G(\epsilon)}{\partial \epsilon} ds' \quad . \tag{B1}$$

Using $\frac{\partial G(\epsilon)}{\partial \epsilon} = - (j\beta + \frac{1}{\epsilon}) \frac{e^{-j\beta\epsilon}}{4\pi\epsilon}$, $ds' = \epsilon^2 \sin\theta' d\theta' d\phi'$, and approximation

$J(\bar{R}') \simeq J(\bar{R})$ for small surface S_ϵ in Equation (B1), we have

$$\bar{J}_1(\bar{R}) = \hat{t} \, J(\bar{R}) \lim_{\epsilon \to 0} \int_0^{2\pi}\int_0^{\pi/2} (-j\beta - \frac{1}{\epsilon}) \frac{e^{-j\beta\epsilon}}{4\pi\epsilon} \epsilon^2 \sin\theta' d\theta' d\phi'$$

$$= - \bar{J}(\bar{R}) \lim_{\epsilon \to 0} \int_0^{2\pi}\int_0^{\pi/2} (\frac{j\beta\epsilon+1}{4\pi}) e^{j\beta\epsilon} \sin\theta' d\theta' d\phi'$$

$$= - \bar{J}(\bar{R}) \int_0^{2\pi}\int_0^{\pi/2} \frac{\sin\theta'}{4\pi} d\theta' d\phi'$$

$$= - \frac{1}{2} \bar{J}(\bar{R}) \tag{B2}$$
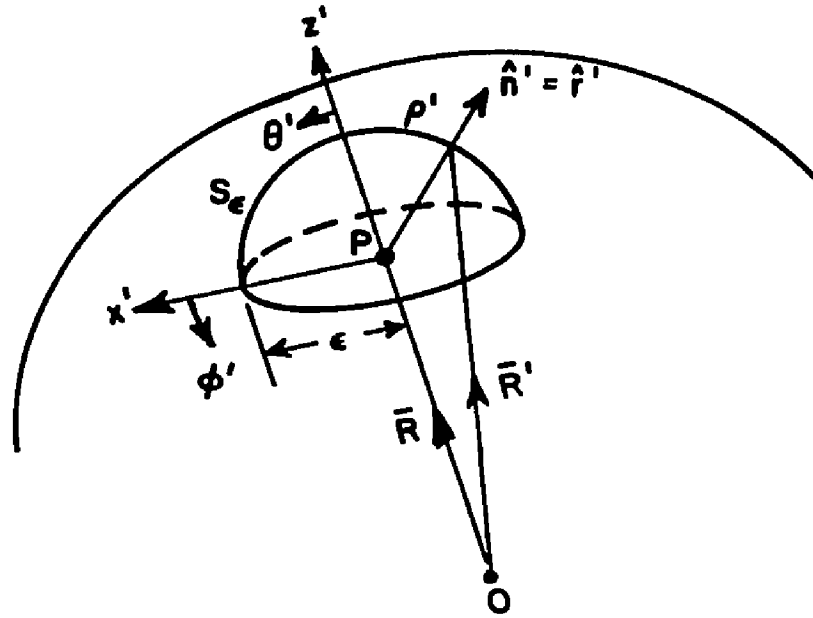
which leads to Equation (6.39).

Figure B1. Hemispherical integration surface around the singular
point P in three dimensional problems.